UPMC HILLMAN CANCER CENTER ACADEMY

FRIDAY, AUGUST 2, 2024

ABSTRACT BOOK

UPMC | HILLMAN CANCER CENTER

University of Pittsburgh

Welcome

Thank you for joining us today to honor our hard-working scholars and laboratories from the Hillman Academy! We strive to provide cutting-edge research and career preparatory experiences to a diverse group of highly motivated high school students who are interested in pursuing higher education and careers in STEM fields. In this hands-on summer program, scholars are placed in laboratories directed by dedicated faculty and trainee mentors across the University of Pittsburgh Campus.

Over the course of its history, the Hillman Academy has become an award-winning science, technology, engineering, and mathematics (STEM) program that prepares students for successful college careers and beyond. The Academy was initiated in 2009 under the directorship of Michael Lotze, MD, and has grown to the program it is today with generous support from the NIH, Doris Duke Charitable Foundation, Jack Kent Cooke Foundation, UPMC, Hillman Foundation, Ear and Eye Foundation, Beckwith Funds, Stan Marks Foundation, Shadyside Hospital Foundation, Pitt, grateful parents and patients, and the many University faculty, trainees, and staff who give selflessly of their time.

Please join us in honoring these students and mentors, as well as the hard work they did this summer to complete an authentic research project. We are so glad that you chose to join us today and are pleased that you have given your scholar a chance to work with our talented faculty, students, and fellows!

Hillman Academy Staff

Program Director: David Boone

Associate Director: Joseph Ayoob

Project Manager: Steven Jones

Hillman Academy Site Directors

Cancer Biology (CB): Dr. Deborah Galson, Dr. Ines Lohse

Computer Science, Biology and Biomedical Informatics (CoSBBI): Dr. David Boone

Computational Biology (CompBio): Dr. Joseph C. Ayoob and Dr. Keisuke Ishihara

Immunology and Cancer Immunotherapy (ICI): Dr. Tullia Bruno and Dr. Greg Delgoffe

Ophthalmology (VISION): Dr. Yuanyuan Chen

Surgery: Dr. Emilia Diego

Tech Drive X (TDX): Dr. Andrew Duncan, Serafina Lanna and Dr. Justin Weinbaum

Women’s Cancer Research Center (WCRC): Dr. Partha Roy and Dr. David Gau

Thank You

This program was made possible with the help of the following people and organizations.

Funding

National Institutes of Health (NIH)

National Cancer Institute Youth Enjoy Science Program

Doris Duke Charitable Foundation (DDCF)

The Beckwith Institute

Hillman Foundation

Shadyside Hospital Foundation

Ear and Eye Foundation

NIH CURE – past

UPMC Center for Engagement and Inclusion – past

Jack Kent Cooke Foundation

Stan Marks Foundation

University of Pittsburgh

UPMC Parking and Security – past

Grateful parents and patients

Partners

Fund for the Advancement of Minority Education (FAME)

Homeless Children's Education Fund (HCEF)

Pittsburgh Public Schools (PPS)

Remake Learning

YWCA

MPowerhouse

STEM PUSH Network

Precollege STEM Programs at Pitt

The Citizen Science Lab

Gene Team

BioZone

Community Engagement Centers

Propel Schools

Pittsburgh Promise

Neighborhood Learning Alliance

Hillman Cancer Center Leadership Team

Dr. Robert Ferris
Dr. Jeremy Rich
Dr. Devin Dressman
Dr. Monica Baskin
Dr. Christopher Bakkenist

Administration

Chris Andersen
Beth Baic
Genine Bartolotta
Michael Becich
Andrea Brasili
Kathy Brickett
Jessica Burrell
Rebecca Case
Rob Ceccehetti
Yvonne Chao
Greg Cooper
Dianna Fennel
Robert Ferris
Toren Finkel
Emma Flynn
Deborah Galson
Harry Hochheiser
Steven Jones
Barbara Karnbauer
Brian Leibowitz
Vladislav Leskovtec
Alison Lithgow
Ines Lohse
Anamarie Martinez
Stephanie Masotti
Lisa McIlvried
Kelsey Meyer
Jessie Nedrow
Toni Porterfield
Rayleigh Richards
Fritz Roth
Nicole Scheff
Mandy Shaheen
Jane Siwek
Lola Thompson
Gina Toy-Cutler
Darryl Washington

Technology

Bill Best
Scot Dunsmore
Keith Durst
Roland Frasher
Ethan Hay
Bryan Krinberg
Mark Schramm

UPMC Hillman Cancer Center Communications Team

Gera Jochum
Anna Daniels

HDS and Interpreters

Jayde Eng
Josh Stresing
Marcus Springer
Michael Nader

Doris Duke Scholars

Mohammed Ali Al-Nagash
Amanda Ferber
Tian LeGrande
Jason Chen
Anthony Kalvi
Samuel Wilson

Instructors, TAs, and Education Team

Adam Forrest
Amanda Locker
Matt Poskus

TECBio REU @ Pitt Mentoring Committee

Michael Grapin (Chair)
Matthey Joyson
Julian Soto
Jules Fetterman
Edgar Maldonado
Alan Wang
Corleigh Forrester
Andrew Pilat

Speakers, Lecturers, and Guests

Joe Ayoob
Brian Doyle
Rebecca Kotcher
Jan Beumer
Wei Du
Stella Lee
David Boone
Andrew Duncan
Tim Lezon
Emmy Brown
Ian Eder
Ruxuan Li
Tullia Bruno
Luisa Escobar-Robledo
Lucy Liang
Tamara Byrd
Adam Forrest
Joseph Long
Racquel Buj-Gomez
Taylor Hobbs
Nate Lord
Alyssa Camerota
Daniel Ibrahim
Raquel Montalvo Perez
Pooja Chawla
Keisuke Ishihara
Ward Richardson
Isabelle Chickanosky
Anders Jeferrson
Asha Seshan
Emilia Diego
Steven Jones
Celine Tohme

Speakers, Lecturers, and Guests (cont.)

Erin Wheeler

John Maier

Soham Mandal

Warren McCoy

Chris Morii-Sciolla

Scott Morley

Jessie Nedrow

Cullen Wilkerson

Andrew Orenberg

Matt Poskus

April Rich

Tina Subic

Ryan Sweeny

Insa Thale Sanghoon Lee

Lina Zwastetzky

Shikhar Uttam

Andreas Vogt

Justin Weinbaum

Sierra White

Michelle William

Professional Development Seminar Series Speakers

Joe Ayoob

David Boone

Tullia Bruno

Steven Jones

Pitt Career Center

Office for Equity, Diversity, & Inclusion - Warren McCoy

Surgeon talk - Emilia Diego, Tamara Byrd, Rebecca Kotcher, Ward Richardson

Offices and Departments

University of Pittsburgh

UPMC Hospital System

UPMC Hillman Cancer Center

UPMC Children's Hospital of Pittsburgh

Pitt School of Medicine

Eye & Ear Foundation of Pittsburgh

UPMC Security Office

UPMC Volunteer office

Disability Resources and Services

Pitt IT/ Technology Help Desk

Panther Central

Department of Biomedical Informatics

Department of Ophthalmology

Computational and Systems Biology

Department of Immunology

Department of Pathology

Department of Surgery

Department of Bioengineering

Magee-Womens Research Institute

McGowan Institute of Regenerative Medicine

Office for Equity, Diversity, & Inclusion

University Counsel

And the many other departments that support this program.

Mentors

Thanks to the hundreds of mentors across campus each of which is recognized on the individual student abstracts and site schedules

UPMC HCC Summer Academy
Cancer Biology Site 2024 Research Symposium
Session A

August 2, 2024, 8:30 am-12:00 pm

Herbermann Conference Center 2nd Floor Room A @ UPMC Cancer Pavilion
5150 Centre Ave, Pittsburgh PA

Join Zoom Meeting https://pitt.zoom.us/j/96725223285 Passcode: 612474

8:30AM Welcoming Remarks

CB Site Education Team:

Deborah L. Galson, PhD (Site Director), Ines Lohse, PhD (Site Co-Director) & Amanda Locker, BS

8:45 AM #1 Roman Allen
PI: Diwaker Davar, MD, MSc

9:00 AM #2 Emma Impelliceceiri
PI: Elise Fourquerel, PhD; Lab Mentor: Rim Nassar, PhD

9:15 AM #3 Kaushal Patel
PI: Jessie Nedrow, PhD; Lab Mentor: Abhinav Bhise, PhD

9:30 AM #4 Tiffany Wang
PI: Dennis Hsu, MD; Lab Mentors: Marwa Ibrahim, PhD & Alex Roberts

9:45 AM #5 Eric Chen
PI: Evan Delgado, PhD; Lab Mentor: Panari Mukesh Patel

10:00 AM #6 Alastair Watt
PI: Patricia Opresko, PhD; Lab Mentor: Samantha Sanford, PhD

10:15-10:30 AM ---------- BREAK ----------

11:30 AM #7 Jason Chen
PI: Tim Burns, MD, PhD; Lab Mentor: Vinod Kumar, PhD

10:45 AM #8 Andrew Li
PI: Kathryn Demanelis, PhD

11:00 AM #9 Julia Lipscomb
PI: Anna Lokshin, PhD; Lab Mentor: Yan Wang, PhD

11:15 AM #10 Gabrielle Generett
PI: Wei Du, MD, PhD; Lab Mentor: Jian Xu, PhD

10:30 AM #11 Hira Payas
PI: Flordeliza Villanueva, MD; Lab Mentors: Xucai Chen, PhD, Anurag Paranjape, PhD & Geetika Fnu, PhD

12:00 PM ------ LUNCHEON (Herbermann Atrium) ------

2:00 PM ACADEMY-WIDE CLOSING CEREMONY
(Assembly Auditorium)

UPMC HCC Summer Academy
Cancer Biology Site 2024 Research Symposium
Session B

August 2, 2024, 8:30 am-12:00 pm

Herbermann Conference Center 2nd Floor Room B @ UPMC Cancer Pavilion
5150 Centre Ave, Pittsburgh PA

Join Zoom Meeting https://pitt.zoom.us/j/96650533051 Passcode: 732708

8:30AM Welcoming Remarks

CB Site Education Team:

Deborah L. Galson, PhD (Site Director), Ines Lohse, PhD (Site Co-Director) & Amanda Locker, BS

8:45 AM #1 Glory Schmigel
PI: Ravi Patel, MD, PhD; Lab Mentor: Robert Edinger, PhD

9:00 AM #2 Gabby Jarvis
PI: Joel Greenberger, MD & Amitava Mukherjee, PhD; Lab Mentor: Renee Fisher

9:15 AM #3 Leni McCann
PI: Xiaosong Wang, MD, PhD; Lab Mentor: Bashir Lawal, PhD

9:30 AM #4 Zacharias Barron
PI: Ines Lohse, PhD & Kurt Weiss, MD; Lab Mentors: Amanda Locker, BS & Tanya Heim, MS

9:45 AM #5 Matteo Foronda
PI: Jing Hong Wang, MD, PhD; Lab Mentor: Zhangguo Chen, PhD

10:00 AM #6 Tiffany Habib
PI: Yu-Chih Chen, PhD; Lab Mentors: Jinxiong Cheng, BSE & Hsiao-Chun Chen, MS

10:15-10:30 AM ---------- BREAK ----------

10:30 AM #7 Matthew Morcos
PI: Chris Bakkenist, PhD; Lab Mentor: Sudipta Pathak, BS

10:45 AM #8 Brandon Williams
PI: Chris Bakkenist, PhD; Lab Mentor: Reyna Jones

11:00 AM #9 Isabel Vilensky
PI: Tatiana Moiseeva, PhD; Lab Mentor: Gregory Zamalloa, PhD

11:15 AM #10 Anthony Kalvi
PI: Yi-Nan Gong, PhD; Lab Mentor: Frank Chang, PhD

11:30 AM #11 Tian LeGrande
PI: Nicole Scheff, PhD; Lab Mentors: Lisa McIlvried, PhD & Megan Atherton

12:00 PM ------ LUNCHEON (Herbermann Atrium) ------

2:00 PM ACADEMY-WIDE CLOSING CEREMONY (Assembly Auditorium)

Computational Biology Site Agenda

August 2, 2024
Murdoch Building (3420 Forbes Ave, Pittsburgh, PA 15213) Floor 8, Room 814
Virtual link: https://pitt.zoom.us/s/96010669627

9:30 – 9:35 AM	**Dr. Joe Ayoob, CompBio Site Head**
9:35 – 9:50 AM	**Oliver Adams** Mentor: Dr. Guangyi Zhao
9:50 – 10:05 AM	**Rhea Arya** Mentors: Dr. Zhiwei Feng, Dr. Sean Xie
10:05 – 10:20 AM	**Grayson Hou** Mentors: Dr. Zhiwei Feng, Dr. Sean Xie
10:20 – 10:35 AM	**Samarth Mandani** Mentors: Dr. Terry McGuire
10:35 – 10:45 AM	**Break**
10:45 – 11:00 AM	**Avery Mills** Mentors: Dr. Fritz Roth, Dr. Warren van Loggerenberg
11:00 – 11:15 AM	**Hussain Raza** Mentor: Dr. Nate Lord, Dr. Anne-Ruxandra Carvunis, Alison Guyer
11:15 – 11:30 AM	**Jame Hsieh** Mentor: Dr. Keisuke Ishihara
11:30 – 11:45 AM	**Alayna Fu** Mentors: Dr. Jim Faeder, Dr. Tina Subic
11:45 AM – 12:00 PM	**Sarah Beth Winikoff** Mentors: Dr. Maria Chikina, Dr. Tina Subic
12:00 – 12:30 PM	**Lunch for Students, Mentors, Family, and Friends** **Murdoch Classroom 814**

Hillman Academy - CoSBBI

August 2, 2024, 8:00 AM
The Offices at Baum, Room 407 A/B
https://us02web.zoom.us/j/85754282549?pwd=elordlNjOE43cFNXOEM4M3RhNGRjZz09

8:00 AM **Welcoming Remarks**
David Boone, PhD

8:05 AM **CoSBBI Scholars Research Presentations – Session 1**

8:05 AM **Divye Arora-Jain**
Mentors: Dr. Liang Zhan and Kai Ye

8:20 AM **Oscar Martinez**
Mentor: Dr. Luija Chen

8:35 AM **Ronit Ginde**
Mentors: Dr. Natasa Miskov-Zivanov and Haomiao Luo

8:50 AM **Vega Mani**
Mentors: Dr. Erik Wright and Sam Blechman

9:05 AM **Rose-Carlie Pierre**
Mentor: Dr. Margaret Rosenzweig

9:20 AM **Daniel Perez**
Mentor: Dr. Olga Kravchenko

9:35 AM **BREAK**

9:40 AM **CoSBBI Scholars Research Presentations – Session 2**

9:40 AM **Amanda Ferber* Doris Duke Undergraduate**
Mentors: Dr. Kayur Mehta, J. Rosen, D. Somaiya, K. Muralidhar

9:55 AM **Tara Olaniyan**
Mentors: Dr. Matt Wohlever and Megan Monroe

10:10 AM **Omisa Shah**
Mentor: Dr. In Hee Lee

10:25 AM **Joshua Petit-Homme**
Mentor: Dr. Jacob Biehl

10:40 AM **Trinidy Manison**
Mentors: Dr. Ana Radovic

10:55 AM **Malynn Jones**
Mentor: Dr. Sandra Murray, Selma Cetin-Ferra, Anthony Cooper

11:10 AM **BREAK**

11:15 AM **CoSBBI Scholars Research Presentations – Session 3**

11:15 AM **Ethan Small**
Mentors: Dr. Murat Akcakaya, Deniz Kocanoagullari, Nate Riek

11:30 AM **Reina Majumdar**
Mentors: Drs. Michael Becich and Rumana Rashid

11:45 AM **Rayan Majumdar**
Mentors: Drs. Michael Becich and Brittany Gomez

12:00 PM **Alex Schafer**
Mentor: Eddie Perez

12:20 PM **Lunch – Baum 4th floor foyer and 407A/B RSVP REQUIRED**

2:00 PM **Hillman Academy Closing Ceremony**
Assembly Building – First Floor Auditorium
5051 Centre Ave or **Zoom for students**:
https://us02web.zoom.us/j/86021100717?pwd=dmVQQ0NvYzFnMUVIOUxKWFdwd2U5UT09

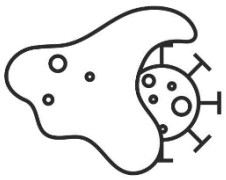

Immunology and Cancer Immunotherapy

Friday, August 2, 2024
9 AM-2 PM EST (West Wing Auditorium)
https://pitt.zoom.us/j/93941059437

Time	Presenter and Mentor
8:30-9:00 AM	Breakfast (optional)
9:00-9:15 AM	**Opening remarks** *Drs. Tullia Bruno and Greg Delgoffe*
9:15-9:30 AM	**Omar Al-bataineh** *Mentor: Dr. Adam Soloff*
9:30-9:45 AM	**Ivan Chen** *Mentors: Drs. Greg Delgoffe and Bingxian Xie*
9:45-10:00 AM	**Anabella Phelps** *Mentor: Dr. Tullia Bruno and Caroline Sweeney*
10:00-10:15 AM	**Jingyuan Zhang** *Mentors: Dr. Greg Delgoffe and Hannah Bumgarner*
10:15-10:30 AM	*Short networking break*
10:30-10:45 AM	**Oluwatobiloba Olaore** *Mentor: Dr. Melissa Kane*
10:45-11:00 AM	**Oliver Francis** *Mentors: Dr. Robert Binder*
11:00-11:15 AM	**Ella Tabish** *Mentors: Drs. Robert Ferris and Lazar Vujanovic*
11:15-11:30 AM	**Lyra Stiglitz** *Mentor: Dr. Alok Joglekar*
11:30-11:45 AM	*Short networking break*
11:45-12:00 PM	**Nora Coen-Pirani** *Mentors: Dr. Hassane Zarour*
12:00-12:15 PM	**Camilla Zarour** *Mentors: Dr. Rodrigo das Neves*
12:15-12:30 PM	**Isabella Kwaw** *Mentor: Dr. Tina Sumpter*
12:30-12:45 PM	**Mohammed Ali** *Mentor: Dr. Daniella Schwartz*
12:45-1:05 PM	**John Presti and Austin Tomer** *Mentor: Dr. Ali Kohan*
1:15 PM	**Final remarks, group picture, and grab and go lunch** *Migrate to Assembly Building*
2:00 PM	**Start of final ceremony in Assembly Auditorium**

We really hope you can join us in person, but if not, here is a virtual link!

Surgery Site

August 2, 2024
Herberman Conference Center Room 202 A
5230 Centre Ave
https://tinyurl.com/2dek8r5y
Meeting ID: 237 965 427 343
Passcode: N3C2Em

10:30 **Opening Remarks**
Dr. Emilia Diego

Time **Research Presentations**

10:45 **Mikaela Dassanaike-Perera**
Mentor, Dr. Alaa Sada

11:00 **Steven Li**
Mentor, Dr. Joshua Brown and Dr. Christine Leeper

11:15 **Mariah Harris**
Mentor, Dr. Genia Dubrovsky and Dr. Anna Sabih

11:30 **Anna Litster**
Mentor, Dr. Melanie Scott

11:45 **Jermaine Taylor**
Mentor, Dr. Samer Tohme

12:00 **Lunch - Herberman Conference Center Room 202 A**

TECH DRIVE X

2024 Research Symposium • Hillman Academy

August 2, 2024

Bridgeside Point II, Room 503, 450 Technology Drive, Pittsburgh, PA 15219
Virtual: https://pitt.zoom.us/j/94395497627

9:00 AM **Welcome**
Dr. Andrew Duncan, Dr. Justin Weinbaum, Serafina Lanna, TDX Site Heads

9:15 AM **Oral Presentations** (10 min. presentations + 5 min. questions); introductions by lab mentors

9:15 AM **Luke An**
Lab, Dr. Jonathan Vande Geest; *Mentor,* Adam Forrest

9:30 AM **Anna Apetrei-Pandrea**
Lab, Dr. Jay Tan; *Mentor,* Dr. Bo Lv

9:45 AM **Isabella Cheatham**
Lab, Dr. Aditi Gurkar; *Mentor,* Swathi Dantuluri

10:00 AM **August Kollar**
Lab, Dr. TK Kozai; *Mentors,* Kevin Stieger, Jazlyn Gallego, & Vanshika Singh

10:15 AM **Sophia Mazer**
Lab, Dr. Vaughn Cooper; *Mentors,* Dr. Abigail Matela & Colton Siatkowski

10:30 AM **BREAK**

10:45 AM **Angie Odeniyi**
Lab, Dr. Justin Weinbaum; *Mentor,* Amanda Pellegrino

11:00 AM **Caroline Praveen**
Lab, Dr. Bryan Brown; *Mentor,* Dr. Mangesh Kulkarni

11:15 AM **Narendra Ray**
Lab, Dr. Tim Chung; *Mentor,* Kat Kerr

11:30 AM **Riley Therrien**
Lab, Dr. Bill Chen; *Mentors,* Dr. Travis Lear & Aine Boudreau

11:45 AM **Samuel Wilson**
Lab, Dr. George Hussey; *Mentors,* Dr. Catalina Pineda Molina & Daniela Romero

12:00 PM **Lunch – Bridgeside Point II, 5th-floor lunchroom**

2:00 PM **Closing Ceremony**
Assembly Building, First Floor Auditorium
5051 Centre Ave, Pittsburgh, PA 15213

VISION Site

August 2, 2024
UPMC Mercy Pavilion – PAV 4.221A
https://pitt.zoom.us/j/99081297659

9:30 **Opening Remarks**

Time	Research Presentations	
	9:40	**Makala Starks** Mentor, Dr. Anthony St. Leger
	10:00	**Sophia Hadi** Mentor, Dr. Yuanyuan Chen and Kate Davoli
	10:20	**Joyce Olawalye** Mentor, Drs. Sandeep Bollepalli and Gary Yam
	10:45	**Ezra Hardy** Mentor, John Ash and Constanza Potilinski
	11:05	**Chimdi Isiguzo** Mentor, Dr. Kun-Che Chang
	11:25	**Justin Chen** Mentor, Dr. Shaohua Pi
	11:45	**Kevin Chen** Mentor, Dr. Shaohua Pi
	12:05	**Ashly Shim** Mentor, Dr. Cheng Zhang
	12:25	**Ismael Aly** Mentor, Dr. Miguel Betegon

WCRC Site

August 2, 2024
The Assembly, Room B 1610
https://pitt.zoom.us/j/99578253974

10:30 am **Welcome**
Partha Roy & David Gau, PhD

10:35 am **Research Presentations**

10:35 – 10:50 am	**Mae Cano** Lab, Dr. Partha Roy; Mentor, Pooja Chawla
10:50 – 11:05 am	**Ava Miller** Lab, Dr. Katherine Aird; Mentor, Dr. Amadine Amalric
11:20 – 11:35 am	**Addison McLane** Lab, Dr. Nadine Hempel; Mentor, Dr. Sierra White and Ya-Yun Cheng
11:35 – 11:50 am	**NyAzia Roberts** Lab, Dr. Adrian Lee, Dr. Steffi Oesterreich; Mentor, Dr. Insa Thale
11:50 – 12:05 pm	**Nathaniel Shelton** Lab, Dr. Adrian Lee, Dr. Steffi Oesterreich; Mentor, Dr. Sanghoon Lee
12:05 – 12:20 pm	**Anvi Chopra** Lab, Dr. Lan Coffman; Mentor, Dr. Huda Atiya
12:20 – 12:35 pm	**Ruth Ayers** Lab, Dr. Ioannis Zervantonakis; Mentor, Matt Laird

12:35 pm **12:35 – 1:45 pm** **Lunch – B 1610, The Assembly**

The Relationship Between ELMO1 and Autoinflammation Using Rac

Mohammed Ali Al-Nagash
University of Pittsburgh
PI: Dr. Daniella M Schwartz
Mentor: Elizabeth Kairis
Site: ICI

The Relationship Between ELMO1 and Autoinflammation Using Rac
Mohammed Ali Al-Nagash
University of Pittsburgh
PI: Dr. Daniella M Schwartz
Mentor: Elizabeth Kairis
Site: ICI

The innate immune system is the human body's first line of defense against antigens in the human body through inflammation using different proteins and phagocytes. Autoinflammation occurs when the innate immune system malfunctions and normal cells are attached as if they were invaders which can lead to periodic fever syndrome. Engulfment and cell motility 1 (ELMO1) is a gene that is known to regulate cell processes by activating Rac, an effector protein that influences actin equilibrium, including cell migration, phagocytosis, and apoptosis. There is no known role for ELMO1 in innate immunity but 5 patients that have been identified with putative gain of function mutations in ELMO1 have signs of autoinflammation. This study aims to test the relationship between ELMO1 and autoinflammation by measuring NF-κB activity as a marker of inflammation. NF-κB is a transcription factor that induces proinflammatory cytokines like IL-1 and IL-18. It is hypothesized that mutant ELMO1 will activate NF-κB more than wild-type (WT) ELMO1, leading to more NF-κB activation and potential autoinflammation. The experimental procedure included seeding HEK293T cells. Cells are then transfected with the respective plasmids of WT vs. mutant GFP-tagged ELMO1, and transfection efficiency is checked with GFP imaging. The cells are then stimulated with 3 concentrations of TNF-α, 2ng, 20ng, and 200ng to promote NF-κB activity, and NF-κB activity is then quantified through a luciferase assay, and results are recorded, and procedure is replicated. The pooled data results display the gain of function mutation T560M in ELMO1, stimulated with 200ng of TNF-α having significantly elevated NF-κB activation (luciferase activity) when compared with WT ELMO1. Other mutations displayed a positive trend, but the data were not significant. A potential relationship between mutations in ELMO1 and autoinflammation can be established, suggesting a novel autoinflammatory disease. More replicates must be done to confirm this conclusion.

Title: The MET-TWIST1 pathway regulates the key glycolytic enzyme, Hexokinase 2 in *MET* altered NSCLC

Scholar: Jason Chen

High School/College/City/State: Johns Hopkins University, Baltimore, MD

PI of group/lab: Dr. Timothy Burns, MD, PhD

Mentors: Vinod Kumar, PhD

Site: Cancer Biology

Lung cancer remains leading cause of cancer deaths both in the U.S. and worldwide. MET is a receptor tyrosine kinase that binds with hepatocyte growth factor (HGF) to mediate many cellular processes evolved in tumorigenesis. The HGF/MET pathway is frequently dysregulated in cancer as a result of MET or HGF protein overexpression, *MET* amplification or *MET* mutations. Patients with *MET* mutated or *MET* amplified non-small cell lung cancer (NSCLC) can be treated with MET tyrosine kinase inhibitors (TKIs) in the clinic. However, long term usage can become ineffective due to *de novo* or acquired resistance, highlighting the need for novel therapeutic strategies. Our research previously identified a significant enrichment of *MET* amplification in lung adenocarcinoma (LUAD) brain metastasis (16%) compared to primary LUAD (3%) and that *MET* amplified BM had a distinct transcriptional signature reflecting high glycolysis. Furthermore, we observed increased glycolysis in *MET* amplified and high MET expressing cell lines. Finally, we found that *MET* altered cell lines are more sensitive to glycolytic inhibitors and that MET inhibition decreased glycolysis. How the HGF/MET pathway regulates glycolysis is still poorly understood. We hypothesized that the HGF/MET pathway increases glycolysis thorough its regulation of the key glycolytic enzyme Hexokinase II (HK2). We observed that MET inhibitor treatment decreased mRNA and protein expression of the key glycolytic enzyme Hexokinase II (HK2). Additionally, we have found that *HK2* is a direct transcriptional target of the transcription factor, TWIST1 which is a key downstream mediator of the MET pathway. Interestingly, knocking down TWIST1 reduced sensitivity to the HK2 inhibitor, 2DG. Conversely, overexpressing TWIST1 in *MET* wild-type cells increased sensitivity to 2DG. We have also found that glycolytic inhibitors are less effective in MET TKI resistant cell lines. Ongoing experiments are testing whether other glycolytic inhibitors will be effective against *MET* altered cell lines.

Title: Contextualizing perceptions of cervical cancer screening among women in Mysore, India

Scholar: Amanda Ferber

College: Johns Hopkins University, Baltimore, MD

Lab PI: Dr. David Boone

Mentors: Dr. Kayur Mehta, Dr. J. Gregory Rosen, Dr. Devanshi Somaiya

Site: Public Health Research Institute of India

We aim to assess the barriers and facilitators to completing a cascade of cervical cancer screening tests among women living in rural Mysore, India. Cervical cancer is the second most common cancer among women in India, with an incidence rate of 18.7 cases in every 100,000 women and around 77348 deaths in 2020. The most common cause of cervical cancer is previous infection with HPV, and the World Health Organization recommends HPV DNA testing as the starting point for cervical cancer screening, but there is no national screening program via HPV test in India. In accordance with the WHO cervical cancer elimination strategy, the Public Health Research Institute of India (PHRII), a research organization and clinic in Mysore, India, began rolling out a cervical cancer screening program where all participating women take self-sampling HPV DNA tests. Upon a positive result, women are invited to proceed in a cascade of diagnostic tests to detect cervical cancer. However, PHRII is experiencing programmatic issues involving loss to follow-up: staff are finding that women are not consistently completing the screening cascade after testing positive for HPV. Cervical cancer detection (beyond just prevention) depends on completion of the entire screening cascade, so poor follow-up can limit the cost-effectiveness in such a program to detect and treat cancer. This project is a collaboration between physicians and researchers at PHRII and the JHU Bloomberg School of Public Health, and we will conduct semi-structured, in-depth interviews with community health workers and screening-eligible women to better understand the factors considered by women when offered cervical cancer screening.

Exploring Cell Death Pathways Induced by Heavy Metals, PAHs, and FTOHs

Scholar: Anthony Kalvi

High School/College/City/State: University of Pittsburgh Greensburg Pa

PI of group/lab: Yi-Nan Gong, Ph.D.

Mentor(s): Frank Chang Ph.D., Julia Ferrick, Donghui Yang, Zhanpeng Cen

Site: Cancer Biology

Exposure to heavy metals, polycyclic aromatic hydrocarbons (PAHs), and fluorotelomer alcohols (FTOHs) poses significant environmental and health risks due to their established carcinogenic properties. These toxic compounds can induce both programmed and unprogrammed cell death. Apoptosis, a form of programmed cell death, involves proapoptotic proteins Bax and Bak, which play crucial roles in caspase activation, leading to controlled cellular demise. In contrast, necrosis is a pathological and unprogrammed form of cell death characterized by cell membrane rupture in response to extreme conditions. Necroptosis, sharing morphological similarities with necrosis, is a highly regulated process combining features of both apoptosis and necrosis. These toxic compounds can cause cell death through mechanisms such as oxidative stress, DNA damage, disrupted cell signaling, and mitochondrial dysfunction. The resultant cell death often contributes to inflammation, a precursor to various cancers. In this study, mouse Lewis Lung Carcinoma (LLC), human pancreatic cancer (Panc-1), and human lung adenocarcinoma (PC9) WT and Bax/Bak double KO cells were exposed to varying concentrations of these substances over time intervals ranging from 30 minutes to 2 days to evaluate their toxicity and the pathways of cell death they activate. Visualization using Sytox Green dye, which binds to nucleic acids once the cell membrane is compromised, and Incucyte imaging revealed dose- and time-dependent cell death responses across the tested concentrations (100 mM - 50 μM) in all cell lines. Our findings indicate that necrosis is a significant form of cell death observed under these conditions.

Title: Sensory nerves in the oral cancer tumor microenvironment sprout in response to tumor cell-secreted nerve growth factor

Scholar: Tian LeGrande

High School/College/City/State: Carnegie Mellon University, Pittsburgh Pa

PI of group/lab: Nicole Scheff, Ph.D

Mentor(s): Megan Atherton, Lisa McIlvried, Ph.D, Nicole Scheff, Ph.D

Site: Cancer Biology

Oral cancer progression may be influenced by reciprocal interactions between peripheral nerves and tumor cells through secreted mediators. Nerve Growth Factor (NGF) and its receptors TrkA and p75 are frequently overexpressed in cancers and correlate with advanced tumor stages, poor outcomes, and pain. Disrupting NGF binding in the tumor microenvironment has been shown to decrease nerve sprouting, tumor size, and pain behaviors in an animal model of bone metastasis . We hypothesize that oral cancer tumor cells secrete NGF, which binds to TrkA/p75 receptors on trigeminal sensory nerves in the tumor microenvironment to increase a sprouting response.

To test this hypothesis, we utilized real-time qPCR and Luminex Multiplex to determine NGF expression and release across various cell lines, as well as the presence of TrkA/p75 receptors on trigeminal sensory neurons. Additionally, trigeminal sensory neuron acute cultures and immunohistochemistry were used to quantify axonal sprouting in response to media from cultured mouse oral cancer and primary non-cancerous cell lines. We found that oral cancer cells expressed significantly less *Ngf* mRNA compared to non-cancer control cells. Conversely, oral cancer cells -secrete significantly more βNGF protein compared to non-cancer control cells. Trigeminal ganglia, which contains sensory neurons that innervate the head and neck region, from MOC-2 tumor-bearing animals expressed genes for NGF receptors, *TrkA* and *p75*. We also found that trigeminal sensory neurons significantly increased sprouting in response to oral cancer cell-conditioned media compared to normal media and conditioned media from non-cancerous primary cells, an effect decreased by neutralizing antibody aNGF.We conclude that NGF may play a key role in sensory neuron sprouting in oral cancer, which could contribute to cancer progression and pain. Future directions should further investigate the mechanisms of NGF and other tumor-secreted mediators in oral cancer, potentially leading to new therapeutic approaches.

Characterizing MBV Uptake in Normal and Cancerous Esophageal Epithelial Cells

Scholar: Samuel Wilson

College: Duquesne University, Pittsburgh, PA

PI: George Hussey, PhD.

Mentor: Daniela J. Romero, PhD., Catalina Pineda Molina, PhD.

Site: TDX

Matrix-Bound Nanovesicles (MBV) are lipid vesicles bound to the Extracellular Matrix (ECM) in all mammalian tissues. They are a subset of Extracellular Vesicles (EV), containing a unique cargo of protein and miRNA that have demonstrated the ability to modulate the phenotype and function of various cell types including macrophages, stem cells, and epithelial cells. Furthermore, in normal and cancerous esophageal epithelial cells treated with MBV, preliminary results have shown different effects on cell viability. Showing decreased survival rates in cancer esophageal epithelial cells when compared with normal esophageal epithelial cells stimulated with MBV. The objective of this study is to determine the process by which normal and cancer esophageal epithelial cells uptake MBV to further understand the interactions between them. MBV isolated from urinary bladder extracellular matrix (UBM) were labeled with CFSE, a fluorescent surface-protein staining dye, and used to treat nonmalignant (Het-1A) and neoplastic (SK-GT-4) esophageal epithelial cells to confirm uptake. Following this, after determining the optimal MBV concentration for treatment via dose-response studies, time course studies were performed to characterize these interactions. Fluorescent microscopy confirmed UBM MBV uptake in Het-1A and SK-GT-4 and showed UBM MBV uptake is possible as early as 30 minutes after treatment. Preliminary results from the dose-response study showed a clear vesicular pattern in the SK-GT-4 cells after each concentration of UBM MBV used for treatment. In contrast, such a pattern was only visible after using the highest concentration of UBM MBV to treat the Het-1A cells, suggesting an exasperated endocytosis response in the neoplastic SK-GT-4 cells. Our next steps include inhibiting mechanisms of cellular uptake in Het-1A and SK-GT-4 to determine the mechanism used to uptake UBM MBV and time-lapse imaging to visualize this process.

RNA-Sequencing Analysis of Pathway Activation in Cannabinoid-Treated and Gemcitabine-Treated Pancreatic Ductal Adenocarcinoma Cells

Oliver E. Adams and Jacob Cuyler
South Fayette High School, McDonald, PA; University of Pittsburgh Hillman Cancer Center Academy, Pittsburgh, PA

Introduction

Pancreatic ductal adenocarcinoma (PDAC), commonly known simply as pancreatic cancer because it accounts for over 85% of pancreatic neoplasms, is a highly lethal disease with a 5-year survival rate of only 12%, partially due to the lack of effective treatment options currently. To improve the presently dismal prognosis, cannabinoids have emerged as a potential option for combination therapy against PDAC. Phytocannabinoids are naturally occurring compounds typically found in plants and interact with the body's endocannabinoid system. Certain cannabinoids possess various anticancer properties such as anti-inflammation, tumor regression, immune modulation, antiproliferation, autophagy induction, and when combined with conventional cancer therapies such as gemcitabine, they have been reported to enhance the cytotoxicity of the drug. However, the synergistic mechanism between gemcitabine and cannabinoids is largely unknown. The objective of my project is to investigate the molecular mechanism of gemcitabine-cannabinoid synergy to evaluate the potential of the combination therapy for usage in PDAC treatment.

Methods

Ingenuity Pathway Analysis (IPA) was used to study bulk RNA-sequencing datasets from Gene Expression Omnibus (GEO) and QIAGEN OmicSoft Lands. Through a comparison analysis of transcriptomes from gemcitabine-treated and cannabinoid-treated pancreatic cancer cells, the similitude in pathway activation is investigated to discover possible reasons behind their synergistic effects.

Results

Various pathways in the gemcitabine treatment were found to be regulated similarly to their regulation in standard cannabinoid treatment, such as the production of nitric oxide and reactive oxygen species in macrophages pathway, the endocannabinoid cancer inhibition pathway, and the glucose metabolism pathway. Other significant cannabinoid-related signaling pathways such as the unfolded protein response pathway and LPS-stimulated MAPK signaling saw marginally mixed upregulation and downregulation across samples.

Discussion

The overlapping pathway modulation between the cannabinoid and gemcitabine treatments suggests that the combination treatment's efficacy results from their relatively similar and highly complementary mechanisms. Cannabinoids enhance the cytotoxicity of gemcitabine by targeting identical structures within the pancreatic cancer cells to amplify the damage caused by gemcitabine. Though these results do not propose significantly novel insight, they further validate the reason behind the synergistic effect observed in the combination therapy and demonstrate the potential for its usage in PDAC treatment.

Figure 1: Cannabinoid-Related Canonical Pathways Modulated in Gemcitabine Treatment Samples

Canonical Pathways	GEM Sample 1	GEM Sample 2	GEM Sample 3	GEM Sample 4	GEM Sample 5	GEM Sample 6
Autophagy	1.941	3.873	2.111	1.897	2.5	2.121
Production of Nitric Oxide and Reactive Oxygen Species in Macı	0.333	2.714	2.121	1.134	1.414	1.342
Endocannabinoid Cancer Inhibition Pathway	1	1	0.707	1.414	1.265	1.414
Role of JAK family kinases in IL-6-type Cytokine Signaling	1.633	2.236	0.447	1	1.134	0
Role of MAPK Signaling in Inhibiting the Pathogenesis of Influenz	1	1.414	N/A	1	0.816	1
LPS-stimulated MAPK Signaling	-0.447	2.121	1	N/A	0.378	0.447
Glucose metabolism	-1.414	-0.447	-1	-0.447	-0.816	0
Unfolded protein response	0.333	0.816	0.707	-0.447	0.378	0

References:

Park, Wungki et al. “Pancreatic Cancer: A Review.” JAMA vol. 326,9 (2021): 851-862. doi:10.1001/jama.2021.13027

Donadelli M, Dando I, Zaniboni T, Costanzo C, Dalla Pozza E, Scupoli MT, Scarpa A, Zappavigna S, Marra M, Abbruzzese A, Bifulco M, Caraglia M, Palmieri M. Gemcitabine/cannabinoid combination triggers autophagy in pancreatic cancer cells through a ROS-mediated mechanism. Cell Death Dis. 2011 Apr 28;2(4):e152. doi: 10.1038/cddis.2011.36. PMID: 21525939; PMCID: PMC3122066.

Dando, I et al. “Cannabinoids inhibit energetic metabolism and induce AMPK-dependent autophagy in pancreatic cancer cells.” Cell death & disease vol. 4,6 e664. 13 Jun. 2013, doi:10.1038/cddis.2013.151

Lowe, Henry et al. “The Endocannabinoid System: A Potential Target for the Treatment of Various Diseases.” International journal of molecular sciences vol. 22,17 9472. 31 Aug. 2021, doi:10.3390/ijms22179472

Brandi J, Dando I, Palmieri M, Donadelli M, Cecconi D. Comparative proteomic and phosphoproteomic profiling of pancreatic adenocarcinoma cells treated with CB1 or CB2 agonists. Electrophoresis. 2013 May;34(9-10):1359-68. doi: 10.1002/elps.201200402. Epub 2013 Apr 11. PMID: 23463621.

OmicSoft Lands Comparison IDs:

LINCS.GPL20573.test109620 (GEM Sample 1)
LINCS.GPL20573.test100425 (GEM Sample 2)
LINCS.GPL20573.test151364 (GEM Sample 3)
LINCS.GPL20573.test97507 (GEM Sample 4)
LINCS.GPL20573.test158032 (GEM Sample 5)
LINCS.GPL20573.test84279 (GEM Sample 6)

The Effect of Microplastics on Macrophage Function and Anti-Tumor Immunity

Scholar: Omar Al-bataineh

High School/College/City/State: Fox Chapel Area High School, Pittsburgh, PA

PI of group/lab: Dr. Adam Soloff

Mentor(s): Dr. Adam Soloff

Site: Immunology and Cancer Immunotherapy (ICI)

Microplastics can have toxic effects when inhaled from the environment. The effect of microplastics on pulmonary immunity is unexplored. Macrophages are essential to maintain lung homeostasis, with the role of phagocytosis of apoptotic cells in the lungs. Alveolar macrophages are linked with multiple pulmonary diseases when their function is hindered. Due to the influx of microplastic exposure in the world today, we investigated the effects of microplastics on macrophage function and anti-tumor immunity. We co-cultured the mouse macrophage cell line, RAW 264.7, in vitro with fluorescent polystyrene bead microplastics at four sizes: 10, 1, 0.1, and 0.02 micrometers in diameter. First, we used fluorescence microscopy to determine if the macrophages were phagocytosing the microplastics. In triplicate, we introduced microplastics at a low (1:1 bead to cell ratio), medium (5:1 bead to cell ratio), and high (10:1 bead to cell ratio) concentration. This helped us determine that the medium concentration of microplastics was most effective for phagocytosis by macrophages. Then, we used flow cytometry to analyze the effects of the microplastics on the macrophages' ability to phagocytose fluorescent green zymosan particles, a component of the yeast cell wall. Compared to macrophages with no microplastic exposure, microplastics significantly inhibited phagocytosis of zymosan green particles (p value = 0.0002) with 10 micrometer microplastics exhibiting the largest inhibition (65% vs 5% uptake, $p < 0.0001$). To revert microplastic-induced dysfunction, we then introduced the drug AICar in three concentrations to the macrophages prior to 0.1 micrometer microplastic exposure. Here, pre-treatment with AICar was able to increase macrophage phagocytosis of zymosan following microplastic exposures, but more experiments are needed to confirm these results. In the future, we plan on continuing to evaluate the relationship between microplastic exposure and chronic lung illnesses/cancer and how to reverse these effects.

Artificial Sweeteners and Their Effect in Immunotherapy Response in Non-small Cell Lung Cancer and Melanoma Patients

Roman Allen, Dr. Diwakar Davar, Drew Hurd, Maddison Nguyen

Pittsburgh Science and Technology Academy, Pittsburgh, PA; Hillman Cancer Center, Pittsburgh, PA

Introduction

The gut microbiome is one of the most important systems within the human body. It provides a key role in human health, taking part in immune system development, synthesis of vitamins, cancer development, and response to immunotherapy.[1] Many factors influence the gut microbiome some of which being location, heredity, and the biggest factor being diet. Artificial sweeteners are one of the most heavily investigated topics in cancer research. Recent studies have shown that these artificial sweeteners, particularly sucralose, adversely affect the gut microbial and overall immune health.[2] The result could be an increase in cancer growth and decline in response to treatment. This project explores four other popular sweeteners; aspartame, aceK, saccharin, and xylitol; found commonly in sugar free food and drink items. Understanding how these sweeteners may be impacting the development and treatment of cancer can lead to improved approaches to preventing, treating, and detecting the disease.

Methods

Dietary data was collected from adv. non-small cell lung cancer (NSCLC) and melanoma patients receiving immunotherapy. Clinical outcome was tracked by overall response to immunotherapy and progression free survival (PFS). A cutpoint was found using the artificial sweetener intake of each cohort to distinguish between low and high intake patients. Based on their overall response and intake, survival curves were created in Stata to visualize how intake of artificial sweeteners may impact immunotherapy response.

Results

A trend was observed of low intake patients responding more effectively to immunotherapy, but p-values and youden index yielded from survival analysis and cutpoint calculation yielded insignificant. Near significance was seen in the NSCLC aceK cohort, giving rational for further exploration.

Discussion

No conclusion can be stated on if artificial sweeteners adversely affect response to immunotherapy. Limitations include sample size; more patient data may provide better accuracy when calculating the cutpoint and creating survival curves; in addition to the DHQ III as response accuracy is not guaranteed from patients. Furthermore, the method of cutpoint calculation can be altered with the current participant pool to calculate a cutpoint that will provide a significant p-value. This would include using different software to find the cutpoint. Other extensions of this research include exploring how artificial sweeteners interact with cell pathways and analyzing other macronutrient information from DHQ III to determine if response is adversely affected by other dietary factors. Focus should be placed on aceK and understanding its mechanics and possible relation to immunotherapy response.

References

[1]Li, X., Liu, Y., Wang, Y., Li, X., Liu, X., Guo, M., Tan, Y., Qin, X., Wang, X., & Jiang, M. (2020). Sucralose Promotes Colitis-Associated Colorectal Cancer Risk in a Murine Model Along With Changes in Microbiota. Frontiers in Oncology, 10, 710. https://doi.org/10.3389/fonc.2020.00710

[2]Amon, P., & Sanderson, I. (2017). What is the microbiome? Archives of Disease in Childhood - Education & Practice Edition, 102(5), 257–260. https://doi.org/10.1136/archdischild-2016-311643

Semi-Automatic Methods for Computing Aortic-Pulmonary Window (AP window) Distance in Patients with Idiopathic Unilateral Vocal-Fold Paralysis (iUVP)

Luke S. An[1], Nathaniel A. Myers[2], Adam M. Forrest[2], Jenny L. Pierce[3], Andrew J. Bierhals[4], Ed Dibella[5], Randal C. Paniello[6], Julia D. Edgar[7], Rebecca Z. German[8], Julie M. Barkmeier-Kraemer[3], Jonathan P. Vande Geest[2]

[1]Upper St. Clair High School, Pittsburgh, PA; [2]Department of Bioengineering, University of Pittsburgh, Pittsburgh, PA; [3]Department of Otolaryngology, University of Utah, Salt Lake City, UT; [4]Mallinckrodt Institute of Radiology, Washington University School of Medicine, St. Louis, MO; [5]Department of Radiology, University of Utah, Salt Lake City, UT; [6]Department of Otolaryngology, Washington University School of Medicine, St. Louis, MO; [7]Communication Disorders Department, Truman State University, Kirksville, MO; [8]Department of Anatomy & Neurobiology, Northeast Ohio Medical University, Rootstown, OH

Abstract: In this project, gated MRI scans of 26 patients, including patients diagnosed with iUVP and healthy age- and sex-matched controls, were analyzed with the goal of finding correlations in the AP window distances of iUVP patients and non-iUVP patients. AP window distance and pulmonary artery (PA) area in the cross-section were analyzed. Additionally, another cross-section of the arteries was taken from a 3-dimensional model and the AP window distance was analyzed.

Introduction: IUVP is one form of unilateral vocal-fold paralysis (UVP) with an unknown cause. UVP occurs when one side of the recurrent laryngeal nerve (RLN) is damaged. It often occurs due to damage in the left RLN[1], which passes between the aortic arch (AA) and PA, through the AP window. Previous work has shown that iUVP patients have hypercompliant aortas[2]. Now, AP window distance is being studied to see if iUVP patients also have shorter AP window distances. The goal of this project is to develop new methods to measure AP window distances.

Methods: In order for the test to remain unbiased, we were blinded to patient identity. We obtained 25 images during the cardiac cycle from the gated MRI scans to capture the vessels under systolic and diastolic conditions. In the first method (LPA cross-section method), which used slices of the left pulmonary artery (LPA) cross-section, the images were analyzed in MATLAB at a manually chosen region of interest (ROI) containing the AP window. Then, an algorithm scaled, binarized, eroded, contoured, and traced boundaries onto the ROI. Ellipses were fit to these boundaries, and the distance between the ellipses and the area of the ellipse that represented the PA were calculated. Algorithm parameters, such as the threshold for the binarization (mask), were manually chosen and tested. Some patients had scans without distinguishable pulmonary arteries or aortic arches, and those scans were ignored. For each patient, the algorithm calculated values for the minimum, maximum, and average distances for the AP window as well as the minimum, maximum, and average area values for the PA area. In the second method (AA cross-section method), a slice with the AA cross-section was extracted from a 3-dimensional model that was created using MATLAB's volshow function. This slice was analyzed using the same process as the LPA cross-section method. Then, coordinates of adjacent points on the boundaries were averaged and connected to form a smoothed border for each artery, and the distance between the arteries was calculated.

Results: The LPA cross-section method generated distances within 30% error (on average) to the manual results. Meanwhile, the PA area was about half the value of the PA area from the manual method (between 25% and 67% smaller). There was relatively high correlation ($R^2 = 0.920$) between the minimum AP window distances of the two methods (Figure 1). The paired t test between this method and the manual had a p value of 0.019, showing significant difference. The AA cross-section method generated distances with less correlation ($R^2 = 0.751$) to the manual. However, the paired t test between this method and the manual had a p value of 0.306, showing no statistical significance.

Discussion: Our goal was to develop viable methods for calculating AP window distance. The LPA cross-section method works as a viable method when computing this distance because of the high correlation in the minimum AP window distances (Figure 1) to the manual method, and this method is more easily repeatable. The typically larger distance (Figure 2) and smaller area in this method compared to the manual method could be attributed to the underestimation of the arteries to prevent them from combining into one object after the contour, something that could be avoided when done manually, as well as other smaller differences stemming from an imperfect mask or erode. Meanwhile, the AA cross-section method introduces a new way of finding consistent measurements across different patients because it is not limited to the acquisition plane, but uses a function to get a plane similar to the other patients'. By improving the accuracy of these methods, we can determine whether AP window distance plays a role in iUVP.

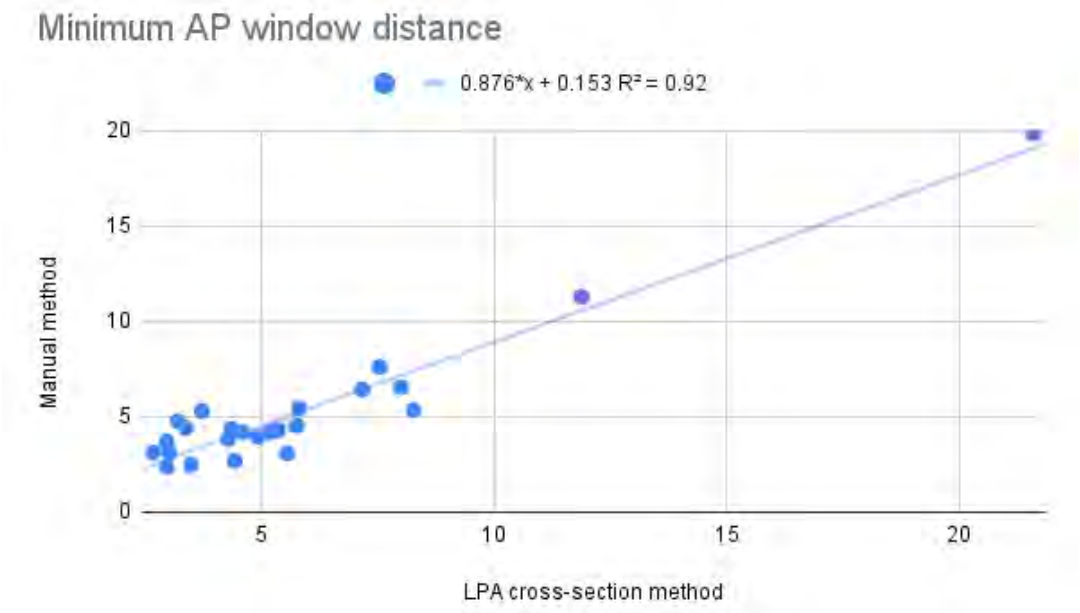

Figure 1. Minimum AP window distance correlation graph.

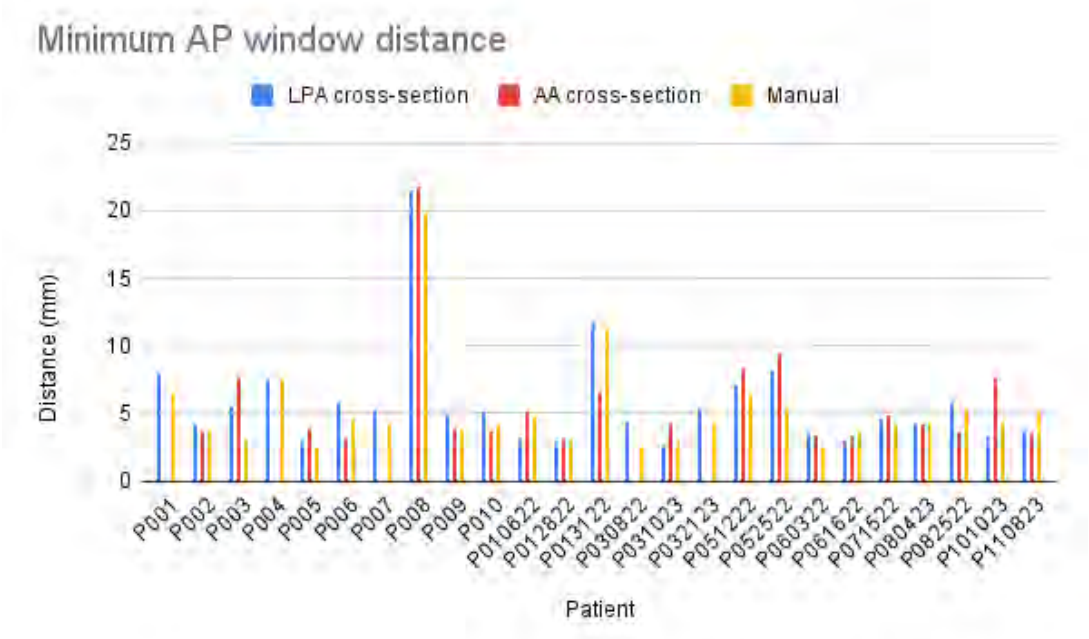

Figure 2. Minimum AP window distances for the semi-automatic and manual methods.

References

1. Williams MJ et. al. A computational study of the role of the aortic arch in idiopathic unilateral vocal-fold paralysis. *J Appl Physiol* 118: 465–474, 2015.
2. Behkam R et. al. Aortic arch compliance and idiopathic unilateral vocal fold paralysis. *J Appl Physiol* 123: 303–309, 2017.

Exploring Hidden Functions of STING Through Proximity Labeling

Scholar: Anna S. Apetrei-Pandrea

High School: Shady Side Academy, Pittsburgh, PA

PI: Jay Xiaojun Tan, Ph.D.

Mentor(s): Bo Lv, Ph.D.

Site: TDX

Background: Innate immunity is the first line of defense against pathogens. The cyclic GMP-AMP synthase (cGAS)-stimulator of interferon genes (STING) pathway is essential in innate immunity, sensing abnormal cytosolic double-stranded DNA from microbes or the host. Upon DNA recognition, cGAS produces cGAMP, which activates STING, triggering STING trafficking, TBK1 signaling, and type-I interferon production. STING is also a proton channel, mediating NLRP3 activation and cell death in a TBK1/interferon-independent manner. We hypothesize that STING's proton channel mediates additional TBK1-independent functions of the DNA-sensing pathway.

Methods: We explored additional STING functions using proximity labeling systems to characterize STING interactome before and after trafficking. We fused STING with biotinylation enzymes: TurboID, miniTurboID, ultraID. DNA fragments were PCR-amplified and cloned into pCDH lentiviral vector, followed by Sanger sequencing. Lentiviruses were packaged in HEK 293T cells by co-transfecting the pCDH vector with packaging vectors pMD2.G and psPAX2. Lentiviruses were used to infect U2OS cells for stable expression of STING fusion proteins, which was verified by western blot. The trafficking of STING fusion proteins was assessed with immunofluorescence. For proximity biotinylation, cells were treated with cGAMP and then biotin. Biotinylation efficiency was examined by fluorescence microscopy.

Results: STING-TurboID, STING-miniTurboID, and STING-ultraID all expressed well. Trafficking analysis revealed that approximately half of STING-TurboID remained in the ER upon cGAMP treatment. STING-miniTurboID and STING-ultraID trafficked similarly to native STING, but STING-ultraID exhibited lower biotinylation efficacy.

Conclusions and Future Directions: MiniTurboID is optimal for proximity labeling to identify effector proteins recruited to STING vesicles. To further minimize the potential artificial impact of miniTurboID on STING trafficking, longer peptide linkers between STING and miniTurboID may be tested. Potential STING effectors could be characterized by mass spectrometry for biotinylated proteins before and after STING activation.

Understanding Late-Life Depression and Cognitive Decline through Brain Functional Networks

Divye Arora-Jain[1], Kai Ye, Ph.d.[2], Liang Zhan, Ph.d[2]
[1]Montour High School, McKees Rocks, PA; [2]Electrical and Computer Engineering, University of Pittsburgh, PA

Abstract

This study aims to investigate the relationship between late-life depression (LLD) and cognitive decline (CD) using fMRI-derived brain functional networks across two datasets. It analyzes 115 subjects with LLD and 274 subjects without LLD to explore brain connectivity and uncover correlations between LLD and CD. Employing machine learning techniques, specifically graph neural networks, the research found that our model could effectively predict cognitive outcomes and accurately classify brain networks with CD and/or LLD.

Introduction

The study of late-life depression (LLD) and its impact on cognitive decline (CD) is crucial for understanding neurological health in aging populations. Utilizing fMRI-derived brain functional networks, this study aims to identify influential brain regions linked to depression and mild cognitive impairment (MCI) while also enhancing our understanding of the underlying neural mechanisms, potentially leading to better diagnostic and therapeutic strategies. By understanding these connections, we hope to uncover key insights into how depression affects cognitive function, ultimately contributing to more time and cost-effective treatments and interventions for those affected by these conditions.

Methods

Using preprocessed brain network data, in the form of adjacency matrices, graph neural networks [1] (GNNs) were employed to run several classification tasks (see Table 1 for specifics) with a focus on hyperparameter tuning to optimize model performance. Hyperparameter adjustments, including epochs, learning rates, layers, and hidden dimensions, were made in Google Colab. The most influential brain regions were then selected from the trial that gave the highest accuracy and lowest loss. Cross Entropy Loss (i.e. $H(p,q) = -\sum_{x\in X}\ p(x)\log\ q(x)$) was used to update the model's weights, thus increasing model performance. The dataset sizes for each classification task varied due to differing specifications, resulting in the following data sizes from the Alzheimer's Disease Neuroimaging Initiative Depression (ADNID) and the Alzheimer's Disease Neuroimaging Initiative (ADNI) [2]: (a) 37, 78; (b) 37, 120; (c) 120, 154; (d) 78, 154. The specifications for each classification is outlined in Table 1. Main outcome measurements included classification accuracy, loss metrics, and significant brain regions linked to depression and MCI.

Results

The classification tasks and model performance metrics are outlined in Table 1, which includes accuracy, loss, and influential brain regions. These results demonstrate that the highest accuracy and lowest loss occurred for the MCI w/D. vs. MCI w/o D. classification showing the promise this model holds for classifying MCI with and without the presence of a diagnostic marker. The saliency maps presented in Figure 1 highlights the influential brain regions for each classification task, revealing specific areas of the brain that are consistently linked to depression and cognitive impairment. Some of the most influential ROIs for classification are the Left Pallidum, Entorhinal Cortex, and the Cuneus.

Discussion

This study demonstrates the potential of graph neural networks (GNNs) to effectively classify normal cognition (NC) and mild cognitive impairment (MCI) by analyzing fMRI-derived brain functional networks. The saliency maps highlighted key brain regions, such as the Entorhinal Cortex and Cuneus, are consistent with known areas involved in mood regulation and cognitive functions, showing the roles they play in depression-related cognitive decline. While our findings hold valuable insight, because of the limited dataset size, the results may not be representative of the broader population. Thus, future research should focus on larger datasets to validate these results and further explore the interaction between depression and cognitive impairment.

Table 1: Model performance comparison and names of most influential brain regions

Classification	Accuracy	Cross Entropy Loss	Influential Brain Regions
(a) MCI w/ D. vs. NC w/ D.	.6957	.6158	22 - ctx-lh-entorhinal 23 - ctx-lh-fusiform 21 - ctx-lh-cuneus 16 - Right-Amygdala 18 - ctx-lh-bankssts
(b) MCI w/ D. vs. MCI w/o D.	.9375	.1584	22 - ctx-lh-entorhinal 5 - Left-Pallidum 9 - Left-Accumbens-area 2 - Left-Thalamus 8 - Left-Amygdala
(c) MCI w/o D. vs. NC w/o D.	.6545	.6753	6 - Brain-Stem 5 - Left-Pallidum 46 - ctx-lh-superiortemporal 35 - ctx-lh-parsorbitalis 25 - ctx-lh-inferiortemporal
(d) NC w/ D. vs. NC w/o D.	.9362	.1764	43 - ctx-lh-rostralmiddlefrontal 31 - ctx-lh-middletemporal 9 - Left-Accumbens-area 21 - ctx-lh-cuneus 23 - ctx-lh-fusiform

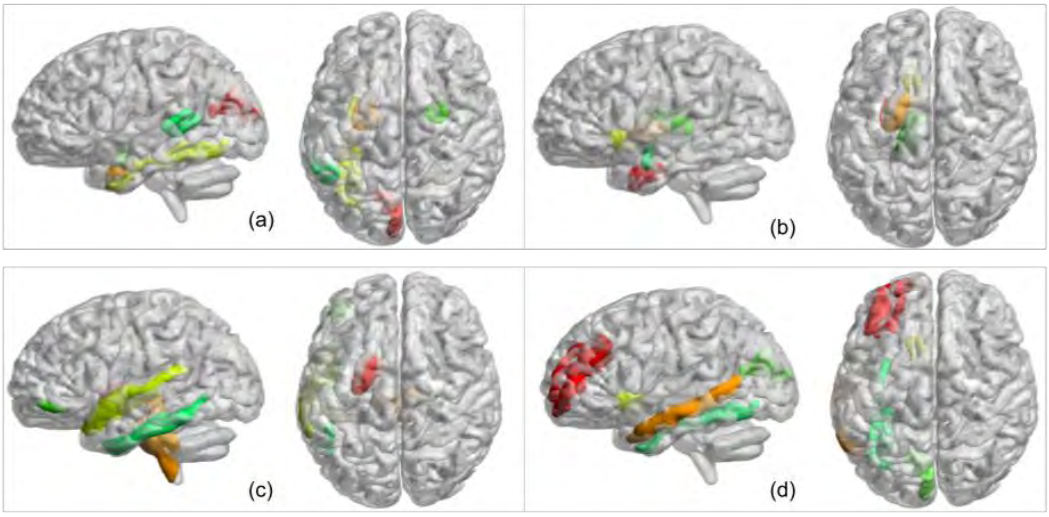

Figure 1: Visualization of top five most influential brain regions

References

1. Kipf, T. N., & Welling, M. (2016). Semi-supervised classification with graph convolutional networks. *arXiv preprint arXiv:1609.02907*.

2. Misra, C., Fan, Y., & Davatzikos, C. (2009). Baseline and longitudinal patterns of brain atrophy in MCI patients, and their use in prediction of short-term conversion to AD: results from ADNI. *Neuroimage*, *44*(4), 1415-1422.

Computational Prediction of Nonabine as a Possible CB_2 Agonist

Rhea Arya, Dr. Roni Lahr
Loveless Academic Magnet Program High School, Montgomery, AL; University of Pittsburgh Hillman Cancer Center Academy, Pittsburgh, PA

Abstract *Targeting the endocannabinoid system, particularly cannabinoid receptor subtype 2 (CB_2), offers promising avenues for cancer drug discovery. Nonabine is a synthetic THC analog discovered in the 1970s and is a potential agonist for CB_2. We compared nonabine to known CB_2 agonists WIN55212 and CP55940 using computational docking. We found shared residues between these known agonists and nonabine, indicating a shared mechanism and a starting point for new CB_2-directed therapeutics.*

Introduction The endocannabinoid system consists of cannabinoid receptor subtypes 1 and 2. CB_1 is localized in the central nervous system (CNS), which can cause psychotropic effects. In contrast, CB_2 is localized to the peripheral immune system; thus, targeting CB_2 helps mitigate these psychotropic effects and aids in apoptosis.
G protein-coupled receptors (GPCRs) help regulate an incredible range of bodily functions, from sensation to growth to hormone responses. GPCRs like these cannabinoid receptors are a major drug target, and CB_2 has been shown to have anti-inflammatory and anti-anxiety properties alongside opportunities for cancer and immune disease treatment, all while avoiding the side effects associated with CB_1.
After a search of THC analogs, we discovered nonabine but had very little information on it, thus making it a candidate for exploration. Nonabine, a THC analog discovered in the 1970s, has been found to have antiemetic effects adjacent to chemotherapeutic drugs. However, there is currently no evidence that nonabine acts through CB_2. This project aims to provide computational evidence that nonabine is a binding partner and possible agonist of CB_2.

Methods We utilized computational docking methods to predict possible CB_2 binding sites and ligand conformations. We employed the docking software, SYBYL, to predict the binding orientations of a receptor and a ligand. Once we gathered information from SYBYL, we used the software PyMOL to create digital models and representations of the ligand-bound CB_2. We compared the ligand in question, nonabine, to known binding ligands WIN55212 and CP55940, known agonists of the CB_2 receptor, to determine if the nonabine binding pocket predicted by experimental docking represents a plausible binding site. We then used the computational program MCCS to determine important residue interactions on CB_2 between the experimental ligand and known CB_2 ligands CP55490 and WIN55212.

Results SYBYL predicted nonabine docking in the main orthosteric binding pocket of CB_2, the same pocket as CP55940 and WIN55212. Nonabine's binding pose resembles that of CP55940 and WIN55212, as they occupy the same position and orientation in the agonist binding pocket. Additionally, MCCS predicted that the CB_2 residues which contribute to binding were similar across CP55940 and nonabine, including the hydrogen bonding SER285 and the hydrophobic PHE94 (Table 1).

Discussion Through computational structural analyses, we found nonabine to share many important properties with known CB_2 ligands with respect to binding pose and key residues on CB_2 (Figure 1). Of note, residue PHE94 appeared in a disordered loop of CB_2 to act as a "lid" holding the ligand in place in the pocket, perhaps stabilizing the agonist binding pose. This provides strong support that nonabine binds to CB_2. Nonabine may make a strong starting point for designing a CB_2-specific candidate. Future studies would include testing the specificity of nonabine *in vitro* through a radio-ligand binding assay and performing site-directed mutagenesis studies to determine the importance of the various residues and contribute to a potential drug repurposing project.

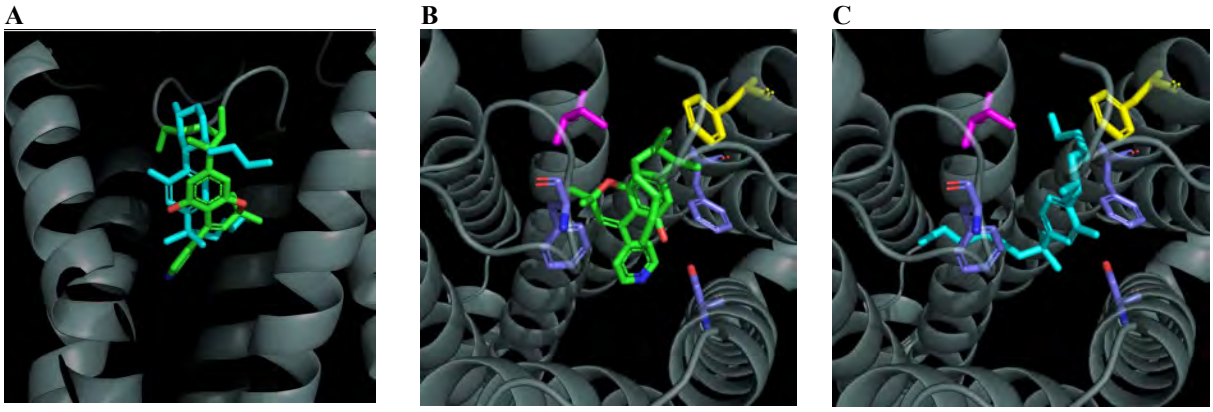

Figure 1. PyMOL-generated images CB2, relevant ligands, and residues (A) CP55490 and nonabine overlaid in the orthostatic binding pocket of CB_2 (B) nonabine interaction with residues, including ILE110 and PHE94 (C) CP55490 interaction with residues, including PHE94, but with a noticeable lack of interaction with ILE110

CP55490 in cyan, nonabine in green, residues in blue, ILE110 in pink, and PHE94 in yellow

Residue	Type of Interaction	Conservation	Free Energy
PHE94	Hydrophobic	Yes	-0.6479
SER285	Hydrogen Bonding	Yes	-0.5629
PHE183	Hydrophobic	Yes	-0.5078
PHE87	Hydrophobic	Yes	-0.3998
ILE110	Hydrophobic	No	-0.3461

Table 1. List of major CB_2 residues interacting with nonabine with corresponding conservation between CP55490 and nonabine.

References

1. Xing et al., 2020, Cell 180, 645–654 February 20, 2020 [a] 2020 Elsevier Inc. https://doi.org/10.1016/j.cell.2020.01.007
2. Sallan SE, Zinberg NE, Frei E 3rd. Antiemetic effect of delta-9-tetrahydrocannabinol in patients receiving cancer chemotherapy. N Engl J Med. 1975 Oct 16;293(16):795-7. doi: 10.1056/NEJM197510162931603. PMID: 1099449.
3. Marzo, Vincenzo Di, Maurizio Bifulco, and Luciano De Petrocellis. "The endocannabinoid system and its therapeutic exploitation." Nature reviews Drug discovery 3.9 (2004): 771-784.
4. The PyMOL Molecular Graphics System, Version 3.0 Schrödinger, LLC.
5. SYBYL;Tripos International: St. Louis, MO, 2008.
6. Chen M, Feng Z, Wang S, Lin W, Xie XQ. MCCS, a novel characterization method for protein-ligand complex. Brief Bioinform. 2021 Jul 20;22(4):bbaa239. doi: 10.1093/bib/bbaa239. PMID: 33051641; PMCID: PMC8293830.

Investigating Mesothelial Cell Mesenchymal Reprogramming Using Immunostaining

Scholar: Ruth Ayers
High School: Pittsburgh Science and Technology Academy, Pittsburgh, PA
PI of Lab: Ioannis Zervantonakis
Mentors: Ioannis Zervantonakis, Matt Laird
Site: Women's Cancer Research Center

Introduction: The majority of patients with ovarian cancer are diagnosed with metastatic disease because of the non-specific symptoms, and lack of effective early screening approaches. This late-diagnosis causes limited treatment options and results in higher mortality rates. Mesothelial cells line the abdominal cavity where a metastatic tumor implants and subsequently proliferate; cancer cells sticking to mesothelial cells is a critical early step in metastatic progression. Thus, mesothelial-cancer interactions facilitate cancer cells spreading around the abdomen and not just stay in the ovaries, where the cancer is easier to treat using surgery. When mesothelial-to-mesenchymal transition occurs, mesothelial cells gain invasive and mobility properties, helping the cancer cells spread. Immunostaining can be used to examine specific proteins in mesothelial cells, allowing for visualization of changes in protein expression, new proteins appearing, and localization caused by the interactions with cancer cells. Comparing mesothelial cells from tumor-free mice to mesothelial cells from mice with metastatic ovarian cancer can help identify proteins that are altered when mesothelial cells are interacting with tumor cells.

Methods: Tissue samples were collected from two mice that had a metastatic ovarian cancer tumor derived from the human ovarian cancer cell line, OVCAR8 and two tumor-free (control) mice. We immunostained each tissue sample with a primary pSMAD1/ pSMAD5 antibody (detected with a Cy5 secondary) as a marker for a mesenchymal state and a pan-Cytokeratin antibody (detected with a GFP secondary). For analysis, we took fluorescent photographs of four sections from each sample that contained mesothelial cells (lining peritoneal organs: e.g. pancreas). Within each section, we circled five cells for each antibody (pSMAD1/pSMAD5, and panCK) and calculated the average gray value to measure the intensity of the fluorescent signal. The average gray value is determined by summing the gray values of all the pixels in the selected area and dividing by the number of pixels. The average intensity values for each antibody type were then compared between the control and cancerous samples to assess differences in fluorescence intensity.

Results:

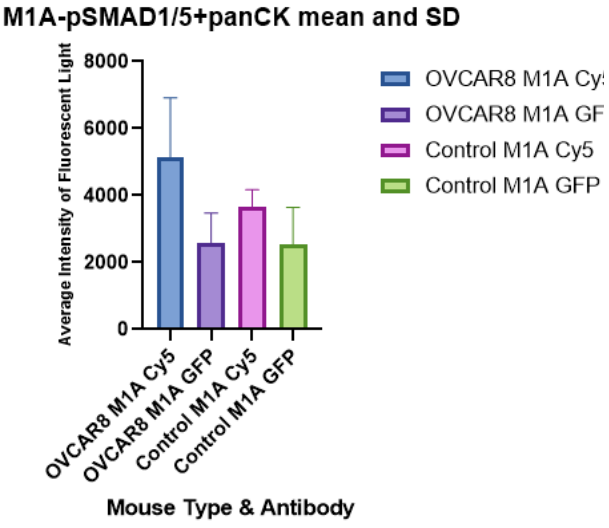

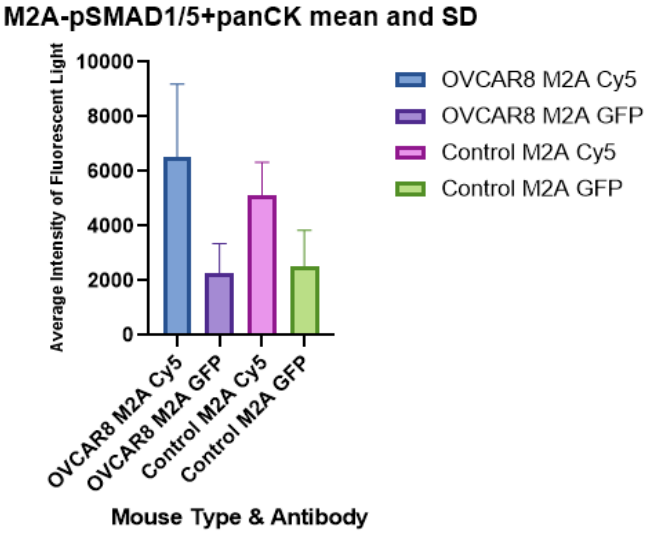

Conclusion: There was increased fluorescence intensity of pSMAD1/5 in all tissue samples with tumor cells from the cell line OVCAR8 in both mouse 1 and 2 suggesting that these markers are increased in the presence of metastatic ovarian cancer from the OVCAR8 cell line.This indicates that cancer cell interactions with mesothelial cells alter the expression of the mesenchymal markers, pSMAD1/5 in mesothelial cells. There was a slight increased fluorescent intensity of panCK in the tumor tissue in mouse 1 and in mouse 2 the tumor tissue had slightly less fluorescent intensity of panCK than the tumor free tissue. This suggests variability in the expression of the mesenchymal marker panCK in the presence of metastatic ovarian cancer.

Detecting osteosarcoma gene expression levels in 2D & 3D cell cultures

Scholar: Zacharias Barron

High School: Woodland Hills High School

Lab: Kurt Weiss, MD**;** Ines Lohse, PhD

Mentors: Tanya Heim, MS; Amanda Locker, MS

Site: Cancer Biology

Background: Osteosarcoma (OS) is the most common primary bone tumor in children and adolescents, with current standard care involving neoadjuvant chemotherapy and surgery, yielding a 5-year survival rate of at least 70% [1-3]. However, for patients with lung metastasis, which occurs in 90% of metastasized cases, there is no established standard care, and the 5-year survival rate remains below 30% [3]. *In vitro* experiments have been useful to explore new treatment strategies for OS LM, however use of monolayer (2D) cultures have their limitations. We grew 3D OS cell models and measured the gene expression of *AR* and *ALDH1A1* compared to their 2D counterparts [4-5].

Methods: The OS cell lines, SaOS-2 and LM2, was cultured in OS media. Next, cells were plated at $3x10^4$ cells per well in a 96-well, ultra-low attachment (ULA), U-bottom plate or in a T75 flask at $1x10^6$. Images were taken of the spheroids at days 2, 4, and 7 and of the 2D cells for up to 3 days. The OS cell lines were collected from the T75 flask after 72 hours and from the U-bottom plate at 7 days. RNA was extracted from LM2 per manufacturer's instructions (Qiagen) and 370 ng was used in a quantitative PCR.

Results: 2D and 3D cells were successfully grown**.** SaOS-2 spheroids expressed higher levels of both *AR* and *ALDH1A1* compared to LM2 spheroids. The expression of both genes was elevated in SaOS-2 3D models compared to their respective 2D models. Conversely, the expression of both genes was reduced in LM2 3D models compared to their respective 2D culture. The expression of both genes was significantly higher in SaOS-2 3D models than in LM2 3D models. ALDH1A1 was significantly higher in both 3D cell types compared to AR.

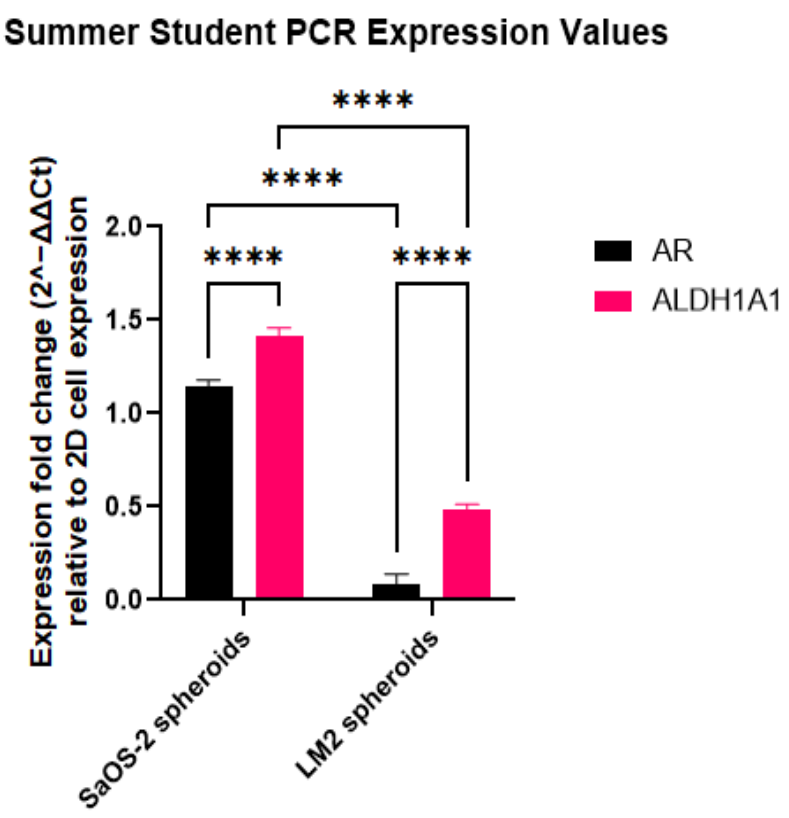

References:

1. Yu, Shibing et al., Lung cells support osteosarcoma cell migration and survival. BMC Cancer, 17:78 (2017).
2. Belayneh, Rebekah et al., Update on Osteosarcoma. Current Oncology Reports, 23:71 (2021).
3. Heim, E. Tanya et al., RNA-sequencing predicts a role of androgen receptor and aldehyde dehydrogenase 1A1 in osteosarcoma lung metastases. Oncogene, 43:1007-1018 (2024).
4. Liu, Xin et al, Epithelial cells in 2D and 3D cultures Exhibit Large Differences Higher-order Genomic Interactions. Genomics Proteomics Bioinformatics, 201:101-109 (2022)
5. Wolff, Anne et al., A Comparative Study on the Adipogenic Differentiation Mesenchymal Stem/Stromal Cells 2D and 3D Culture. Cells, 11(8):1313 (2022).

Scholar: Mae Cano

High School: Mount Lebanon High School, Mount Lebanon Pennsylvania

Lab: Partha Roy, PhD

Mentor: Pooja Chawla, MS

Site: Women's Cancer Research Center

MRTF-dependent Paracrine Regulation of Osteoclast Differentiation

Background: Triple negative breast cancer (TNBC) is the most aggressive breast cancer. It frequently metastasizes; I focused on bone metastasis. MRTF is a transcription factor involved in cell migration, development and metabolism. Previous studies have shown decreasing MRTF in TNBC cells decreases osteoclast differentiation, decreasing metastasis. Also, depletion of MRTF depletes secreted factor G-CSF. Secreted factor CTGF is previously tested: with MRTF knockdown in breast cancer conditioned media, CTGF partially rescues the repression of osteoclast differentiation. G-CSF must be tested to determine if it further rescues the differentiation defect. We also investigate MRTF's effect on differentiation activation. I hypothesize G-CSF addition will rescue the repression of osteoclast differentiation upon MRTF-depletion. Breast cancer conditioned media will promote early activation of differentiation; MRTF-depletion will reduce early activation.

Methods: Western blots measured G-CSF, CTGF, and MRTF to determine rescue assays treating monocytes with MDA-231/D2A1 conditioned media with/without MRTF knockdown. I also performed RNA extraction from osteoclast cells treated with D2A1 conditioned media at a 24 hour time point for a qPCR for Acp5 (the gene encoding early ocl differentiation activation marker TRAP). We performed differentiation assays on a bone-mimicking plate to quantify bone breakdown.

Results: The bone-mimicking plate showed upon depletion of MRTF, there is less bone breakdown. In one differentiation assay, cells were supplied with suboptimal levels of RANKL; there were few developing osteoclasts, but they presented purple, meaning TRAP was turned on. More were in the control conditioned media group compared to knockdown, suggesting the presence of MRTF increases differentiation. Recombinant G-CSF did not show on western blot gel, preventing rescue assays.

Conclusions: MRTF has great impact on TNBC bone metastasis. Decreasing its expression will also decrease osteoclast differentiation and metastasis in the bone. G-CSF seems to work in tandem with CTGF to differentiate osteoclasts, although more research must be done to confirm.

DNA Damage Detection in Senescent Cells In Cardiac Tissue

Scholar: Isabella Cheatham

High School: Fox Chapel Area High School, Pittsburgh, PA

Lab: Aditi Gurkar, PhD

Mentor: Alberto Bertozzi

Site: Technology Drive X

Background: Cellular senescence is a state of permanent cell cycle arrest in which the cell stops multiplying but also does not proliferate. Cellular senescence increases with age and links to diseases associated with oxidative stress. When DNA damage occurs on chromosomes, telomeres can become shortened and dysfunctional. There is growth in cellular senescence when telomeres are dysfunctional so if cardiac cells have DNA damage on telomeres they are at higher risk. By producing oxidative lesion 8-oxoguanine (8oxoG) at telomeres there is an acceleration of cells becoming senescent. DNA damage in telomeres can be marked by a green fluorescent protein (GFP) which produces fluorescence under a microscope anywhere DNA damage occurs in cardiac cells.

Methods: FAP-Mcer-TRF1-H2B expressing retina cell lines were treated with 100 nm of MG2I dye. Once incubated for 15 minutes MG2I dye attached to FAP. The cells were irrigated under a 600 nm red light to produce highly reactive oxygen (8oxoG). The 8oxoG is produced next to DNA and binds to guanine bases creating DNA damage. DOGG1-GFP recognises the DNA damage, binds, and shows fluorescence when observed under the microscope.

Results: In the first attempt, DOGG1-GFP staining was not specific to the nucleus but there was a stronger fluorescent signal in the cells induced with DNA damage than the control with no DNA damage. In the second attempt, both the DNA damage induced cells and the control showed the same intensity of GFP but the damage was primarily observed in the nucleus.

Conclusion: Our study showed that DNA damage is produced by 8oxoG but not specific to the telomeres. DOGG1-GFP marks for DNA damage induced by 8oxoG. DNA damage was not specific to the nucleus and was not at a higher intensity in the induced over control cells which means the experiment should be tested again.

Title: Identifying whether epigenetic inhibitors can promote gene expression in HCC cells

Scholar: Eric Chen

High School/College/City/State: Shady Side Academy, Pittsburgh, PA

PI of group/lab: Evan Delgado, Ph.D.

Mentor(s): Evan Delgado, Ph.D.

Site: Cancer Biology

Background: Hepatocellular carcinoma (HCC) is the most common type of primary liver cancer. Currently, liver transplantation is the most effective treatment, but a lack of healthy donor livers impacts the use of this method. New approaches to treating HCC are crucial because HCC is a heterogeneous disease, causing the efficacy of immunotherapy to only demonstrate a response in approximately 30% of patients. Some groups have turned to utilizing a combination of histone deacetylase inhibition (HDACi) and DNA methyltransferase inhibition (DNMTi) to promote the expression of genes that assist immune cell recruitment and function. This study aimed to investigate the effective dose and specific conditions of combining DNMTi and HDACi in HCC cell lines to potentially promote the expression of genes that assist in immune cell responses.

Methods: The murine HCC cell line Hepa 1-6 was treated with varying doses of Belinostat while 5-aza concentrations remained constant. Cells were treated for 24, 48, and 72 hours. Quantitative PCR was used to assess gene expressions of chemokines (CCL5, CXCL1, CXCL2). Luminescence-based assays were used to measure changes to cell viability, and fluorescence-based assays were used to measure HDAC activity.

Results: Hepa 1-6 cells treated with 5-aza and Belinostat showed a significant decrease in CCL5, CXCL1, and CXCL2 gene expression at high concentrations of Belinostat in a dose-dependent manner. Cell viability was also impacted in a dose-dependent and time-dependent manner with respect to altering Belinostat. Confirmation of HDAC inhibition is underway, as is assessment of cells treated with lower concentrations of HDACi.

Conclusion: Our study determined that at high doses of Belinostat, HDACi is detrimental to the expression of immune-related genes in HCC cell lines. Further studies will be conducted to confirm whether Belinostat effectively alters the expression of genes in both normal and cancerous human hepatocytes.

Intracellular Lactate and T-Cell Function

Scholar: Ivan Chen

High School: Seneca Valley High School, Seneca Valley Pennsylvania

Lab: Greg Delgoffe, PhD

Mentor: Bingxian Xie

Site: Immunology and Cancer Immunotherapy

Background: T-cell therapy is a form of immunotherapy that enhances a patient's T-cells so that they may detect and kill tumor cells more directly and efficiently. For instance, immunotherapies like CAR-T therapy, TCR therapy, and TIL therapy are all effective against liquid cancers such as lymphoma and leukemia. However, they are less effective against solid tumors such as lung cancer and liver cancer. The main reason for this is due to the tumor microenvironment. The tumor microenvironment is immunosuppressive due to many factors, with one being the large amount of lactic acid produced due to the Warburg effect, which states that tumor cells will always prefer aerobic glycolysis over other processes like the citric acid cycle, even in an environment with an abundance of oxygen. This project focuses on measuring the intracellular level of lactate inside T-cells to determine if they are a factor in reducing T-cell activation.

Methods: Xcelligence systems were used to detect tumor killing efficiency of T-cells in different lactate concentrations. iLACCO, a lactate biosensor, was overexpressed in Jurkat cell line via retrovirus infection as a way to detect intracellular lactate concentrations in T-cells. Flow cytometry was used to confirm that the iLACCO gene could detect different concentrations of lactate, and then CD69, a T-cell activation marker, was stained on the Jurkat cells to be analyzed through flow cytometry again to determine T-cell activation in varying lactate concentrations.

Results: We found that higher extracellular lactate inhibits T cell killing of tumor cells. iLACCO was able to help in accurately detecting different concentrations of intracellular lactate. Through CD69, we detected that higher lactate concentrations often resulted in less CD69 activation, which means less T-cell activation.

Conclusion: Our project shows that intracellular lactate levels can impact T-cell activation.

Development of Prototype for Optomotor Reflex in Mice

Justin Chen, Kevin Chen, Lingyun Wang, Dr. Shaohua Pi,

University of Pittsburgh Department of Ophthalmology, Pittsburgh, PA

Abstract

We developed a prototype similar to StriaTech's OptoDrum, referred to as 'optodrum', to accurately assess the optomotor reflex in mice. Our research provides a standardized method to measure visual function in mice, which is crucial for consistent and reliable assessment across studies. Specifically, our optodrum can test different factors that may affect the frequency or the duration of the reflex with flexible parameters to control the pattern being displayed.

Introduction

The optomotor reflex (OMR) is the reflexive head movement an animal makes when tracking a moving pattern. However, this reflex is completely gone in mice with the P23H mutation due to retina degeneration. To test the strength of the reflex, our optodrum can record factors such as the duration and frequency that the behavior occurs, which can provide information about the effects that certain drugs or mutations have on the mice's vision.

Methods

Four monitors were placed in a square to make up the walls of the chamber (Figure 1). To display the pattern, a program was created in the Processing software. Parameters such as pattern speed, width, and intensity were included to allow for different patterns. Additionally, black and white 3D printed stands were used to sit the animals (75mm for mice, 150mm for rats). A camera was also mounted on the ceiling to record the response of the animals.

Results

Wild-type (N=4) and P23H mice (N=2) were used to test the device. For each mouse, various parameters including the pattern width (Low: 169 px, Medium: 349 px, High: 554 px), speed (Low: 1.6 RPM, Medium: 3.3 RPM, High: 5.0 RPM), brightness (Low: 0.5, Medium: 0.7, High: 1.0), and direction (Clockwise and Counterclockwise) of the stimulus pattern were changed. The response was recorded for three minutes at 30 FPS, for a total of 5,400 images for each individual pattern. The wild-type mice showed significant amounts of OMR behavior. On the other hand, the P23H mice did not show any instances of OMR behavior.

Discussion

The optodrum successfully passed the test trial with the blind P23H mice and the wildtype mice. This means we can use the prototype for further research. However, we currently lack quantitative measurements of the reflex and are developing software to do so.

Figure 1. This shows the inside and outside of the optodrum.

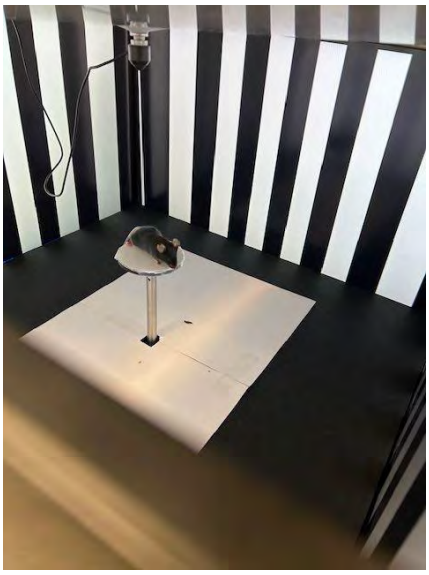

Development of Deep Learning Object Detection Algorithm for Optomotor Reflex Device in Mice

Kevin Chen, Justin Chen, Dr. Shaohua Pi
University of Pittsburgh Department of Ophthalmology, Pittsburgh, PA

Abstract

Ocular functions such as visual acuity and contrast sensitivity are key for assessing vision quality, especially in mice models for their popularity in clinical trials. This project presents a tool that accurately records a behavior encapsulating both of these functions: the optomotor response (OMR), minute head movements stimulated in order to stabilize vision. This project also uses a deep learning neural network, the Single Shot MultiBox Detector (SSD), for its forte in object classification and localization to detect the mice's body parts to aid us in tracking OMR.

Introduction

When an organism sees a moving pattern, it instinctively moves its eyes and head to maintain focus. This head movement is the optomotor reflex, and because it is only triggered from visual stimuli, its presence of this response can tell researchers just how acute and sensitive the testee's vision is. With our project, we are currently training and testing an SSD model, an extension of a convolutional neural network (CNN) that is capable of recognizing the location and classification of objects within an image (Figure 1). It achieves this task by first using a backbone CNN (Resnet50 in our project) to extract feature maps of varying size. Each feature map has a specialized confidence and localization predictor both consisting of multiple convolutional layers that predict potential object locations and classifications within that feature map. These outputs are then combined and Non-Maximum-Suppression (NMS) is applied to reduce multiple bounding boxes that are recognizing the same object.

Methods

Mice were placed on a raised platform inside a chamber with four monitors displaying stripes of varying width, speed, and contrast to trigger OMR, which was captured by a camera. We manually labeled the mouse's nose, head, lower body, ear (moving parts) and tail (baseline reference) using the Labelme program on 1000 recorded images for training and validation of the SSD model to create a total of 5000 annotations in a json format. We compiled these annotations, rescaled the data to be in a 300 x 300 pixel size (input size for SSD), and converted the annotations to xml files (input type for SSD). We then started training the model, but because it had difficulty recognizing some parts, we eliminated the head, nose, and lower body and just had the classes include the ears and tail.

Results

OMR was visually observed during experimentation, but significant difficulties arose in training the model to recognize the mice's features (Figure 2). But, after numerous modifications in the training data and retraining, the model was able to detect the ear positions with a 99% accuracy and it could detect the tail with a 95% accuracy (Figure 3).

Discussion

We conclude initial failures stemmed from poor training data, as there were no defining features in the nose, lower body, or head because the mice's pigments were almost pure black. The results of the last training support this conclusion, as after we trained the model to identify the bright-pink colored tail and ears, the performance drastically increased as both labels provided an easy pattern for the model to learn. With this, we have goals to develop an algorithm to take the SSD predictions and computationally calculate where OMR has occurred in mice when given a set of frames.

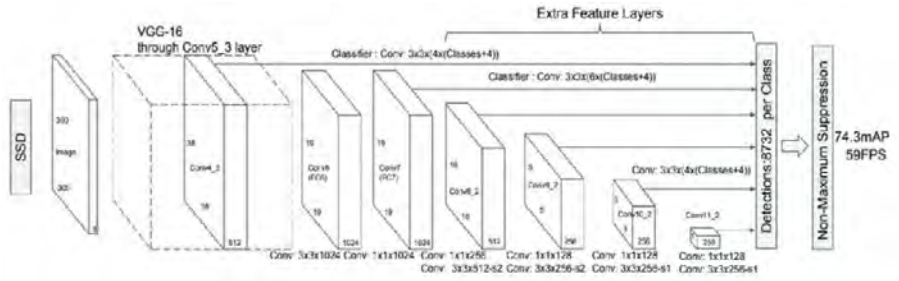

Figure 1: Diagram of SSD architecture

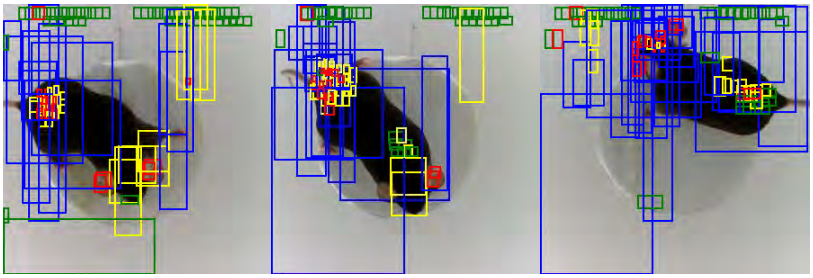

Figure 2: Sampled images of failed object detection

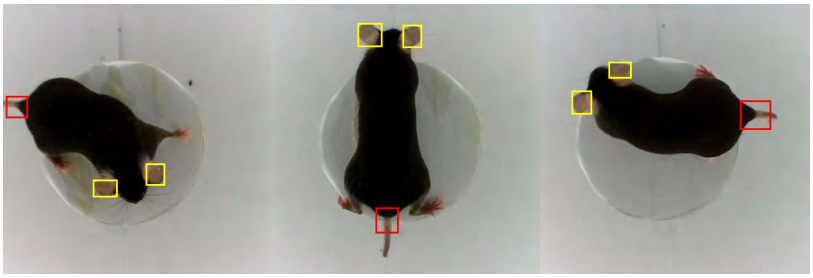

Figure 3: Sampled images of successful object detection

References

1. Yuko Sugita , Haruka Yamamoto , Yamato Maeda and Takahisa Furukawa. Influence of Aging on the Retina and Visual Motion Processing for Optokinetic Responses in Mice. December 2020, Osaka University
2. Wei Liu, Dragomir Anguelov, Dumitru Erhan, Christian Szegedy, Scott Reed, Cheng-Yang Fu, Alexander C. Berg. SSD: Single Shot MultiBox Detector. December 2016, Cornell University
3. Cong Shi, Xuedong Yuan, Karen Chang, Kin-Sang Cho, Xinmin Simon Xie, Dong Feng Chen, Gang Luo. Optimization of Optomotor Response-based Visual Function Assessment in Mice. June 2018, Scientific reports

Title: Role of CD10 stromal expression in regulating CD4 T cells within the OCCC tumor microenvironment

Scholar: Anvi Chopra

High School/College/City/State: North Allegheny Senior High School, Wexford, PA

Lab: Coffman Lab

Mentor(s): Huda Atiya, Ph.D. and Lan Coffman, M.D., Ph.D.

Site: WCRC

Background: Ovarian clear cell carcinoma (OCCC) is a rare, aggressive, chemo-resistance ovarian cancer subtype. OCCC is different from other ovarian cancer subtypes due to its origin from endometriosis which is a chronic inflammatory disease characterized by the growth of endometrial tissue outside of the uterus cavity. Our lab found a subset of endometriosis-associated stroma (enMSCs), marked by low CD10 expression, supports OCCC growth and metastasis. However, how this low CD10 stroma affects the OCCC immune microenvironment is still unknown. Recently, our lab found that OCCC tumors have significantly lower CD4+ T helper cells compared to other ovarian cancer subtypes. CD4 T cells is known to control the activation of other immune cells. This leads us to the questions: (1) What is the relationship between low CD10 stromal expression and CD4 T cells? And (2) how low CD10 enMSC affects CD4 T cells?

Methods: **First:** Using immunohistochemistry (IHC), patient OCCC tissue sections were stained with anti-CD10 and anti-CD4 antibodies. After imaging using a light microscope, the images were analyzed for CD10 and CD4 positive cell number using Q path. **Second:** Patients-derived enMSCs lines were processed for RNA extraction followed by cDNA synthesis and then qRT-PCR. CD10 and MGP genes expression were calculated as fold change after normalization and calculate the delta-delta Cq value.

Results: Our IHC data showed that low CD10 stromal expression is associated with low CD4 T cells. In contrast, the presence of CD10 stromal expression is correlated with more CD4 T cells. To determine how low CD10 stromal expression reduces CD4 T cells, our qRT-PCR showed a negative connection between CD10 and MGP expression (MGP has a role in effecting CD4 T cells). Our data showed that as CD10 expression increased, MGP expression tended to decrease.

Conclusion: Low CD10 enMSCs-derived MGP impact CD4 T cells within OCCC tumors.

Title: 9-mer and 15-mer peptide (*Galt*) increases the IFN type I signaling in T cells.

Scholar: Nora Coen-Pirani

High School/College/City/State: Winchester Thurston School, Pittsburgh, PA

PI of group/lab: Hassane Zarour, MD, PhD

Mentor(s): (name or names of who directly guided your research. If it was the PI, place hers

or his name here as well, even if already mentioned): Florent Amatore, MD, PhD & Rodrigo Das Nevas, MD, PhD

Site: Immunology and Cancer Immunotherapy

Background: Neoadjuvant intratumoral TLR9 agonists (CMP-001) and anti-PD-1 provide durable clinical responses in patients with high-risk resectable melanoma. Response is associated with broad immune activation, especially with increased activity of $CD8^+$ cells in the tumor microenvironment and in the blood. Therefore, treatment efficacy may be driven by the immune response against tumor neoantigens. Neoantigens are peptides derived from mutations presented by HLAs and targeted by antitumor $CD8^+$ cells. Testing peptides of different lengths to determine if one can stimulate more immune cells, such as CD4 and CD8 cells, could enhance T-cell-mediated tumor killing.

Objective: To determine if a long peptide including the class I and predicted class II sequences can stimulate both CD4 and CD8 cells.

Methods: HLA-A* 0201 healthy donor buffy coat ordered and processed. Peripheral Blood Mononuclear Cells (PBMC) are isolated during processing. Proceed with HLA-A2 PE and isotype control IgG PE staining to identify HLA-A2 positive cells by flow cytometry. Use HLA-A2 positive PBMCs and extract CD8 cells with CD8 selection beads (Miltenyi). Perform a co-culture for CD4 and CD8 cells with the 2 high-affinity peptides and irradiated PBMCs in the presence of IL-6 + IL-12 for 1 week. Repeat with IL-2 and IL-7 for weeks two and three. To prepare for ELISPOT assay, add in 15-mer peptide with CD4 and both 9-mer and 15-mer peptides with CD3. Perform IFN-g ELISPOT assay to measure how often IFN-g and IL-5 are secreted by CD4 and CD8 cells.

Results: Unlike the “short” 9-mer peptide which stimulated just CD8 cells, the “long” 15-mer peptide was able to stimulate both CD4 and CD8 T-cells.

Conclusion: The “long”, 15-mer peptides are good candidates for further evaluation of their immunogenicity and characterization of the CD4 and CD8 cells that they stimulate. Other peptides of different lengths will be screened and the best ones proposed for further assessment.

Adrenalectomy for Mild Autonomous Cortisol Secretion: Can We Predict Patients at Risk for Postoperative Adrenal Insufficiency?

Scholar: Mikaela Dassanaike-Perera

High School: North Allegheny High School, Pittsburgh, PA

PI of group/lab: Dr. Alaa Sada, MD, MS

Mentor: Dr. Alaa Sada, MD, MS

Site: Surgery

Background: Mild autonomous cortisol secretion (MACS), defined by an AM cortisol ≥1.8 µg/dL following a 1 mg overnight dexamethasone suppression test (DST), is prevalent in patients with adrenal incidentalomas. Adrenalectomy is generally recommended for MACS, which can be associated with postoperative adrenal insufficiency (AI). Currently, patients undergo postoperative day 1 (POD1) AM cortisol testing to determine if a glucocorticoid taper is indicated to prevent AI. Our goal is to analyze if preoperative hormonal work-up for could predict who need a postoperative taper.

Methods: This is a retrospective review of 24 patients who underwent unilateral laparoscopic adrenalectomy for MACS. All patients with POD1 AM cortisol <10 µg/dL were started on a glucocorticoid taper. We compared the preoperative hormonal work-up between those who needed a taper and those who did not. We utilized JMP software to compare data using Fisher's exact and Wilcoxon rank-sum tests.

Results: Median (IQR) age was 55.5 (42, 66) years, and 83% were females. Among the cohort, 58% of patients were started on a glucocorticoid taper. Patients who required a postoperative taper had higher 8 AM cortisol levels on their preoperative DST test. Median (IQR) AM cortisol levels after the 1 mg DST were 4.9 (3.4, 7.1) and 2.65 (2.07, 3.37) for the taper and no-taper groups, respectively ($p=0.03$). There was no difference in baseline preoperative ACTH and DHEAS levels between groups, both $p>0.05$.

Conclusion: Our study shows that preoperative AM cortisol levels after the 1 mg DST can predict patients at risk for adrenal insufficiency who need to be started on glucocorticoids following adrenalectomy for MACS. Further studies are needed to optimize the glucocorticoid taper regimen and duration.

"The Effect of PI3K Inhibitors on CD8+ T-Cell Activation by Chemotherapy-Treated Tumor Cells"

High School /City/State: Hampton High School, Pittsburgh, PA

PI of the lab: Dr. Jing Hong Wang

Mentor(s): Dr. Jing Hong Wang, Dr. Chen Zhangguo

Site: Cancer Biology

Background: Chemotherapy drugs are a mainstay of cancer treatment and can be used to elicit immunogenicity in tumors.[1] My lab previously found that CD8+ T-cells, immune cells critical for tumor clearance, are strongly activated by chemotherapy-treated tumor cells.[3] In addition to chemotherapy drugs, kinase inhibitors are also used to slow the growth of tumors. One family of kinases, PI3Ks, is integral to cell survival, motility, and activation.[2] PI3K inhibitors are commonly used in cancer treatment.[2] My work seeks to understand the effect of one such inhibitor on CD8+ T-cells' ability to recognize chemotherapy-treated tumor cells

Method: CD8+ T-cells were isolated from mice spleen. A20 lymphoma cells were purchased from ATCC.

*Co-Culture:*16 hours before co-culturing, cancer cells were cultured in either media with or without Doxorubicin (a chemotherapy drug). CD8+ T-cells were then cultured alone, with A66 (a PI3Kα inhibitor), with Doxorubicin-treated tumor cells, or with Doxorubicin-treated tumor cells and A66, for four days.

T-Cell Stimulation: CD8+ T-cells were cultured alone, with anti-CD3/CD28 beads with A66, or with Dynabeads and A66, for 3 days.

T*umor Growth:* Tumor cells cultured alone or with A66 were collected and counted each day for three days.

CD8+ T-cell activation was measured by flow cytometry and tumor proliferation was measured by cell counting.

Results: We observed that PI3Kα inhibitor, A66, can limit tumor proliferation. We also found that A66 inhibited the activation of CD8+ T-cells induced by anti-CD3/CD28 beads. In addition to this, We observed that CD8+ T-cells can be activated by chemotherapy-treated tumor cells, however, this effect was lost after administering A66.

Conclusion: PI3K inhibitors are commonly used as anti-cancer drugs to limit tumor growth. However, the immune system's anti-tumor responses can also be detrimentally affected by them. This may explain why many cancer patients don't respond well to such drugs.

Works Cited

1. Blankenstein, Thomas, et al. “The determinants of tumour immunogenicity.” Nature reviews. Cancervol. 12,4 307-13. 1 Mar. 2012, doi:10.1038/nrc3246. Accessed 25 July 2024.

2. Liu, Pixu, et al. “Targeting the phosphoinositide 3-kinase pathway in cancer.” Nature reviews. Drug discovery vol. 8,8 (2009): 627-44. doi:10.1038/nrd2926. Accessed 25 July 2024.

3. Wang, X., Waschke, B.C., Woolaver, R.A. et al. MHC class I-independent activation of virtual memory CD8 T cells induced by chemotherapeutic agent-treated cancer cells.Cell Mol Immunol 18, 723–734 (2021). https://doi.org/10.1038/s41423-020-0463-2. Accessed 25 July 2024.

Investigation of the interaction between CD91 and kinases Axl and Fgr

Scholar: Oliver Francis

Highschool: Taylor Allderdice, Pittsburgh, PA

PI: Robert Binder, PhD

Mentor: Trey Harkness

Site: Immunology

Background: Due to DNA damage accumulation cells become cancerous leading to uncontrolled growth. These cells get recognized by the immune system via CD8 T cells and natural killer cells in order to get eliminated. Our lab has shown that a receptor known as CD91, which is expressed on antigen presenting cells, is required to initiate this response. This is achieved by CD91 facilitating all of the signals necessary for T cell activation (antigen presentation, costimulation, and cytokine production). An important aspect of CD91s function is a signaling pathway that is initiated upon phosphorylation of two tyrosine residues on the beta chain of CD91. This signaling pathway and subsequent cytokine production has been shown to be dependent on Axl and Fgr. Our investigation focuses on determining how Axl and Fgr associate with the tyrosine residues of CD91.

Methods: Using immortalized bone marrow derived macrophages, we targeted each of the tyrosine residues of CD91 using CRISPR. cRNA and tracrRNA were complexed to create guide RNA targeting CD91, this was then complexed to the cas9 enzyme prior to delivery into cells via nucleofection. Efficiency of delivery into cells was measured using flow cytometry. CD91 tyrosine mutations were detected by sanger sequencing.

Results: SF DN100 was identified as the optimal nucleofection condition for iBMDMs, with approximately 35% of cells taking up GFP. Using this nucleofection condition cutting of the HPRT protein with a positive control CRISPR gRNA was detected.

Conclusions: Control kits for CRISPR were verified to be working in iBMDMs. Sequencing for CD91 mutations is underway. After confirming mutations these cells will be used for immunoprecipitation to test for interaction with Axl and Fgr.

Simulating Dynamics of RNA Polymerase II During Transcription Using Computational Modeling

Alayna Fu[1,3], Sarah Winikoff[2,3], Dr. Keisuke Ishihara,[4] Dr. James R. Faeder[4], Dr. Maria Chikina[4], Dr. Tina Subic[4]
[1]North Allegheny Senior High School, Pittsburgh, PA; [2]Pittsburgh CAPA, Pittsburgh, PA; [3]UPMC Hillman Cancer Center Academy and [4]Department of Computational and Systems Biology, University of Pittsburgh School of Medicine, Pittsburgh, PA

Abstract: ChIPMOD[1], a computational model published in 2013, simulates rudimentary dynamics of RNA polymerase II during transcription. Adding new features to the model, we updated ChIPMOD to match findings from recent research studies. We observed how promoter-proximal pausing affects RNAPII during transcription by varying different factors of the polymerase through mathematical models that display patterns representing the relationships between parameters.

Introduction: In eukaryotic cells, RNAPII promoter-proximal pausing is an important step in the regulation of the transcription process. However, the physical dynamics of RNAPII is not well understood. Computational modeling of RNAPII can allow researchers to understand how certain parameters affect the overall process of transcription and predict behaviors of RNAPII.

Methods: ChIPMOD follows the steps RNAPII takes during transcription, modeling around initiation, elongation, and termination. Taking insight from recent findings, we redesigned RNAPII pausing and processivity by having the pause site affect the processivity. To further improve ChIPMOD, we adjusted the stochastic models, changing the uniform randomness of the binding of polymerase to the gene to follow a Poisson distribution. Rather than graphing ChIP-seq density, we focused on the distribution of polymerase on the gene across multiple cells, as well as the position of the polymerase at certain time points.

Results: Comparing the plots created by the updated ChIPMOD to experimental data from a published paper[3], we saw an increase in resemblance compared to the plots created by the original ChIPMOD. In both the experimental data and in the graph created by the updated ChIPMOD, we saw a peak in density of the polymerase in multiple cells, alluding to the idea that promoter-proximal pausing increases the stability of the polymerase through processivity. Other patterns appeared across multiple plots but were not represented in the experimental data. Further research of such patterns will be needed to ensure if they are a feature in transcription or simply a numerical artifact.

Discussion: Transcription, when RNA polymerase transcribes RNA from DNA, is a fundamental step in gene expression, where the genetic information in DNA is being read and carried out. Transcription errors in certain genes have the potential to be the cause of some degenerative diseases. Research using both experimental data and a physically consistent computational modeling such as the updated ChIPMOD can assist in the understanding of mechanisms that affect transcription.

References

1. Andreas H. Ehrensberger, Gavin P. Kelly, Jesper Q. Svejstrup, Mechanistic interpretation of promoter-proximal peaks and RNAPII density maps, Cell, Volume 154, Issue 4, 2013, Pages 713-715, ISSN 0092-8674
2. Wissink, E.M., Vihervaara, A., Tippens, N.D. et al. Nascent RNA analyses: tracking transcription and its regulation. Nat Rev Genet 20, 705–723 (2019)
3. Zhang J, Cavallaro M, Hebenstreit D. Timing RNA polymerase pausing with TV-PRO-seq. Cell Rep Methods. 2021 Oct 25;1(6):None. doi: 10.1016/j.crmeth.2021.100083. PMID: 34723238; PMCID: PMC8547241

Exploring the Role of Immune Receptor TREM1 in Human Acute Myeloid Leukemia (AML)

Scholar: Gabrielle Generett

High School/College/City/State: Fox Chapel Area High School, Pittsburgh, PA

PI of group/lab: Wei Du, MD, PhD

Mentor(s): Jian Xu, PhD

Site: Cancer Biology

The immune receptor TREM1 (CD354) is a key regulator of the inflammatory response. Evidence indicates that TREM1 plays significant roles in various solid tumors, but its role in blood cancers is unclear. Earlier research has shown that TREM1, along with a weakened DNA damage response (DDR), leads to the expansion of the pre-leukemic hematopoietic stem cells in mice lacking the Fanconi Anemia gene *Fanca*. It was also found that ongoing DNA damage and oncogenic stress-induced TREM1 can promote leukemia in mice. Data from the Cancer Genome Atlas (TCGA) was analyzed showing that TREM1 is upregulated in several types of leukemia. Higher TREM1 levels are associated with poor patient survival and are inversely related to DDR gene expression. We measured TREM1 expression in human leukemia cell lines with various mutations using antibodies against human TREM1 and B-actin as a loading control. Additionally, we assessed the sensitivity of these leukemia cells with different TREM1 levels to the pharmacological TREM1 inhibitor LR12, through cell growth curves, and flow cytometry analysis for cell cycle and apoptosis. Leukemia cell maturation was evaluated by Wright-Giemsa staining with LR12. Immunohistochemistry (IHC) staining on bone sections from mice transplanted with MA9 leukemia cells, targeting mouse TREM1 and g-H2AX (a DNA double-strand break marker). Our studies show that TREM1 inhibition suppresses cell growth, induces cell death, and promotes the maturation of TREM1-high leukemia cells. Future directions include figuring out if the inhibition of TREM1 delays leukemia development *in vivo* using the human-NSGS xenograft model and if correct DDR deficiency limits TREM1 upregulation, delaying leukemia development.

Evaluating Biological Systems Using A Simulator For Large Discrete Models

Ronit Ginde[1], Dr. Natasa Miskov- Zivanov[2], Haomiao Luo[3]
[1]North Allegheny Intermediate High School, Wexford, PA; [2]University of Pittsburgh Hillman Cancer Center Academy, Pittsburgh, PA

Abstract: Biological simulators are beneficial because they reduce costs and enable detailed analysis of complex systems. However, many struggle with accurately modeling biological complexity and validating predictions with real-world results. To address these challenges, the DiSH simulator fused timing features by spontaneous degradation propagation delay, and enabled discrete models for simulation. In this work, the T cell differentiation model was used for synthesizing data and mainly analyzed data to evaluate the effects of these timing features.

Introduction: From previous work, the naive CD4 positive T cell differentiation model uses a boolean model which is constructed by boolean variables and part of dummy variables for delay and multi-level representation. Instead, the DiSH simulator is able to run discrete models and simulate timing settings. Timing in DiSH is arranged by spontaneous behavior, balancing behavior, and delay. To enable assigning elements with discrete variables, DiSH introduced increments settings and function type options. Increments are categorized as proportional or 1-level, and function types are classified into arithmetic or logical scoring. To evaluate biological systems effectively, it is essential to analyze the main features that define DiSH. Therefore, focusing on how spontaneous behavior, balancing behavior, and delay affects the results and how combinations of those timing features affect the results.

Methods: In the timing component, we tested multiple setups with DiSH using logical and arithmetic scoring, and increments, activating one timing feature while others remained at zero, such as A0.S0.B0.D1.I1 or A0.S0.B1.D0.I1 (Figures 1, 2). For the combination of these key components, we conducted an Ablation test, scoring results from 0 (optimal) to 4 (worst), based on different setups adjusting spontaneous, balancing, or delay timing. Key setups included A2.S2.B0.D1.I1, A2.S0.B2.D1.I1, and A2.S2.B2.D0.I1. Each setup altered one timing feature to have no activation and measured its impact on the results. All results ranked and measured by their steady state level (Figure 3).

Results: All three timings produced mainly unexpected results, with minimal expected outcomes. Results showed the steady states of FOXP3 (SS_FOXP3) and IL2 (SS_IL2) yielded unexpected results; as the initial value of T Cell Receptor increased, SS_FOXP3 rose while SS_IL2 declined. Analyzing the combination data, showed that balanced scored 2, delay scored 3, and spontaneous scored 4 on the ablation test. When all were activated, the score was 0. This indicates that balanced behavior (A2.S2.B0.D1.I1) exerted the least influence, delay had a greater impact (A2.S2.B2.D0.I1), and spontaneous behavior (A2.S0.B2.D1.I1) had the most severe impact. The best results occurred when all three timings were activated together (A2.S2.B2.D1.I1).

Discussion: The results of identifying key features in the DiSH simulator helped demonstrate DiSH's ability to provide detailed insights into complex biological systems, proving its usefulness in exploring and understanding intricate biological behaviors.

Figure 1: FOXP3 and IL2 interaction with T Cell Receptor when delayed timing is activated

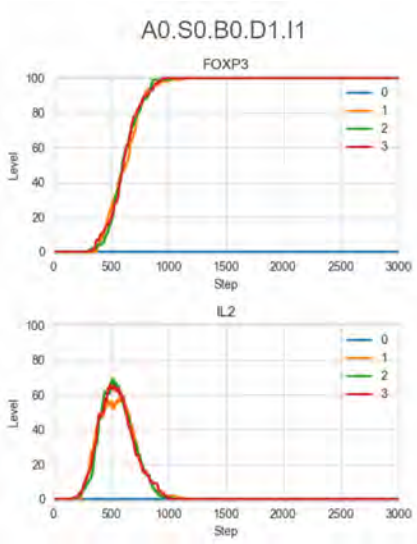

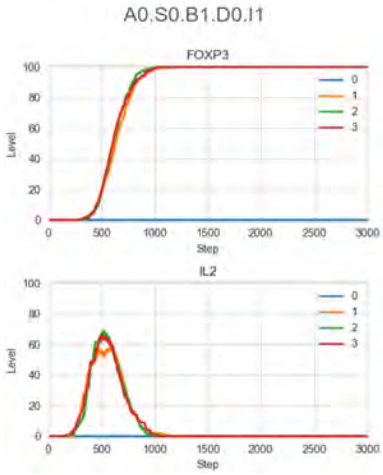

Figure 2: FOXP3 and IL2 interaction with T Cell Receptor when delayed timing is activated

Ablation test				
optimal setups	A2.S2.B2.D1.I2/I1			
steups comb	max/min of FOXP3(ss)	steady states(N=4,N=5,N=6)	eliminated setup	
A2.S2.B0.D1.I1	100/70	3,3,4	Balancing	0
A2.S2.B1.D1.I1	100/60	4,4,5		1
A2.S2.B2.D1.I1	100/0	3,4,4		2
A2.S0.B2.D1.I1	100/100	2,2,2	Spontaneous	3
A2.S1.B2.D1.I1	100/0	3,3,4		4
A2.S2.B2.D1.I1	100/0	3,4,4		
A2.S2.B2.D0.I1	100/0	2,3,2	delay	
A2.S2.B2.D1.I1	100/0	3,4,4		
A2.S1.B2.D0.I1	100/0	2,3,2		
A2.S1.B2.D1.I1	100/0	3,3,3		
A2.S2.B2.D1.I1	100/0	3,4,4		

Figure 3: Ablation test for combination timing features

References:

1. A. K. Chakraborty, J. Das, Pairing computation with experimentation: A powerful coupling for understanding T cell signaling. *Nat. Rev. Immunol.* **10**, 59–71 (2010).

2. K. Palucka, J. Banchereau, Cancer immunotherapy via dendritic cells. *Nat. Rev. Cancer* **12**, 265-277 (2012).

Title: Improving Microfluidic Single-Cell Migration Assays with Stromal Cells to Better Mimic Tumor Microenvironments

Scholar: Tiffany Habib

High School: Hampton High School, Pittsburgh PA

Lab: Dr. Yu-Chih Chen

Mentor: Hsiao-Chun Chen and Jinxiong Cheng

Site: Cancer Biology

Metastasis remains the leading cause of mortality in breast cancer patients, with cell migration playing a crucial role in this process. Our objective is to inhibit cancer cell movement to impede or halt metastasis. Previously, the Chen lab screened 2,726 compounds for their efficacy in blocking cell migration, identifying several promising candidates. However, these studies exclusively utilized cancer cells in migration assays. To more accurately replicate the tumor microenvironment, we propose the inclusion of stromal cells, specifically cancer-associated fibroblasts and mesenchymal stem cells (MSCs), which are critical for modeling tumor dynamics. In this study, we substituted 40,000 breast cancer cells per well with a co-culture of 25,000 cancer cells, 10,000 fibroblasts, and 5,000 MSCs. Our findings indicate overall consistent migration results between mono-cultured and co-cultured cancer cells, though some compounds exhibited differential effects. Due to time constraints, it remains uncertain whether these differences are genuine or attributable to experimental issues. Further investigations are required to validate these observations and elucidate the underlying mechanisms.

Key Words: Cell Migration, Breast Cancer, Tumor Microenvironment

Retinal Degeneration in P23H Mutated Mice Identification Via Histology

Sophia Hadi[1], Dr. Yuanyuan Chen, PhD[2]
Taylor Allderdice High School, PA, Department of Ophthalmology, University of Pittsburgh School of Medicine, Pittsburgh, PA

Background

Retinitis pigmentosa (RP) is a hereditary autosomal dominant disease (of rhodopsin P23H gene mutation) resulting in apoptotic degeneration of retinal rod and cone photoreceptors, causing blindness and affecting thousands worldwide. Histology sections of mice with said mutated gene knocked in allow for a better understanding of how RP affects retinal layers and how certain treatments could potentially prevent degeneration.

Method

Mouse eyes were marked by a cautery scar at the superior side and enucleated from a litter of pups at P30 from two heterozygous (P23H +/-) parents. These eyes were then fixed in Hartmann's fixative and stored in 70% ethanol. Next, they were embedded in wax and cut into 5 microns using a microtome. The wax sections containing optic nerve were collected on slides and stained with Hematoxylin and Eosin. Tail or ear lobe tissues were used to extract genome DNA to genotype the pups. Another group of P23H/+ mice was I.P.treated with 0.5 mg/kg of PP (a potential treatment for retinal degeneration) or saline every two to three days from P15 to P30, and their retina cross-sections were prepared and stained.

Result

The number of photoreceptors in the retina and the overall retinal thickness was greatest in the wild-type mice compared to both the heterozygous and homozygous, with homozygous being the thinnest. The PP-treated mice had major retinal degeneration compared to the vehicle control.

Conclusion

As expected, the homozygous mice experienced the most retinal degeneration, and the wild type the least. Since the PP-treated mouse retinal sections showed a thinner outer nuclear layer than those injected with a saline solution, it can be concluded that the drug was toxic, even in small doses.

References

1. Hartong, Dyonne., et al. "Retinitis Pigmentosa." ScienceDirect, 2006, vol. 368, no. 9549, pp. 1795-1809, The Lancet, https://www.sciencedirect.com/science/article/pii/S0140673606697407?via%3Dihub.

AAT in a Light Damage Mouse Model

Scholar: Ezra Hardy

High School/College/City/State: Pittsburgh Science and Technology Academy, Pittsburgh, PA

PI of group/lab: John Ash

Mentor(s): Connie, Haitao Liu

Site: VISION

Background:AAT (alpha 1 antitrypsin) is a protein mainly produced in the liver that inhibits proteases (enzymes that break down proteins) and has anti-inflammatory properties. In this study we are looking at how AAT can prevent light damage (LD) in the eyes.

Methods: Male albino mice were treated with either AAT or PBS (Phosphate buffered saline) and then half were exposed to 1200 lux light for 4 hours. A week later an ERG (electroretinogram) was performed on all the mice to measure the amount of electrical activity in the retina in response to light stimulus and an OCT (optical coherence tomography) was performed on all the mice to measure retina thickness. These results were compiled together and put on 2 separate graphs.

Results: The LD mice that were treated with AAT showed higher activity than LD mice that were treated with PBS in the ERG, there was no significant differences between non LD mice. There was a small difference between groups in the OCT.

Conclusions: The ERG did show a noticeable difference between LD AAT and LD PBS suggesting that AAT is effective at helping prevent LD but the OCT results shows that the method of light damage was not effective.

Future Directions: This experiment used exclusively male mice to have as little variance as possible between test subjects. We want to repeat this procedure with only female mice in order to get more data and see if the sex of the mouse has any effect on the results. Because the OCT results showed little difference between LD and non-LD mice, we want to look at our method of light damage and try to adjust either the intensity of the lights or the amount of exposure to hopefully get better results next time.

Title: Drain Liquid Biopsy to Improve Staging of Patients with PDAC after Surgery

Scholar: Mariah Harris
High School/City: Pittsburgh CAPA 6-12, L Pittsburgh Pa
PI of group/lab: Dr. Genia Dubrovsky
Mentors: Dr. Dubrovsky, Dr. Qurat UI Ain Sabih
Site: UPMC Department of Surgery

Introduction: Pancreatic ductal adenocarcinoma (PDAC) is a highly aggressive form of cancer and the most common type of pancreatic cancer. After surgery for PDAC, most patients will have the cancer come back within five years. However, currently it is difficult to predict which patients will have a recurrence and when. Therefore, new tests are needed to better predict which patients will have a recurrence, and which patients need more treatment after surgery. We hypothesize that surgical drain fluid is more sensitive than blood for identifying ctDNA and predicting tumor recurrence.

Methods: We analyzed data from 5 patients who were diagnosed with PDAC and underwent surgical treatment. These patients all had a KRAS G12D mutation in their tumor. Resected tumors were evaluated by pathology. Surgical drain fluid and blood was collected on postoperative day 1. Droplet digital polymerase chain reaction(ddPCR) was performed on all samples. Mutant allele frequency (MAF) of KRAS ctDNA was compared for blood and drain fluid, and across patients with different pathologic stages.

Results: Surgical drain fluid and blood was successfully collected on all 5 patients that we evaluated. Pathologic staging showed 40% of patients had T1 and 60% had T2 tumors. 40% of patients also had N0 disease, and 60% were N1-2. 60% had R0 resection margins, while 40% had a microscopically positive margin. All patients had a mixed response to neoadjuvant chemotherapy based on pathologic evaluation. ddPCR results are still pending at this time.

Conclusion: In this study, we show that drain fluid and blood can be successfully collected on patients undergoing curative intent resection for PDAC. This fluid can be processed for downstream analysis via ddPCR to evaluate for known tumor mutations. Results of those studies are still pending at this time, but may provide insights into patient recurrence risk and overall survival.

Microbubble mediated delivery of microRNA-27a-5p in head and neck squamous cell carcinoma cells

Scholar: Payas Hira

High School/College/City/State: Centennial High School, Dallas, Tx

PI: Dr. Flordeliza S. Villanueva

Mentor(s): Dr. Anurag Paranjape, Dr. Geetika Wadhwa, Dr. Xucai Chen, Dr. Flordeliza S. Villanueva

Site: Cancer Biology

Head and neck squamous cell carcinoma (HNSCC) is the sixth most frequently diagnosed cancer. Thus far, only small improvements in survival rates for HNSCC have been observed. The lack of effective treatments using current methods shows a need to develop novel therapeutic methods targeting oncogenes dysregulated in HNSCC. MicroRNA-27a-5p (miR-27a*) was shown to downregulate expression of several oncogenes in HNSCC. In this study we used ultrasound-targeted microbubble cavitation (UTMC) technology, pioneered by Dr. Villanueva's lab to deliver miR-27a* to HNSCCs. In UTMC, gas-filled microbubbles (MBs) loaded with oligonucleotides deliver molecular therapeutics to tissues in the presence of ultrasound (US). The US (frequency 1 MHz; PNP 500 kPa; pulse length 10 μs; pulse interval 1 ms; treatment duration 10 s) causes the MBs to cavitate (expand and contract), then pop, leading to transient pore formation on cell membrane (sonoporation), allowing RNA delivery to the cells. In this study, Human HNSCC cells were exposed to miR-Negative Control (NC) and miR-27a* loaded MBs (n=3 wells each), then treated with US. After 48 hour incubation, total RNA was isolated and qPCRs were performed to investigate expression of target genes (EGFR and mTOR). A significant reduction in the expression of mTOR was observed, whereas EGFR was less conclusive. An additional experiment confirmed the delivery of miRs into cells. The cells were treated with Cy3-antimiR-NC loaded MBs and US and incubated for 1 hour. Then they were fixed in 2% paraformaldehyde, treated with DAPI (a nuclear stain) and phalloidin (stains F-actin). Confocal imaging confirmed that UTMC allowed antimiR to enter the cells. This study showed that UTMC can deliver RNA inside the HNSCCs, and UTMC-mediated delivery of miR-27a* represses the expression of target gene mTOR. Further research could focus on assessing additional targets by Western blot and delivery of miR27a* using a mouse xenograft model.

Physical Modeling of Cell Mechanical Interactions

Scholar: James Hsieh

High School: Taylor Allderdice High School, Pittsburgh, Pennsylvania

Lab: Keisuke Ishihara, PhD

Mentor: Keisuke Ishihara

Site: Computational Biology

Intro & Background: Mechanical interactions among cells is important for organ development and disease. Mechanical forces can affect the proliferation and migration of cancer cells in tumors. Previous experiments in the Ishihara lab showed that externally applied osmotic pressure prevents cancer cells from clumping. However, it is unknown how mechanics affect cell-cell interactions.

Methods: To explore mechanical interactions at different length scales, I used physical simulations to model cell movement in 2D over time. I modeled attraction and repulsion between two cells by defining the potential energy as a function based on their distance. I used the Lennard-Jones Equation for ideal gases as the base dynamics of the simulation. Simulation results were compared to microscopy movies of cancer cells under osmotic presure.

Results: Modifications were made to set limits such that the equation refrains from exponentially increasing infinitely. First, I used the Lennard-Jones Equation and found that nearby cells attracted each other but repelled at closer distances. Second, I limited repulsion, allowing cells to get closer. However, all of the cells clustered and orbited each other. Third, I also limited attraction to prevent orbiting and added a slowing mechanism. Now, I observed stable pairs of cells that were only disrupted by a third cell approaching with a high velocity.

Discussion: In this study, I modeled cell-cell interactions with 2D simulations. By balancing the attractive and repulsive forces, I found a condition that resembles cancer cell interactions under osmotic pressure. However, I have yet to find a condition that mimics the clumping behaviour in the unperturbed cancer cells. Understanding different mechanical conditions may lead to new therapeutic strategies to inhibit malignant tumor growth.

Title: Outlining the Roles of BRCA1 and BRCA2 In Centromeric DNA Repair After Inducing Oxidative Damage

Scholar: Emma Impellicceiri

High School/ City/ State: Bethel Park High School, Pittsburgh, PA.

PI of lab: Elise Fouquerel

Mentors: Rim Nassar, Lily Thompson

Site: Cancer Biology

BRCA1 and BRCA2 are well-known biomarkers of cancer but their role in centromeric damage repair, especially double strand breaks at centromeres, is seldom known. My goal over the summer was to research the effect of BRCA1/2 on oxidative DNA damage repair triggered by oxidative stress (OS). Our hypothesis is that oxidative stress at the centromere results in replication stress, potentially leading to persisting double strand breaks and eventually mutations and cancer. To induce OS, I used a chemoptogenetic tool and I performed protein knockdown via siRNA and verified the decrease of expression by running the protein extractions on a western blot. I then used IF/FISH to assess the DNA damage response at the centromeres without BRCA1/2 present. I am looking for the proteins γH2AX and 53BP1 which are markers of DNA damage and double strand breaks. The BRCA1/2 knockdown was successful at the 96-hour time point. Then I induced OS at the centromere before collecting for IF/FISH experiment. I collected cells after 0-hour and 24-hours of recovery and performed IF/FISH to see γH2AX and 53BP1 recruited at the centromere. Through taking a backwards approach to this research, I can see if oxidative lesions recruit or use certain proteins like BRCA1/2 to help with DNA repair. If γH2AX and 53BP1 are present after inducing OS at the centromere, it shows that the DNA is trying to repair itself. If I observe γH2AX and 53BP1 recruited at the centromere, it can allow further experiments to see their role in more detail. Knowing the significance of BRCA1/2 in the repair of oxidative lesions at centromeres can translate to a wider range of cancer-fighting drugs and further research of these proteins could promote the development of enhanced cancer combating alternatives.

Title: Retinal Ganglion Cells Regeneration

Scholar: Chimdi Isiguzo

High School: Pittsburgh Science and Technology Academy, Pittsburgh, PA

PI of group/lab: Kun-Che Chang

Mentor(s): Mishal Rao

Site: Vision

Introduction:

Retinal ganglion cells (RGCs) are crucial for vision, and their degeneration leads to vision loss in diseases like glaucoma. This study examines if TPPP3 expression can enhance retinal function over time compared to Brn3a. By assessing these markers in an animal model, we aim to identify new therapeutic targets to improve RGC function and prevent vision loss.

Methods:

We used mice for their well-understood retinal structure. A viral vector with Brn3a and TPPP3 genes was injected into the vitreous humor of anesthetized mice using a microsyringe under a surgical microscope. After two weeks, an optic nerve crush was performed. Anesthetized mice had their optic nerve exposed and crushed with fine forceps. Two weeks post-injury, PERG assessments were conducted. Lightly anesthetized mice were placed in front of a visual stimulus display, and electrodes were attached to the cornea. PERG signals were recorded for amplitude and latency to assess RGC function.

Results:

Following the virus injection and optic nerve crush procedures, the PERG assessments showed that the Brn3a group experienced a moderate increase in PERG amplitude and a slight reduction in latency. The TPPP3 group demonstrated a significant increase in PERG amplitude and a notable reduction in latency, indicating a higher level of RGC function improvement. In contrast, the control group showed no significant changes in PERG amplitude or latency. Overall, TPPP3 exhibited a greater enhancement in RGC function compared to Brn3a.

Discussion:

This study demonstrates that TPPP3 expression in retinal ganglion cells can significantly improve their function following an optic nerve injury. The findings indicate that TPPP3 may serve as a promising therapeutic target for conditions involving RGC degeneration, such as glaucoma. Further research is warranted to explore the long-term effects and potential clinical applications of TPPP3 in retinal therapies.

Investigation of the Relationship between Primary Senescence and Secondary Senescence and the Effects of Deletion of Fgr Tyrosine Kinase on Inflammation in the Irradiated Lung

Scholar: Gabby Jarvis

High School/College/City/State: Shady Side Academy, Pittsburgh, PA

PI of group/lab: Dr. Joel Greenberger, MD

Mentor(s): Dr. Amitava Mukherjee, PhD, Renee Fisher

Site: Cancer Biology

Background: Late effects of radiotherapy in the thoracic region induce fibrosis in healthy lung tissue, making it increasingly difficult for a patient to breathe over time. It has been shown that exposure to radiation leads to cellular senescence and can precede radiation-induced pulmonary fibrosis (RIPF). However, the role of cellular senescence in RIPF and the underlying mechanisms are unknown. Our laboratory has previously shown that induction of tyrosine kinase Fgr in radiation-induced senescent cells upregulates inflammatory proteins and biomarkers of fibrosis (1-2).

Methods: Using senescence-associated beta-Gal staining, we evaluated radiation-induced senescence in human primary lung epithelial cells and in fibroblasts. To understand whether irradiation-induced primary senescent cells cause secondary senescence in non-irradiated neighboring cells, we used a non-contact trans-well cell culture system with senescent cells on top wells, and control cells in the bottom wells. In separate studies in mice, quantitative RT-PCR was used to evaluate the expression of IL-6 and p16 in control and Fgr knockout mice. Western Blotting to evaluate proinflammatory proteins, including p21 and Fgr, and GAPDH as control is ongoing.

Results: After seven days, primary human senescent cells caused a statistically significant induction of secondary human senescent cells. The quantitative RT-PCR results showed thoracic radiation induced senescence biomarker p16, and profibrotic cytokine IL-6 in the control mouse lungs which were significantly reduced in Fgr knockout mouse lungs. GAPDH Western Blot showed equal loading, and evaluation of other inflammatory proteins are ongoing.

Conclusions: Taken together, we have shown that radiation 1) induces senescent cells, 2) causes secondary senescence, 3) induces IL-6 and p16, and 4) with the absence of Fgr reduces profibrotic proteins IL-6 and p16. Hence, Fgr could be a potential therapeutic target for the prevention of RIPF. Further studies will use RNA sequencing to investigate the difference between primary and secondary senescence relevant in cancer.

1. Mukherjee, A., Epperly, M.W., Fisher, R. *et al.* Inhibition of tyrosine kinase Fgr prevents radiation-induced pulmonary fibrosis (RIPF). *Cell Death Discov.* **9**, 252 (2023). https://doi.org/10.1038/s41420-023-01538-3
2. Mukherjee, A., Epperly, M.W., Shields, D. *et al.* Ionizing irradiation-induced Fgr in senescent cells mediates fibrosis. *Cell Death Discov.* **7**, 349 (2021). https://doi.org/10.1038/s41420-021-00741-4

Motion of Gap Junction Plaques

Malynn G. Jones
Dr. Sandra A, Murray, PhD
Rising Freshman at Howard University Site:
CoSBBI, David Boone

Abstract

Gap junctions are channels that allow direct cell-cell communication. The purpose of this study is to determine patterns of motion of gap junction plaque structures on the cell surface and annular gap junction structures in the cytoplasm by using the spot tracking function of Imaris software to analyze time-lapse microscopy data. Results from this study and further investigation will increase our understanding of how gap junction communication and dynamics regulate cellular behavior. Introduction Cell-to-cell communication via gap junctions is essential to cellular function and has roles in health and the development of some diseases. Gap junction channels are made of proteins called connexins. With over 20 types of connexins within the connexin family, connexin 43 (Cx43) is the most abundant in many different cell types. Contacting cells that have connexins at their plasma membrane make connections by docking these connexins to create gap junction channels that facilitate communication. Clustering of these channels forms structures called gap junction plaques that often appear linear under the microscope. These plaques regularly release round vesicular structures, called annular gap junctions, into either of the contacting cell's cytoplasm via internalization. The communication of materials via gap junctions can control how groups of cells behave, and the loss of this communication can affect normal cell function and play a role in some diseases such as cardiovascular diseases and cancer. The majority of annular gap junctions are known to fuse with lysosomes that contain degrading enzymes but some of them have also been shown to either form contacts with cytoplasmic organelles or move back to plasma membrane to join existing gap junction plaques or form new gap junction plaques. Thus, internalization is a common method of removal of the gap junction plaques and a process that reduces cellular communication.While much is known about how gap junction plaques assemble, some details of the mechanism of gap junction plaque removal from the cell surface are still unclear. Therefore, further investigation of gap junction patterns of motion will increase our understanding of the influence of gap junction structure dynamics on cell communication and behavior.

Methods

To determine patterns of motion and directions of annular gap junctions and/or gap junction plaques, the spot tracking function of Imaris image analysis software was used on time lapse images. This software helps scientists visualizing 2D and 3D images to measure structural properties and investigate patterns of motion to answer biology research questions. Time-lapse images of cells expressing fluorescent gap junctions were used as the initial dataset. After converting the files to Imaris file format and, we used optimized spot tracking using the spot tracking wizard and performed tracking to generate tracks of gap junction plaques and annular gap junctions over time. After tracking was completed, the outcome measures were exported from Imaris to a spreadsheet and further analysis was done to evaluate track length and duration. The track speeds were calculated from track length and duration values. The
directions of the movement and straightness of the tracks were also evaluated.

Results

A total of 736 tracks were generated from 5 time-lapse image files. The average track displacement for gap junction structures detected with Imaris spot tracking was 46 ± 3 μm. On average, gap junction structures were tracked for 5 ± 0.2h. Speeds were calculated at an average of 2.5 ± 0.1 nm/s.

Summary

We determined the average speed and the duration of the annular gap junctions.
Further investigation will be done to measure the directionality of the annular gap junction movements. In addition, tracking parameters will be used to identify the cytoskeletal and/or motor proteins that regulate the movement of gap junction structures.

Acknowledgments:

- Dr. Sandra Murray
- Dr. David Boone
- Dr. Selma Cetin-Ferra
- Dr. Anthonya Cooper
- UPMC Presbyterian
- DBMI Building
- University of Pittsburgh Center for Biologic Imaging

Microglial Calcium Activity and Inflammatory Response to Electrode Insertion

Scholar: August Kollar

High School/College/City/State: Mt. Lebanon High School, Mt. Lebanon, PA

PI of group/lab: TK Kozai, PhD.

Mentor(s): Kevin Stieger, Vanshika Singh

Site: TDX

Background: Implanting electrodes into the brain allows for both stimulating and recording the brain's activity. These implants can be used for both studying the electrical signals from the brain as well as controlling and treating specific conditions such as Parkinson's Disease, epilepsy, and depression. However, the electrode's effectiveness deteriorates over time due to natural immune responses in the brain, which cause scarring and inflammation at the site of the implantation. Microglia, a glial cell in the brain, influences this immune response, and therefore a better understanding of the microglia's behavior and response to electrode insertion will support treatments to help improve the longevity of implanted electrodes. Calcium activity is known to indicate inflammatory phenotypes in these microglia, therefore, surveying microglial relationships with transient calcium events will also aid in better understanding the behavior of brain cells during probe insertion related injury. We hypothesize that calcium events closer to the probe within the insertion hemisphere will be more intense than events further from the probe and events in the contralateral (control) hemisphere.

Methods: We used a mouse model utilizing GCaMP6f-tdTomato selectively expressed in microglia to view microglia morphology (tdTomato) and track calcium events (GCaMP6f). Single-shank Michigan-style electrodes were implanted into the brains of these mice. We then imaged microglia for ~15 minutes over a field of view of 275 μm near the electrode and on the contralateral hemisphere at 3, 6, and 12 hours post-implantation, and daily for 14 days post-implantation. The collected data was analyzed through a custom algorithm that detected transient calcium events not part of the glial scar, which were then analyzed using Python scripts. The magnitude of changes in fluorescence intensities were calculated to analyze any potential relationships between calcium events, their proximity to the probe, and time since probe insertion—to test our hypothesis. For this study, data from 3 animals over 17 trials (3 trials the day of probe insertion plus one trial each day for two weeks following insertion) was analyzed.

Results: Data suggests that calcium event intensity increases during the first 2 days and is generally greater than contralateral event intensities (2-Way ANOVA: day-to-day $p = 6e\text{-}5$, hemisphere $p = 1.6e\text{-}3$). Event intensity peaks on day 2 post implantation, which was significantly greater than day 0 events and day 2 events in the contralateral hemisphere. There were no significant increases in contralateral event intensity compared to day 0 contralateral events.

Conclusion: Our study supports past findings claiming that calcium activity is most intense during the first few days following insertion, which suggests that microglial calcium activity is an indicator of inflammatory responses to electrode insertion injury. More data may support more significant differences in calcium event behavior over time.

How Neurokinin A Affects Neutrophil Migration Into the Skin

Scholar: Isabella Kwaw

High School/College/City/State: Andover High School, Andover, KS

PI of group/lab: Tina L. Sumpter

Mentor(s): Tina L. Sumpter, Ahnika Hay

Site: ICI (Immunology and Cancer Immunotherapy)

Allergic contact dermatitis (ACD) affects up to 20% of people and about 8% of adults. DNFB is a common contact allergen causing ACD. DNFB induces inflammation when applied to the skin and affects resident skin cells, including mast cells and neurons. DNFB also initiates a cellular cascade that results in neutrophil migration. Neuro-inflammation is a component of ACD, and pro-inflammatory neuropeptides increase inflammation. However, there is limited information about anti-inflammatory neuropeptides regulating ACD. Our data has shown that the neuropeptide Neurokinin A (NKA) reduces DNFB-induced neutrophil migration. Although the anti-inflammatory mechanism that NKA uses is unknown, we hypothesize that NKA regulates chemokines that recruit neutrophils into the skin. Mast cells make chemokines that recruit neutrophils into the skin, including CXCL1, CXCL2, CXCL12, and CCL2. We have previously discovered that CCL2 is downregulated by NKA, and our study explores what other chemokines are affected by NKA and how mast cells play a role in this process. Mice with mast cells (Mcpt5 Cre LM), and mice without mast cells (Mcpt5 Cre DTA), were injected with PBS or NKA and treated with DNFB to induce inflammation. RT-PCR was used to detect the levels of CXCL1, CXCL2, and CXCL12 in the ear skin. Higher levels of CXCL1 were found in the skin of both types of mice when injected with DNFB. In the skin of mast cell-deficient mice, we found lower levels of CXCL1 compared to normal (LM) mice when injected with NKA. Flow staining showed that neutrophils had the CXCR2 receptor. To date, our data shows that NKA regulates CXCL1 in a mast cell-dependent manner. Further studies will be done to decipher if the capacity for NKA to down-regulate CXCL1 requires mast cell-derived IL-10.

Impact of chemical exposures on stochastic epimutational burden and lung cancer risk

Andrew Li, Dr. Kathyrn Demanelis
North Allegheny Senior High School, Pittsburgh, PA; University of Pittsburgh Hillman Cancer Center Academy, Pittsburgh, PA

Introduction: Lung cancer (LC) is the leading cause of cancer death in the United States. While smoking is the primary risk factor for LC, there are additional factors that influence its development. In particular, the chemical exposome, the combination of endogenous and exogenous compound exposures encountered throughout an individual's lifetime, can provide a greater understanding of environmental influences on both LC and biomarkers of cancer-enabling processes. One of these biomarkers is stochastic epigenetic mutational burden (SEMs), the sum of all random alterations of DNA methylation across the genome due to aging, lifestyle factors, disease, and environmental exposures. Currently, exposome wide analyses are limited by the inability to efficiently and universally resolve necessary chemical identifiers (IDs), such as CAS and KEGG IDs. The objectives of my project were to 1) develop a pipeline in R and Python to better assign chemical IDs in chemical exposome data and 2) evaluate the relationship between compounds identified in the chemical exposome on SEMs in a pilot study using samples from the Pittsburgh Lung Screening Study (PLuSS).

Methods: The chemical exposome was measured in the plasma of 44 case-control pairs (matched on age, sex, smoking status, pack-years of smoking, and date of sample collection) from PLuSS using high-resolution mass spectrometry. The TidyMass package was utilized to putatively annotate compound peaks. The chemical exposome data was quantified using cutpoints (non-detectable, below median, and above median peak areas). Conditional logistic regression models evaluated the impact of each compound on LC risk using R's "survival" package. Among the controls, linear regression models were used to examine the impact of the chemical exposome on total stochastic epimutational burden (SEMs derived from Illumina EPIC DNA methylation array data), and were adjusted for age, sex, and smoking status. SEMs were stratified by their direction: hyperSEMs (gain of methylation) and hypoSEMs (loss of methylation).

Results: We focused specifically on resolving CAS IDs and KEGG IDs. Of 6960 total compounds in our exposome data, there were originally 2912 (42%) compounds with CAS IDs and 1575 (23%) with KEGG IDs. By referencing MetaboAnalyst's API, the Chemical Translation Service (CTS) from the Fiehn lab at UC Davis, MetaCyc's Metabolite Translation Service, and PubChem as part of our pipeline, we were able to successfully fill in 2865 CAS IDs and 1536 KEGG IDs. After implementing our pipeline, 5777 (83%) compounds had CAS IDs and 3111 (45%) had KEGG IDs. Within our exposome data, we discovered 31 compounds associated with hyperSEMs and 33 compounds associated with hypoSEMs ($p < 0.05$). Twenty compounds associated with hyperSEMs and 18 associated with hypoSEMs were positively associated. In addition, nine compounds associated with hyperSEMs or hypoSEMs, including piperine and acetaldehyde, overlapped with compounds associated with LC risk. Notably, acetaldehyde (OR = 2.16, 95% CI = 1.22 - 3.84, $p = 0.008$), a primary metabolite of ethanol and Group I carcinogen, was found to be significant among hyperSEMs, hypoSEMs, and LC risk.

Discussion: We successfully resolved most CAS IDs for our compounds and nearly all metabolites with available KEGG IDs using our pipeline, helping to better 1) characterize these compounds and 2) prepare data for pathway analysis. We also discovered several compounds associated with both SEMs and LC risk. Of interest is acetaldehyde, a known carcinogen that can influence DNA damage repair function and encourage tumor growth. As a pilot study, the sample size is relatively small and may not capture the full spectrum of chemical exposures and their effects, warranting caution when interpreting our results. In addition, annotations of compounds were putative and not confirmed. Further examination into the role of environmental exposures in LC and the development of efficient and accurate methods for resolving these chemical IDs in exposome data is essential for improving our understanding of LC etiology and for guiding LC prevention and intervention strategies.

Variation in EMS quality metrics and correlation to patient outcome

Scholar: Steven Li
School: Fox Chapel Area High School, Pittsburgh, PA
PI of lab: Joshua Brown
Mentor: Joshua Brown, Christine Leeper
Site: Surgery

Abstract

Prior work shows that EMS quality metrics, such as scene time and pain treatment, predict a greater likelihood of trauma patient survival. EMS agencies are heterogeneous with significant variation in quality metric adherence. It is unclear whether specific characteristics of EMS agencies such as volunteer versus paid employees, operational model, or geographic area impact quality metric adherence. Therefore, our objective was to evaluate the relationship between agency characteristics and achievement of quality metrics.

We utilized the 2022 ESO database, an electronic medical record of patient and EMS agency-level data. Agency-level variables include volunteer versus paid employee status, funding source (community non-profit, fire-based, non-fire governmental, hospital-based, and private for-profit), and geographic service area size (square miles). National EMS quality criteria generated a trauma-specific quality score for each agency. Linear regression determined the relationship between agency characteristics and overall quality score.

728 agencies were included in the analysis with 77,573 total patients transported. Agencies with paid employees had higher quality scores than volunteer agencies (coef 0.002; 95% CI 0.001, 0.004, $p<0.01$). Fire-based agencies and hospital-based agencies had lower quality scores compared to non-profit agencies (coef -0.020; 95% CI -0.022, -0.019, $p<0.01$; coef -0.006; 95% CI -0.011, -0.002, $p<0.01$), while non-fire governmental agencies and private non-hospital agencies had higher quality scores compared to non-profit agencies (coef 0.003, 95% CI 0.002, 0.005, $p<0.01$; coef 0.071, 95% CI 0.068, 0.073, $p<0.01$). A larger service area was also associated with a higher quality score (coeff 0.024; 95%CI 0.022-0.026, $p<0.01$).

Our findings demonstrate that agency characteristics significantly impact adherence to quality metrics. Since lower quality scores have been linked with worse in-hospital survival after injury, this information can be used to identify agencies that would benefit most from interventions such as education, simulations, and inter-agency provider sharing.

Optimizing Karyotyping Protocols for Analyzing Chromosomal Instability in Fallopian Tube Epithelial Cells with p53 Mutations

Scholar: Julia Lipscomb

High School: Seneca Valley Senior High School, Harmony, Pennsylvania

Lab: Anna Lokshin, PhD

Mentor: Yan Wang, PhD

Background: Karyotyping, or chromosome analysis, is commonly used for the detection of chromosomal instability (CIN). CIN is one of the primary issues associated with cell lines, as it can cause genetic heterogeneity or unstable cell properties. Mutated TP53 also affects various cellular responses, such as genomic instability, as well as promoting cancer cell proliferation, metastasis, and drug resistance. Additionally, the more a cell line is passaged, the greater the risk of chromosomal changes. Conducting *in vitro* studies in similar environmental and cellular conditions as the cells *in vivo* is instrumental when implementing the work in clinical trials. This study was done on fallopian tube epithelial cell (FTEC) cultures from healthy donors that were immortalized with hTERT. It focuses on detecting if there is CIN in the control and TP53 mutations on passage 30, as well as finding any differences between the different cell lines. We examined the effect of the two mutations (TP53 R175H and TP53 R273H) the lab made to mimic the early pre-lesion in humans called the P53 signature.

Methods: Fallopian tube epithelial cell cultures are isolated from healthy donors. The following protocol was adapted from Howe, Umrigar, and Tsien. The donor cells assessed were CH001, Donor #6, and Donor #26. Three cell lines were used from each: empty vector control, R175H mutation, and R273H mutation. Those cells were treated with colchicine, pelleted, incubated in KCl, and fixed. Donor #26's cells were treated with 0-, 5-, 10-, 20- and 25-minute incubation time with KCl to optimize the hypotonic step for best resolution. Slides were made from all cell lines, stained without G-banding, and studied under 400x magnification. All cell lines were G-banded, and the GFP slides were studied under 1000x magnification with oil.

Results: This study found the cells show no clear difference in the G-banded cells of the control and the mutations. However, a difference in nucleus size was noted between the WT and mutants when treated with KCl. The mutants' nuclei varied widely in size compared to the control whose nuclei were closer in size. In addition, the optimized hypotonic step for the FTEC is 20 minutes in potassium chloride (KCl) and the trypsin time for G-banding steps was 12-15 seconds.

Conclusion: There is no chromosomal instability detected in the fallopian tube epithelial cell line with TP53 R273H and R175H mutation after being passaged 30 times. Further analysis is needed to view the chromosomes and analyze them.

Title: The Relationship Between Liver Damage and Coagulation

Scholar: Anna Litster

High School/City/State: Shady Side Academy, Pittsburgh, PA

Lab PI: Dr. Melanie Scott

Mentors: Melanie Scott MD PHD, Joud Mulla MS

Site: Surgery

Introduction: The liver plays an essential role in blood clotting (hemostasis) as it produces almost all coagulation factors. The two main pathways of coagulation activation (intrinsic and extrinsic), converge at the common pathway for hemostasis. Intrinsic pathway function is tested using activated partial thromboplastin time (aPTT), and extrinsic pathway using prothrombin time (PT). We determined the relationship between liver damage and coagulation in acute liver damage models in mice.

Methods: Three models were used: 1.polytrauma (multi-injury trauma induced by hypovolemic shock [25% total blood volume removal], liver crush via hemostat, and pseudo-fracture [soft-tissue injury+injected bone solution]); 2.acetaminophen (APAP)-induced acute liver failure (600mg intraperitoneal APAP); 3.liver crush alone. Blood was collected via cardiac puncture 6h after polytrauma/liver crush, or 24h after APAP, and plasma separated and frozen at -80°C. Alanine aminotransferase (ALT) and aspartate transferase (AST) were analyzed using HESKA to determine acute liver damage level. aPTT and PT were analyzed by Diagnostica Stago Start machine. Data given as mean+/-standard error of mean (SEM). Statistical analysis performed using Student's t-test with $p<0.05$ considered significant.

Results: As expected, ALT/AST increased significantly in each model indicating acute liver damage. However, ALT/AST were significantly lower in APAP mice compared with polytrauma or liver crush mice (AST:1472±397 vs 2485±382 or 3305±420 respectively; $p<0.05$: ALT 647±77 vs 4107±727 or 5592±769 respectively; $p<0.05$). Interestingly, both aPTT and PT were not significantly different from normal in polytrauma and liver crush mice at 6h (aPTT: 32±2.2 vs 27.3±1.9 or 28.1 ± 2.05 respectively; PT: 11.8±0.15 vs 12.5±0.6 or 11.8±0.3 respectively; p=NS), but APAP mice had significant changes in both aPTT and PT suggesting alteration in coagulation function (coagulopathy) (aPTT 32±2.2 vs 45.7±5.4; PT 11.8±0.15 vs 18.3±1.7; $p<0.05$).

Conclusion: Our data suggest no relationship between liver damage and coagulation function/coagulopathy in these models. In future experiments I would look at multiple time points for each liver model and compare with coagulation function over time.

Utilization of Principal Component Analysis (PCA) to Hyperspectral Imaging - Potential Commercial Medical Applications

Rayan Majumdar[1], Michael Becich[2], MD, PhD, Brittany Gomez[2]
[1]La Salle High School College, Philadelphia, PA; [2]University of Pittsburgh Hillman Cancer Center Academy, Pittsburgh, PA

Abstract

This project investigates the enhancement of image quality in blood vessels using Hyperspectral Imaging (HSI) and Principal Component Analysis (PCA) for improved clinical diagnostics. By reducing the dimensionality of HSI data from placenta samples, PCA effectively captures the most significant variance, demonstrating improved visualization and potential applications in Extracorporeal Membrane Oxygenation (ECMO) and cardiovascular monitoring.

Introduction

Hyperspectral Imaging (HSI) is utilized in various clinical applications such as skin disease diagnosis, blood flow visualization, and surgical navigation. However, the high-dimensional data generated by HSI poses computational challenges. This study explores the use of Principal Component Analysis (PCA) to manage these challenges by transforming high-dimensional HSI data into a lower-dimensional space while retaining critical information.

Methods

The study involved applying PCA to HSI data obtained from placenta samples. The analysis focused on reducing data dimensionality and improving image visualization. A comparative assessment of visualization quality was conducted between PCA-treated images from individual datacubes and the whole dataset. Mean Squared Error (MSE) metrics were used to quantify visualization improvement.

Results

Applying PCA to individual datacubes resulted in a significant reduction in MSE from 0.02 to 0.0079, demonstrating a 2.5x improvement in image quality. Conversely, analyzing the whole dataset with multiple datacubes led to a loss in visualization quality. The results highlight PCA's effectiveness in enhancing the visualization of HSI data.

Discussion

The application of PCA to HSI data significantly enhances image quality, offering promising implications for clinical diagnostics. Specifically, in ECMO and cardiovascular applications, PCA can aid in monitoring tissue and blood oxygenation, potentially improving patient outcomes. The development of AI-based algorithms leveraging PCA-treated HSI data could lead to better diagnostic tools for critically ill patients.

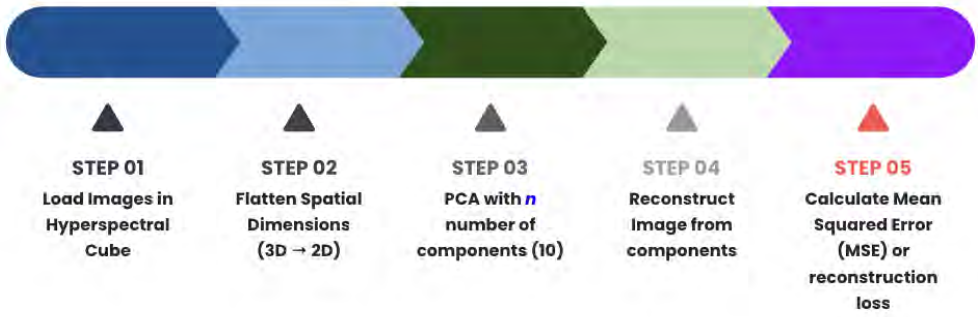

Figure 1: 5 Key steps in converting raw Hyperspectral Imaging (HSI) data and applying PCA

Figure 2: Loss of information when PCA is applied to the whole dataset (one datacube), MSE = 0.02 *vs.* Minimal loss of information when PCA is applied to one datacube only on itself, MSE = 0.0079

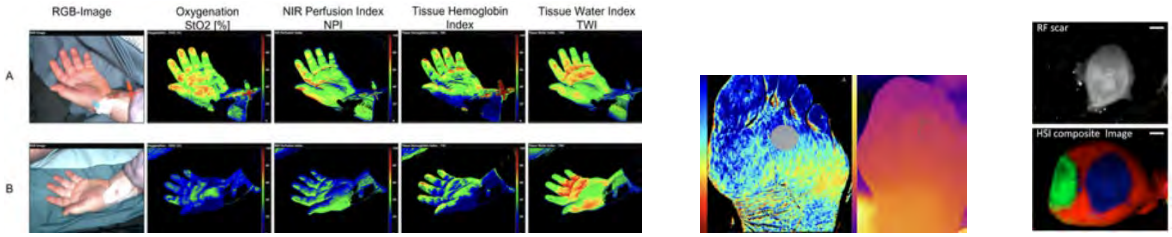

Figure 4: Potential commercial applications of HSI in ECMO and cardiovascular applications

References:

1. Yoon, J. (2022). Hyperspectral Imaging for Clinical Applications. BioChip Journal, 16, 1-12
2. Kuhlmann, H., Garczarek, L., Künne, D., Pattberg, K., Skarabis, A., Frank, M., Schmidt, B., Arends, S., Herbstreit, F., Brenner, T., et al. (2023). Bedside Hyperspectral Imaging and Organ Dysfunction Severity in Critically Ill COVID-19 Patients—A Prospective, Monocentric Observational Study. Bioengineering, 10(10), 1167.
3. Cheng, S., Zheng, Y., Zhang, Z., Zhu, J., Yuan, X., Yin, M., Zhao, Y., Zhang, W., Luo, X., Shi, H., et al. (2014). Optical coherence tomography in ophthalmology: Basic principles and recent advances. J Biomed Opt, 19(1), 010901
4. Greenman, J., Yudovsky, D., Khaodhiar, L., Nouvong, A., & Mojaradi, B. (2022). Investigation of the Performance of Hyperspectral Imaging by Principal Component Analysis in the Prediction of Healing of Diabetic Foot Ulcers. Journal of Imaging, 16, 1-12.

Role of Replication Stress and BAP1 Mutation in Patient Survival

Reina Majumdar[1], Michael Becich[2], MD, PhD, Rumana Rashid[2]

[1]Lansdale Catholic High School, Lansdale, PA; [2]University of Pittsburgh Hillman Cancer Center Academy, Pittsburgh, PA

Abstract

This study examines the impact of replication stress and BAP1 mutations on patient survival in mesothelioma. Analysis of 189 patients using Kaplan-Meier survival curves and correlation analyses revealed significant associations between BAP1 mutations and both overall survival (OS) and progression-free survival (PFS).

Introduction

Mesothelioma is an aggressive cancer with poor prognosis, primarily due to late-stage detection and treatment resistance. BAP1 mutations, which affect DNA repair and replication, contribute to genetic instability and tumor progression. Understanding the roles of BAP1 mutations and replication stress (RS) in mesothelioma could uncover new therapeutic targets.

Methods

Data from 189 mesothelioma patients, including PFS and OS, were analyzed using Kaplan-Meier survival curves. Correlation analyses and histograms explored relationships between clinical outcomes and molecular markers. The cohort included epithelioid (53.8%), biphasic (34.6%), and sarcomatoid (11.6%) subtypes, with 60% of patients harboring BAP1 mutations. RS scores were analyzed across all subtypes.

Results

Kaplan-Meier survival analysis showed distinct PFS and OS patterns across subtypes. Median PFS times were 12 months (epithelioid), 8 months (biphasic), and 5 months (sarcomatoid). Median OS times were 18 months (epithelioid), 12 months (biphasic), and 9 months (sarcomatoid). Significant correlations were found between BAP1 mutations and OS ($p < 0.1$) and PFS ($p < 0.05$), particularly in biphasic ($p=0.0002$) and sarcomatoid ($p=0.025$) subtypes. RS scores did not demonstrate any significant correlation with OS and PFS in this study

Discussion

The study highlights the significant impact of BAP1 mutations on mesothelioma survival, with marked differences in PFS and OS across subtypes. No significant correlations were found between replication stress and survival outcomes. Future research should incorporate spatial biology to further investigate replication stress and its role in patient survival.

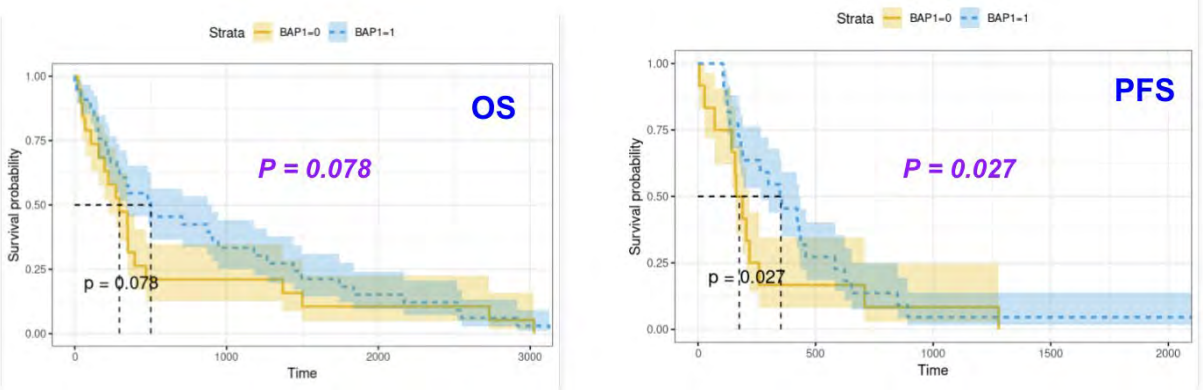

Figure 1: The Kaplan-Meier curves for BAP1 with p<0.1 values across all cancer subtypes demonstrating significant correlation with OS and PFS.

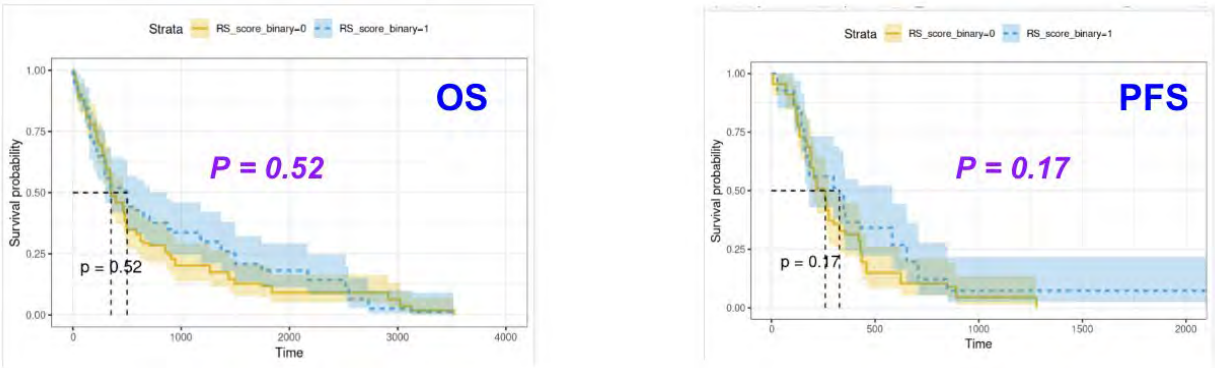

Figure 2: The Kaplan-Meier curves for Replication Stress (RS) scores did not demonstrate any significant correlation with OS and PFS.

References:

1. Kwon, J., Lee, D., & Lee, S.-A. (2023). BAP1 as a guardian of genome stability: Implications in human cancer. Experimental & Molecular Medicine, 55, 745-754
2. Hajj, G. N. M., Cavarson, C. H., Pinto, C. A. L., Venturi, G., Navarro, J. R., & Cordeiro de Lima, V. C. (2021). Malignant pleural mesothelioma: an update. J Bras Pneumol, 47(6), e20210129
3. Bodenmiller, B. (2016). Multiplexed Epitope-Based Tissue Imaging for Discovery and Healthcare Applications. Cell Systems, 2, April 27
4. Rozenblatt-Rosen, O., Regev, A., Oberdoerffer, P., Nawy, T., Hupalowska, A., et al. (2020). The Human Tumor Atlas Network: Charting Tumor Transitions across Space and Time at Single-Cell Resolution. Cell, 181(2), 236-249. doi:10.1016/j.cell.2020.03.053

Pharmacokinetic modeling of Pemigatinib to evaluate potential drug-drug interactions

Scholar: Samarth Mandani

High School: Moon Area High School, Moon Township, PA

Lab: Xiang-Qun (Sean) Xie, MD, PhD, EMBA

Mentor: Terence (Terry) McGuire

Site: Computational Biology

Intro:

Pemigatinib, sold under the brand name Pemazyre, is an effective treatment for bile duct cancer. Pemigatinib inhibits the fibroblast growth factor receptor (FGFR) family of receptor tyrosine kinases and limits the growth of bile duct cancer cells. Pemigatinib additionally interacts with the cellular machinery as a substrate of cytochrome P450 (CYP) 3A4 and as an inhibitor of P-glycoprotein (P-gp) or organic cation transporter-2 (OCT2)/multidrug and toxin extrusion protein-1 (MATE1). The possible drug-drug interactions (DDIs) of Pemigatinib with other drugs sharing common cellular targets or pathways are currently unknown and understudied. Here, we present results from an *in silico* analysis utilizing Simcyp Simulator to evaluate potential DDIs arising from interactions of Pemigatinib with other CYP3A4 inhibitors/inducers or substrates of P-gp or OCT2/MATE1 to provide accurate dosing recommendations for future clinical trials.

Methods:

In accordance with a corresponding case study exploring the DDI's of Pemigatinib through Simcyp, physiochemical parameters for the compound were utilized whilst developing our own PBPK model.

Results:

After much trial and error, an accurate PBPK model of Pemigatinib was develop through simcyp. The model successfully replicated results of clinical trials regarding Pemigatinib administration in healthy as well as cancerous populations within a reasonable range, demonstrating its accuracy and efficacy.

Discussion:

A more comprehensive study is needed to fully understand the interactions between Pemigatinib and other drugs. Future directions will involve utilizing this model to recommend safer and more effective dosing plans for clinical studies.

Predicting Pathogen Susceptibility to Antibiotics in Bloodstream Infections based on Patient's Clinical History and Prior Resistance

Vega Mani[1], Samuel Blechman, MS [2]
[1]Taylor Allderdice, Pittsburgh, PA ; [2]Department of Biomedical Informatics, Pittsburgh, PA

Abstract

In this project, UPMC's Electronic Health Records and patient data on antibiotic usage were used to develop machine learning models that predict if a patient's infecting pathogens in a bloodstream infection are susceptible or resistant to a certain antibiotic based on recent prescriptions and past resistance. The most commonly tested and prescribed antibiotics were extracted from the data set to use. The input features were added to the columns and placed into a binary Random Forest model, and then were run through performance evaluations.

Introduction

Antibiotics can be detrimental to patients when used incorrectly or without necessity because it creates antibiotic resistant bacteria that can be difficult to treat. Clinicians must prescribe an antibiotic before Antibiotic Susceptibility Test (AST) results become available, posing a risk because the patient's infection may be resistant to the chosen empiric therapy. The objective of this study is to evaluate how well machine learning models are able to predict pathogen's susceptibility to a certain antibiotic based on their past resistance and recent prescriptions of the antibiotic.

Methods

The data included patient records of demographics, antibiotic susceptibility test results, hospital location, recent antibiotic prescriptions, and past antibiotic resistance. These features were placed into multiple binary classifiers. The recent prescription feature flags prescriptions based on if the start date of the antibiotics was before the order date of the AST. The whole data incorporates past medical history ranging from 2004 -2024. The data with cultures of bloodstream infections only ranges from 2016-2024 therefore it uses a patient's past medical data, the earliest from 2004 to predict a patient's susceptibility. The past resistance feature checks if the patient has had past resistance to the given antibiotic in the past 6 months, 2 years, or ever. The data was split into test and train groups based on the year which spanned from 2016-2024. The years before 2021 were placed in the train group and the years after were tested on. A Random Forest model was created from the Caret library in R to predict a patient's susceptibility using these features. Next, a 10-fold cross validation was run to evaluate the accuracy and robustness of the predictions. Sensitivity, Specificity, and Positive Predictive Value (PPV) was calculated to create an ROC curve and a Precision-Recall curve which determined how well the model was performing. Once this was calculated the model parameters were tuned multiple times until it was able to perform at the highest possible accuracy and precision.

Results

The model depicted how well clinical history was able to be useful predictors for a patient's AST results. When the patient had a greater number of bloodstream infection cultures, the accuracy increased because there was more previous data to rely on. This poses a limitation because the model requires clinical history from at least 6 months prior. The model also was able to display if past resistance or recent prescription to other antibiotics was able to aid in predictions, building similarities between some of the antibiotics.

Discussion

The results look promising, because the Sensitivity and Specificity scores were high for most of the antibiotics. This establishes the beneficial role that past clinical history plays in predicting bloodstream pathogen's susceptibility.

Figure 1. Depicts the AUC (Sensitivity vs. Specificity) scores for each of the antibiotics

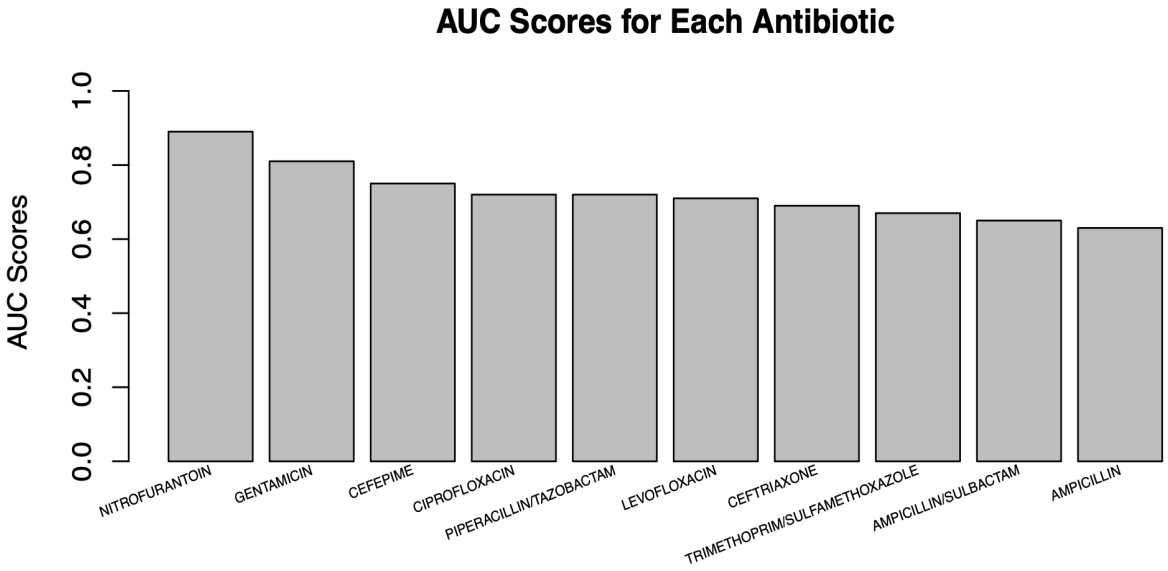

References

1. Hebert, Courtney et al. "Prediction of Antibiotic Susceptibility for Urinary Tract Infection in a Hospital Setting." *Antimicrobial agents and chemotherapy* vol. 64,7 e02236-19. 23 June. 2020, doi:10.1128/AAC.02236-19

2. Kanjilal, Sanjat et al. "A decision algorithm to promote outpatient antimicrobial stewardship for uncomplicated urinary tract infection." *Science translational medicine* vol. 12,568 (2020): eaay5067. doi:10.1126/scitranslmed.aay5067

3. Yelin, Idan et al. "Personal clinical history predicts antibiotic resistance of urinary tract infections." *Nature medicine* vol. 25,7 (2019): 1143-1152. doi:10.1038/s41591-019-0503-6

Title: What the numbers say part 2

Scholar: Trinidy Manison

High School/College/City/State: Uprep Milliones/ Pennsylvania State University

PI of group/lab: Dr. Ana Radovic

Mentor(s): Ana Radovic , Kayla Odenthal, & Jenny Frye

Site: CoSBBI

Supporting Our Valued Adolescents (SOVA) is an initiative by the University of Pittsburgh dedicated to helping adolescents, especially those from underserved and marginalized groups like BIPOC (Black, Indigenous, and People of Color) and LGBTQ+ communities. SOVA aims to prevent mental health issues by offering tailored tools, information, and support systems. Additionally, SOVA provides ongoing support and resources to adolescents already dealing with mental health conditions.

In 2023, the SOVA Lab conducted presentations across Allegheny County, each reaching over 40 students. These sessions covered various mental health topics, offering practical advice and strategies for improving well-being. This year's research builds on previous projects with a significant shift: actively seeking input and feedback from focus groups. This participatory method engages our target audience more deeply and gathers valuable insights from those we aim to support.

To collect and analyze data effectively, SOVA uses the "Rose, Bud, Thorn" method within focus groups. This technique involves participants identifying positive aspects (Roses), potential opportunities (Buds), and areas for improvement (Thorns). By utilizing this method, SOVA captures a comprehensive range of perspectives and experiences, enabling us to refine and improve our mental health curriculum and support services based on real-world feedback.

We conducted three focus groups with the same children to gather comparable yet differing perspectives on our improvements and to obtain their consent for their suggestions. We collectively explored how to make our sessions more engaging through the feedback we received . Less crowded slides , understandable vocabulary and interactive techniques. In the future, these focus groups will help create a curriculum for other speakers and attract more youth.

Through these efforts, SOVA promotes mental health and well-being among adolescents, particularly from marginalized communities. By adapting evidence-based strategies and involving the target audience in development, SOVA ensures its resources and support systems are both relevant and effective.

Oscar Martinez
Claremont High School
Ontario, California, USA

Mentor: Dr. Chen Luija:

Academic Degrees: BS in Biological Technology, MS in Biomedical Informatics, and PhD in Biomedical Informatics.

Affiliation: Assistant Professor, Department of Biomedical Informatics, University of Pittsburgh

Abstract

This study compares cellular states in normal and flu-infected lungs using time-series single-cell transcriptomes, focusing on aging and gender effects. Data from young and old, male and female mice were analyzed to understand the dynamic transcriptomic processes during influenza infection and repair.

Introduction

Understanding the role of aging in influenza response and tissue repair is crucial. This study aims to investigate variations in cellular states in normal and flu-infected lungs using time-series single-cell RNA sequencing (scRNA-seq) data from young and old, male and female mice.

Methods

Single-cell RNA-seq data were collected from young (8-12 weeks) and old (22 months), male and female mice at four time points: day 0 (control), day 3 (early sensing), day 7 (peak inflammation), and day 11 (repair initiation). Approximately 160,000 cells from 16 samples were analyzed. The data underwent cell clustering, labeling, differential gene expression analysis, and pathway enrichment.

Results

Key findings include significant differences in cell subpopulation dynamics and cell-cell communication between young and old, male and female groups during influenza infection and repair. These differences were identified through comprehensive analysis of cell clustering and pathway enrichment.

Discussion

The study reveals important insights into how aging and gender influence the cellular response to influenza. This knowledge can inform future research and potential therapeutic strategies for age-related susceptibility to influenza and other respiratory infections.

The Effect of High Biofilm Production in *Pseudomonas fluorescens* on the Rate of Phagocytosis by *Dictyostelium discoideum*

Scholar: Sophia Mazer

High School: Shaler Area High School, Pittsburgh, PA

Lab: Dr. Vaughn Cooper

Mentors: Dr. Abigail Matela, Colton Siatkowski

Site: Tech Drive X

Background: Biofilms, which consist of bacteria and their extracellular matrix, are essential to microbial life as they assist with bacterial survival and resistance to the immune system, specifically macrophages, during infections. *Pseudomonas fluorescens*, a bacterium similar to the infection-causing pathogen *Pseudomonas aeruginosa*, is capable of producing biofilm under certain conditions, with some mutants exhibiting more biofilm production than others. In this study, an ancestor strain (SBW25) and four high-biofilm-producing mutant strains of *P. fluorescens* were used to determine the rate at which these strains were phagocytosed by *Dictyostelium discoideum*, a slime mold that mimics how a human macrophage would act in the presence of a pathogen.

Methods: The ancestor and mutant strains were plated as confluent lawns on SM/5 agar plates. Filter discs soaked in a *D. discoideum* solution were placed onto the center of the bacterial lawns. Plates were kept at room temperature in a dark and humid environment. Area measurements were first taken after 96 hours, then every 24 hours for a total of four measurements per plate to determine how much bacteria was being phagocytosed per hour. Data were quantified using Fiji software.

Results: The WspF mutant was phagocytosed at the slowest rate, with its average rate being 0.124 cm^2 per hour. The WspA mutant was phagocytosed at the fastest rate, with its average rate being 0.305 cm^2 per hour.

Conclusion: Overall, this study demonstrates that some high-biofilm-producing mutants of *Pseudomonas fluorescens* can more effectively resist phagocytosis by *Dictyostelium discoideum* than others. In understanding these resistance mechanisms and biofilm pathways, the development of more treatments for biofilm-producing infections could be possible. More studies will focus on exploring those resistance mechanisms and exploring ways to work around biofilm resistance in both *P. fluorescens* and *P. aeruginosa*.

Investigating the oncogenic effects of EPHA3d4-5 in HGSC and Determining transcription factor signatures to predict treatment outcome in kidney cancer

Scholar: Leni McCann

High School: Mt Lebanon High School, Pittsburgh, PA

Lab: Dr. Xiaosong Wang, MD, PhD

Mentor: Dr. Bashir Lawal, PhD

Site: Cancer Biology

During the summer research period, two distinct projects were conducted, each addressing critical questions in cancer research. Below are the abstracts for these projects:

Project 1: Oncogenic Role of EPHA3 Exon 4-5 Duplication in High-Grade Serous Ovarian Carcinoma: Ovarian cancer, particularly high-grade serous carcinoma (HGSC), remains a significant focus in cancer research due to its status as the deadliest gynecologic cancer. HGSC accounts for 75% of ovarian cancers and most related deaths. Analysis of The Cancer Genome Atlas data reveals that HGSC tumors possess the highest frequency of intragenic rearrangements (IGRs) compared to other tumor types. Notably, a duplication of exons 4 and 5 of the Ephrin Tyrosine Kinase A3 (EPHA3) gene, termed EPHA3d4-5, is present in 8% of HGSC cases. This study aimed to elucidate the oncogenic function of EPHA3d4-5 in cell line models. The OVCAR3 cell line, which expresses EPHA3d4-5, was transfected with siRNAs targeting EPHA3d4-5 and wild-type EPHA3. Subsequent assays, including western blotting, cell viability, migration, and colony formation, were conducted to assess the impact of EPHA3d4-5 knockdown. The results demonstrated that silencing EPHA3d4-5 led to a significant reduction in cell proliferation, migratory capacity, and colony formation, indicating that EPHA3d4-5 contributes to the growth and oncogenic properties of HGSC cells.

Project 2: Predictive Transcription Factor Signatures for Immunotherapy Response in Kidney Cancer: Immunotherapy offers a promising avenue for cancer treatment; however, its efficacy varies among patients, with some experiencing adverse effects. This project aimed to identify transcription factors that could predict patient responses to treatment with atezolizumab, atezolizumab combined with bevacizumab, or sunitinib, in kidney cancer. By analyzing data from kidney cancer patients, we identified specific transcription factor signatures associated with sensitivity or resistance to these therapies. These predictive signatures could help forecast patient response prior to treatment, potentially allowing for more personalized therapeutic strategies and reducing the likelihood of unfavorable outcomes.

Characterizing Drp1 00/00 Variant Mouse Embryonic Fibroblasts (MEFs)

Scholar: Addison McLane

High School: Seneca Valley Senior High School, Harmony, PA

PI: Nadine Hempel, PhD

Mentor: Ya-Yun Cheng, PhD and Sierra White, PhD

Site: Women's Cancer Research Center

Background: Mitochondria are an organelle responsible for multiple jobs within the cell, including energy production and cell death regulation, and are essential for proper cellular function and survival. Fusion and fission dynamics determine the shape and size of the mitochondria, which is linked to its function and regulation; Dynamin Related Protein 1 (Drp1) is the protein that facilitates this process, therefore Drp1 is an essential protein. Splice variants of Drp1 exist that localize to different areas within the cell and differentially affect fission capacity, which is why different variants of the protein may impact mitochondrial functions and cell behavior. The splice variants that are of interest to our project are those relating to exons 16 and 17 in the variable domain of the protein. Patients with ovarian cancer containing high levels of Drp1 that lack exon 16 have a significantly decreased survival rate. The absence of exon 16 increases mitochondrial fission and enhances cancer cell proliferation. This brings to question whether there is a functional difference to the Drp1 splice variants. The different variants aren't widely studied, and we would like to further our understanding about what mechanisms the different Drp1 splice variants control through the use of Mouse Embryonic Fibroblasts (MEFs) isolated from genetically engineered mice lacking exon 16 and 17 of Drp1. The aim is to characterize the expression of fusion and fission markers, and determine if expression is altered by presence of only one specific Drp1 splice variant lacking exons 16 and 17.

Methods: Protein lysates from Wildtype (WT), homozygous lacking exons 16 and 17 (00/00), and heterozygous (WT/00) MEFs were extracted and quantified using a Bradford Assay. Western Blot procedure was followed to detect and identify differences in expression for the marker proteins of mitochondrial fusion and fission, including MFN1, MFN2, MFF, and OPA1, as well as markers of autophagy (necessary for clearance of damaged mitochondria through mitophagy) P62 and LC3B, and the stress marker ATF4.

Results: Based on preliminary data, changes for the expression of OPA1 and P62 have been observed in homozygous MEFs compared to WT MEFs. There was no change detected in expression for the markers we tested here between the heterozygous WT/00 and wildtype cells.

Conclusion: The absence of exons 16 and 17 in Drp1 relates to a shift in expression of certain fusion and fission markers in MEFs, suggesting a change in mitochondrial dynamics and regulation of autophagy.

Validating the Knockdown of the Protein SLC38A3 in Ovarian Cancer Cells

Scholar: Ava Miller

High School: Plum Senior High School, Plum, PA

Lab: Katherine M. Aird, PhD

Mentor: Amandine Amalric, PhD

Site: Women's Cancer Research Center

Background: Ovarian cancer presents with non-specific symptoms that lead to the majority of cases being diagnosed late stage. OVCAR8 is one of the human ovarian cancer cell lines that exhibits similar features to high-grade serous ovarian carcinoma (HGSOC). HGSOCs are the most common form of epithelial ovarian cancer and are often chemoresistant. Chemoresistance has a direct correlation to over 70% of ovarian cancer deaths. The mechanisms that make OVCAR8 chemoresistant are multifactorial, and therefore allow insight into the complex phenomenon of chemoresistance in ovarian cancer. Dr. Amandine Amalric's project is to assess whether the protein SLC38A3 is involved in chemoresistance in ovarian cancer. The specific protein SLC38A3 (Solute Carrier Family 38 Member 3) serves as a carrier of amino acids, and it is located in the plasma membrane of the cell. I will be validating that there is a decrease in SLC38A3 protein level after knockdown of SLC38A3 in ovarian cancer cells.

Methods: I performed Western Blot experiments. This is a routine technique for protein analysis. I took the proteins, denatured them and gave them all negative charges. Then I loaded the proteins into a well atop an acrylamide gel, and ran an electrical current through the gel, this moved the proteins to the bottom. In addition to the proteins I ran a 'ladder'. A 'ladder' is a solution that is designed to estimate protein molecular weight. These results from the gel were transferred to a membrane that allowed them to be analyzed. I then compared the signal for SLC38A3 of shSLC38A3 to the shCONTROL OVCAR8. In this context, SLC38A3 knockdown should show a decrease in SLC38A3 protein level.

Results: The results of the Western Blots were observed through chemiluminescence detection. The bands for SLC38A3 are compared, shSLC38A3 to the control. There was a decrease in SLC38A3 protein level was observed in shSLC38A3 compared to the OVCAR8 control.

Conclusion: When comparing the two shSLC38A3 samples to the control, significant knockdown could be seen. These experiments show that SLC38A3 level has been decreased in the OVCAR8 cell line using shRNA targeting SLC38A3. This is the validation we needed before treating the cells with cisplatin (chemotherapy) to assess the chemoresistance of SLC38A3 knockdown cells compared to the control cells.

Site-Directed Mutagenesis of Synonymous-Like Nonsense Mutations in Alpha-1 Antitrypsin

Avery Mills[1,2], Warren van Loggerenberg[3], Kirby Fawcett[3], Andrew Pilat[3], Keisuke Ishihara[3], Frederick P. Roth, PhD[3]
[1]The Ellis School, Pittsburgh, PA; [2]Hillman Cancer Center Academy, University of Pittsburgh, Pittsburgh, PA and [3]Computational and Systems Biology, University of Pittsburgh, Pittsburgh, PA

Abstract A scalable human-cell-based fluorescence assay for Alpha-1 antitrypsin (AAT) variant function has been used to measure the impact of all possible AAT amino acid substitutions, thus providing a comprehensive variant effect (VE) map[1]. Interestingly, we observe nonsense variants towards the N-terminus of AAT to act synonymous-like. Here, we use site-directed mutagenesis to confirm our map results and investigate sequence-structure-function-relationships that might govern use of an alternative translation initiation site.

Introduction AAT is encoded by the gene *SERPINA1* and is primarily secreted by hepatocytes[1]. Genetic variation in AAT can cause Alpha-1 antitrypsin deficiency (AATD), the most common genetic disorder in caucasians (affecting ~1 in 2500 individuals), resulting in liver and lung disease. While sequencing is a first line diagnostic tool, it remains challenged by the difficulty of distinguishing tolerated from damaging variants, leaving most interpreted as variants of uncertain significance (VUS). To address the VUS problem and sequence-structure-function relationships, we previously measured nearly all AAT amino acid substitutions and generated a comprehensive "variant effects map". Interestingly, we observed nonsense protein-truncating variants at the N-terminus to be synonymous-like, supporting a recent report of an alternative translation initiation site (Met82)[3]. Because the assays are based on the expression of mature cDNA from a 'landing pad' in the AAVS1 locus of HEK293T cells, our 5'UTR length is consistent, which refutes previous suggestion that length of the 5'UTR controls the proportion of non-secretory AAT isoform[1]. Here, we use site-directed mutagenesis and a human-cell-based fluorescence assay to investigate the impact of nonsense variants at the N-terminus of AAT to elucidate the mechanism of alternative translation initiation.

Methods Sequencing data from multiplexed assays of variant effect was processed using the TileSeq analysis pipeline to generate variant effect (VE) maps. In brief, we quantified variant allele frequencies of non- and select conditions using TileSeq_MutCount, which incorporates Bowtie2 for aligning paired sequencing reads to the reference template[2]. Next, we generated a score for each variant using the tileseqMave pipeline. A "high" and "low" map were generated, the former reporting enrichment of aggregating variants and the latter degradation (Figure 1). We selected 3 nonsense variants (amino acid (AA) position 15, 32, and 40) that appeared synonymous-like and 2 (61 and 70) nonsense variants with deleterious scores from the map for site-directed mutagenesis. To this end, we designed pairs of forward and reverse 5'-phosphorylated primers. AAT template DNA was diluted, and a polymerase chain reaction (PCR) setup for each variant consisting of DNA template, primers, 2X Phusion Master Mix (New England Biolabs), and PCR H_2O. Gel electrophoresis confirmed that the anticipated product was amplified (Figure 2A.), and the PCR products were treated with DpnI to remove excess template DNA. Next, we circularized the amplified products using T4 DNA Ligase (New England Biolabs) and made a solution with the ligase buffer, DpnI-treated DNA, H2O, and DNA ligase. After incubation, we transformed the ligation mix into NEB DH5alpha chemically competent *E. Coli* cells (Figure 2B). Transformants were then plated on LB-Ampicillin agar and grown overnight. Single colonies for each variant were selected and grown overnight in LB-Ampicillin media. Plasmids were purified using the QIAprep Spin Miniprep Kit (QIAGEN), and each variant was sequenced and verified (Plasmidsaurus).

Results To further evaluate sequence-structure-function relationships for AAT, we reassessed sequencing results from multiplexed human-cell-based fluorescence assays with the previously described TileSeq pipeline and performed site-directed mutagenesis. We unexpectedly observed nonsense variants upstream of AA position 40, for both high and low AAT abundance maps, to be tolerated. Site-directed mutagenesis by PCR amplification of 3 nonsense variants with tolerated (AA15, AA32, AA40) and 2 with deleterious (AA61 and AA70) scores resulted in the expected length 6630bp. Initially, we observed non-specific amplification for PCR reactions of AA15 and AA70. However, increasing the annealing temperature by 7°F reduced this off-target amplification. After cloning, sequencing revealed fragmentation of the AA61 and AA70 constructs, possibly due to error in circularization during enzymatic ligation of the amplified products.

Discussion Here, we re-evaluated the functional impact of nearly all missense variants of AAT in the human population on a VE map and identified nonsense variants that were reported as tolerated on the map towards the N-terminus. Site-directed mutagenesis was successfully used to generate 3 tolerated nonsense variants (AA15, AA32, and AA40), which support use of a previously suggested alternative translation initiation site (Met82) in AAT[3]. One major caveat is that these nonsense variants may only rule out experimental noise observed in our map. Thus, we are proceeding to generate deletions in the AAT region upstream of amino acid position 40, and will evaluate AAT abundance for all variants — nonsense and deletions — in a human-cell-based fluorescence assay.

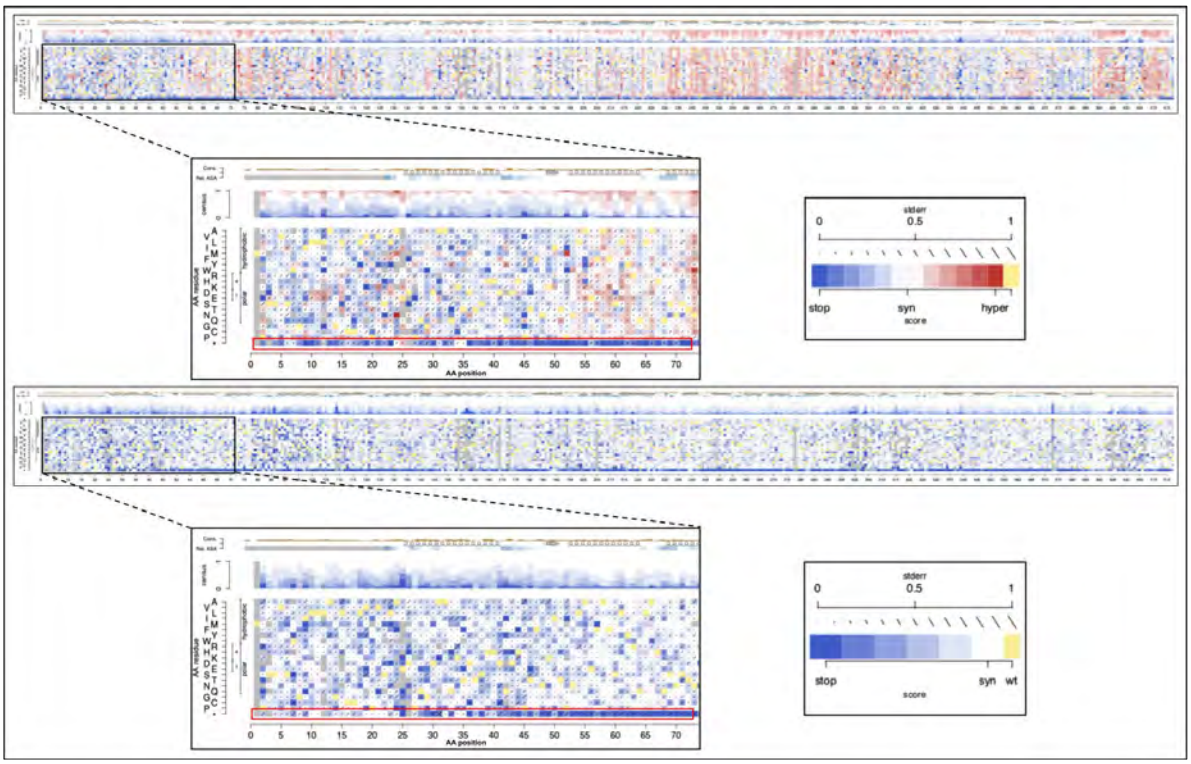

Figure 1. AAT Variant effects maps. Near full functional impact landscapes for AAT. Mutations leading to loss of abundance are shown in blue and tolerated in white. Yellow fields indicate the wildtype amino acid at each position. Red corresponds to polymerization propensity, and gray fields indicate missing data. Expanded view shows the N-terminus of both maps, where nonsense (bottom track) appears tolerated.

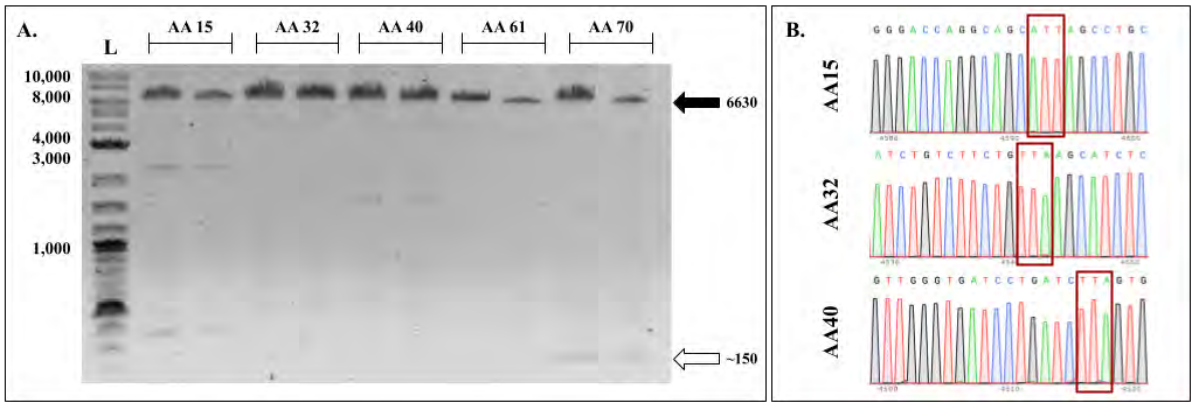

Figure 2. Site-directed mutagenesis for nonsense variants of AAT at the N-terminus. A) PCR amplified products run on 0.8% agarose gel containing a 10X concentration dye. Lane L represents the template DNA ladder in base pairs (bp). The expected length of each variant is 6630 bp, marked by the black arrow. Non-specific off-target amplification in variant AA70 is marked by the white arrow. **B)** Chromatogram results of extracted plasmid from transformed DH5Alpha cells. Variants AA15, AA32 and AA40 showed stop codon insertion at the predicted nucleotide positions.

References

1. W. van Loggerenberg, *man. in prog.*
2. Weile J, Sun S, Cote AG, Knapp J, Verby M, Mellor JC, Wu Y, Pons C, Wong C, van Lieshout N, Yang F, Tasan M, Tan G, Yang S, Fowler DM, Nussbaum R, Bloom JD, Vidal M, Hill DE, Aloy P, Roth FP. A framework for exhaustively mapping functional missense variants. Mol Syst Biol. 2017 Dec 21;13(12):957. doi: 10.15252/msb.20177908. PMID: 29269382; PMCID: PMC5740498.
3. Maslakova AA, Golyshev SA, Potashnikova DM, Moisenovich AM, Orlovsky IV, Smirnova OV, Rubtsov MA. SERPINA1 long transcripts produce non-secretory alpha1-antitrypsin isoform: In vitro translation in living cells. Int J Biol Macromol. 2023 Jun 30;241:124433. doi: 10.1016/j.ijbiomac.2023.124433. Epub 2023 Apr 21. PMID: 37086761.

Title: Mesenchymal Stem Cell-Derived Extracellular Vesicle effect on Endothelial Colony-Forming Cells

Scholar: Angie Odeniyi

High School/College/City/State: Roy C. Ketcham Senior High School, Wappingers Falls, NY

PI of group/lab: Justin Weinbaum, PhD

Mentor(s): Amanda Pellegrino

Site: Technology Drive X

Background: Tissue-engineered vascular grafts (TEVGs) are a promising alternative to occluded blood vessels. Within these grafts lie endothelial cells (ECs), impersonating the endothelium layer of blood vessels. The formation of an endothelial cell monolayer on a graft is called endothelialization. This is especially notable in a mechanism known as fallout endothelialization, where the endothelial colony forming cells (ECFCs) attach, differentiate to ECs, and grow to form a monolayer on TEVGs. Various ways to differentiate ECFCs into endothelial cells have been studied, including shear stress and vascular endothelial growth factor (VEGF). Mesenchymal stem cell-derived extracellular vesicles (MSC-EVs) are nanoparticles secreted from parent cells that contain proteins and RNA. These EVs contain VEGF, which is known to spark differentiation along with proliferation and migration of cells. This study investigates the differentiation of ECFCs into ECs with the implementation of MSC-EVs.

Methods: Micro bicinchoninic acid assays (BCA) were run for quantifying proteins in MSC-EVs. Immunofluorescent staining assays were run to identify specific antibodies in three separate groups: the ECFCs with and without EVs, and the ECs. Western blotting was used to determine the specific proteins in the ECFCs and the ECs. 2-D tube formation assays on collagen gel were used as functional assays to observe the number of tubes formed by the cells and the rate at which they formed.

Results: MSC-EVs demonstrated little to no protein in the microBCA. Immunofluorescent staining of the ECFCs and ECs showed a presence of von Willebrand factor (vWf) and CD34, but not a significant amount of CD31. ECs showed slight tube formation via 2-D tube formation assay, but neither ECFC groups showed any tube formation. A BCA on cell lysates showed protein used for western blot. The western blot showed the presence of VEGF-2 receptor (KDR), but not CD34 or vWf.

Conclusion: The study does not distinctly show that our hypothesis was supported, as the data varies across the three groups. There is no direct similarity between the ECFC + EV and the EC group in the 2-D tube formation assay and the immunofluorescent staining. Therefore, this study will need to be investigated further. One method is to increase EV dosage since there was little to no protein in the microBCA for the dosage used, and another method is to use a different experimental approach, such as flow cytometry.

Title: Using Escherichia coli for nanobody production

Scholar: Tara Olaniyan

High School: Science and Technology Academy, Pittsburgh, PA

Lab: Matthew L. Wohlever, Ph.D.

Mentor: Megan Monroe

Site: COSBBI

Background: Antibodies are one of the most prevalent tools in modern biological research due to their robust and specific binding ability. While antibodies are naturally produced by the immune system, the process is slow and costly. Nanobodies, which are small fragments of antibodies that retain the key binding characteristics, are an attractive alternative to antibodies as the smaller size allows them to be produced in *E. coli* rather than in animals, thus saving time and money. Here, we produced nanobodies against the ALFA tag, a synthetic epitope common in cell biology research. To aid visualization of the nanobody/ALFA tag complex, we fused it to Green Fluorescent Protein (GFP).

Method: E. coli cells were used to express three types of anti-ALFA-tag nanobodies that have fluorescent tags. Competent cells were transformed with our nanobody plasmid. Cultures were induced to produce nanobodies. Then to purify the protein, we use columns that have resin that select our tagged proteins. Western blots were then used to validate that our nanobodies can recognize ALFA-tagged proteins.

Results: After the protein purification process, we could isolate the proteins needed for the nanobody production. Then, we verified them using a Western blot.

Conclusion: We successfully used E. coli cells to produce nanobodies in this study. Using a western blot, we confirmed the presence of the nanobodies. Using technology, we have an inexpensive method to produce nanobodies for research.

Title: Effects of RanBP2 on Mx2-Mediated Inhibition of Specific Nuclear Import Pathways
Scholar: Oluwatobiloba Olaore
High School: Pittsburgh CAPA, Pittsburgh, PA
Lab: Kane Lab
Mentor: Melissa Kane, PhD
Site: Immunology and Cancer Immunotherapy

Background: Mx2 is an interferon-stimulated protein that localizes to the nuclear pore complex (NPC), and inhibits human immunodeficiency virus (HIV-1) infection. RanBP2 is a component of the NPC; it consists of eight filaments that project from the NPC into the cytoplasm and serves as docking platforms for nucleocytoplasmic transport receptors. Previous research demonstrates that RanBP2 is involved in HIV-1 infection, and it is suggested to interact with Mx2. This study focuses on understanding whether mutations in RanBP2 affect Mx2's ability to localize to the NPC, inhibit HIV-1, and whether it prevents certain nuclear localization signals (NLS) from entering the nucleus.

Methods: We conducted the experiment on four different HT1080 cell lines; three clones of mutated ΔC915 (cells that have a deletion of RanBP2 up until the kinesin binding domain) and one control cell line. Each of the four cell lines were transduced with 11 different NLS that were attached to a GFP-lacZ protein. Then, doxycycline was added to half of the cells to induce Mx2. Subsequently, the cells were fixed and stained with Hoechst and HCS CellMask for imaging of the nucleus and cytoplasm. Using automated imaging and flow cytometry, we determined the GFP signal localization and intensity in the cells.

Results: Our results show that mutation of RanBP2 significantly affected nuclear import of the Rex and CIRBP NLS. Additionally, we found that Mx2 affected NLS functionality at varying levels. Furthermore, we saw Mx2's ability to inhibit nuclear import decreased in ΔC915 clones.

Conclusion: Our study shows that deletion up until the kinesin binding domain (KBD) from RanBP2 only affects nuclear import for some NLSs. Further research will be done to understand why KBD deletion affected Mx2 inhibition and nuclear import, and to analyze the impact of different deletions on RanBP2 and whether it further alters nuclear import and Mx2's inhibition of HIV-1.

Title: Corneal Autophagy

Scholar: Jay Olawaiye

High School/College/City/State: Quaker Valley High School, Pittsburgh, PA

PI of group/lab: Dr. Yuanyuan Chen

Mentor(s): Gary Yam, Mithun Santra

Site: Biology and Translational Medicine in VISION site

Background: A healthy cornea transmits and refracts light for normal vision. Various injuries cause the following: Corneal damage with inflammation and fibrosis, and opacities that compromise corneal clarity, resulting in vision loss. Our lab demonstrated that corneal stromal stem cell (CSSC) treatment inhibits opacity development in injured mouse corneas, through suppressing inflammatory and fibrotic responses. Autophagy is a process that destroys defective cell material and is fundamental for cell and tissue recovery. My work investigated whether CSSC treatment restored corneal functions and clarity via modulating the autophagy response.

Methods: cDNA samples from *in vivo* CSSC treatment studies were assayed for autophagy-associated gene expression using specific primers targeting ATG5, Beclin1, and LC3B. Mouse samples included naïve corneas (n=3), injured corneas, and injured corneas treated with CSSCs were examined for autophagy and fibrosis gene expression. A mixture of 5ng cDNA, specific forward and reverse primers (0.125uM each), and SYBR Green RT master mix was amplified in a QuantStudio3 RT PCR System. Rapamycin (an autophagy inducer) was used as a positive control. RNA abundance was determined with the ddCT method, normalized with 18S, and fold changes were expressed as mean±SD compared with injured controls. Statistical significance was determined using the Mann-Whitney U test.

Results: The injured mouse corneas showed reduced expression of fibrosis associated genes after 14 days of CSSC treatment; however, there were insignificant changes in expression of ATG 5 Beclin 1 and LC3B ($P>0.05$, Mann Whitney U-test), when compared to the injury only control group.

Conclusion: My work presents a pilot study indicating that autophagy was not involved as a mechanism in the corneal clarity improvement after CSSC treatment. Further assays are required to validate this.

1G9 Anti-CEACAM5 Antibody: Targeting Cancer Cells with Precision

Scholar: Kaushal S. Patel

High School: South Fayette High School, McDonald, Pennsylvania

Lab: Jessie Nedrow, PhD

Mentor: Abhinav Bhise, PhD

Site: Cancer Biology

Background: CEACAM5 is a tumor-associated protein found in a variety of gastrointestinal cancers and is a target for imaging and therapeutic applications in CEACAM5-expressing tumors. Based on a newly identified anti-CEACAM5 antibody (1G9), we generated conjugated antibodies and modified them for zirconium (III) chloride cold labeling to create anti-CEACAM5 antibody PET tracers. The focus of this study was to assess whether modifications of anti-CEACAM5 antibodies would provide high-affinity PET and radiotherapeutic agents.

Methods: The antibody conjugation was composed of a 100-200 µL carbonate buffer that was incubated at 37ºC for 60 minutes and the antibody-DFO solution. The concentrations used for SPR (Surface Plasmon Resonance) were 100 nM, 50 nM, 25 nM, 12.5 nM, 6.25 nM, and 3.125 nM. Each concentration was made with the 1G9 antibody and diluted with an HBS buffer. SPR was used to determine the dissociation constant (K_D).

Results: The results demonstrated that the modified 1G9 antibodies retained high specificity and affinity for CEACAM5. A significant difference between the modified antibody and unmodified antibody was not observed. Accordingly, the graphs that illustrated the pharmacokinetics of a modified antibody and an unmodified antibody looked similar.

Conclusion: These findings suggest that modified 1G9 antibodies are promising candidates for the development of targeted imaging and therapeutic agents for CEACAM5-positive cancers. Further clinical evaluation is warranted to assess their potential in improving cancer diagnosis and treatment outcomes.

Evaluating Statin Prescription Patterns for Secondary Prevention in ASCVD Patients: Insights from the All of Us Dataset

Daniel L. Perez[1], Olga V. Kravchenko, PhD[2]

[1]Holy Ghost Preparatory School, Bensalem, PA; [2]University of Pittsburgh, Pittsburgh, PA

Abstract

We conducted exploratory analysis to investigate how racial factors may influence statin prescription patterns in the ASCVD patients using All of Us cohort. We found that Asian and Middle Eastern or North African patients were less likely to receive high-intensity statins than other groups, while Black or African American patients were more likely to be on a high intensity statin.

Introduction

Atherosclerotic cardiovascular disease (ASCVD) is a set of conditions caused by progressive buildup of plaque in arterial walls that can restrict blood flow by narrowing the arteries and lead to serious cardiovascular events such as heart attacks or strokes. These conditions include coronary heart disease (CHD), cerebrovascular disease, peripheral artery disease, and aortic atherosclerotic disease. ASCVD is a major contributor to cardiovascular morbidity and mortality worldwide and is a primary focus for preventative strategies (1,2).

Primary prevention of ASCVD aims to prevent or delay the onset of disease in at-risk individuals, while secondary prevention targets those who have already experienced a cardiovascular event to prevent recurrence. For individuals with ASCVD, high-intensity statins are recommended for aggressive lipid control, to lower LDL cholesterol levels, prevent further plaque buildup and to reduce the risk of subsequent heart attacks and strokes (3).

Prior studies have shown that many patients with ASCVD do not receive guideline-recommended statin therapy and have suggested disparities in statin prescribing practices across different racial and minority groups. This work focuses on secondary prevention, aiming to evaluate statin prescription patterns among ASCVD patients to identify potential disparities in prescribing practices.

Methods

We conducted a retrospective cohort study using the All of Us dataset. All of Us is a comprehensive database that contains healthcare records from a diverse group of participants across the United States. It includes demographic details, electronic health records, genomic data, survey responses and other factors. The study cohort consisted of patients diagnosed with ASCVD, defined according to the American Heart Association criteria. Included in the cohort were individuals 18-75 y.o. who had

LDL cholesterol levels available and had one or more of the following conditions: coronary arteriosclerosis, myocardial infarction, angina pectoris, coronary artery stenosis, cerebrovascular disease, transient cerebral ischemia, ischemic stroke, silent myocardial ischemia, acute coronary syndrome, peripheral arterial disease, intermittent claudication, abdominal aortic aneurysm, and aneurysm of descending thoracic aorta. The cohort was further categorized based on intensity of statin therapy (none, low/moderate, or high intensity).

We have used descriptive statistics to summarize the demographic and clinical characteristics of the study cohort. To investigate potential disparities, we performed chi-square tests to compare the proportions of

patients prescribed high-intensity statins across demographic groups, focusing on race and gender. Additionally, we employed logistic regression to further examine factors influencing statin prescription intensity.

Results

There was a total of 26854 people in the cohort, 44% male, 53% female, 1.5% identified as gender minorities. The race distribution was 51.6% White, 25.1% Black or African American, 15.4%, 1.7% Asian, 1.4% More than one population, 0.5% Middle Eastern or North African. In terms of statin use, 44.0% of the cohort have not been taking any statin, 30.9% were taking high intensity statin, and 25.1% were on low/moderate intensity statin regimen.

The chi-square test results for selected races (Asian, Black or African American, Middle Eastern or North African, Native Hawaiian or Other Pacific Islander) among individuals 75 or younger showed a significant association between race and high-intensity statin prescription patterns, $\chi^2(6, N = 26,854) = 61.24$, $p < .001$. Specifically, Black or African American patients were more likely to be prescribed high-intensity statins, while Asian and Middle Eastern or North African patients were less likely to receive high-intensity statins compared to other racial groups.

Discussion

Our analysis showed that Black or African American patients were more likely to be prescribed high-intensity statins, while Asian and Middle Eastern or North African patients were less likely to receive high-intensity statins compared to other groups. Native Hawaiian or Other Pacific Islander patients showed mixed results. The finding that Black or African American patients were more likely to receive high-intensity statins compared to White patients was surprising, given that prior studied indicated the opposite. One possibility is that our analysis considered only the latest prescription date, which may occur when a patient has a more advanced form of the disease, leading to more aggressive treatment. Additionally, the All of Us dataset may not be fully representative of the general population. As well, participants in the All of Us cohort are generally more actively engaged with their health. Further research is necessary to understand these factors and ensure equitable statin therapy across all racial groups.

References

1. Cardiovascular diseases (CVDs) [Internet]. [cited 2024 Jun 26]. Available from: https://www.who.int/news-room/fact-sheets/detail/cardiovascular-diseases-(cvds)

2. Secondary Prevention- Clinical ASCVD | Clinical Guidance [Internet]. [cited 2024 Jul 29]. Available from: https://www.healio.com/clinical-guidance/lipid-management/secondary-prevention-clinical-ascvd-cardiovascular-disease-prevention

3. Frank DA, Johnson AE, Hausmann LRM, Gellad WF, Roberts ET, Vajravelu RK. Disparities in Guideline-Recommended Statin Use for Prevention of Atherosclerotic Cardiovascular Disease by Race, Ethnicity, and Gender. Ann Intern Med. 2023 Aug 15;176(8):1057–66.

Augmented Reality used in Medicine

Scholar- Joshua A. Petit-Homme

High School- Pittsburgh Central Catholic High School

Lab- Jacob T. Biehl, PhD

Mentors- Jacob T. Biehl, Shovan Bhatia, Michael Kann, Edward Andrews

Site- CosBBI

Augmented Reality is the real-time integration of digital information into a user's environment or adding layers of virtual objects to a real environment. Augmented Reality is used in medicine to eliminate room for error mainly through planning operations, physicians can visualize/overlay images of patients veins, arteries, bones, tumors, and more in a real world view. Currently the majority of its use goes into the education of med students/residents by creating simulations of procedures.

The methodological approaches I used were observational studies and surveying of literature. I had the opportunity of shadowing different surgeries to better understand workflows in the operating room, and to figure out what AR technology could make physicians jobs easier. The observations will be used to synthesize potential AR tools that can be used in an OR setting. These will then be presented to physicians to receive feedback. I also created an annotated bibliography of papers detailing prior and current use of AR in medicine.

I found that the technology works well in aiding surgeons in mapping out procedures. In STA-MCA Bypass procedures done at UPMC Mercy and Presbyterian the Surreality Lab used the technology to overlay a CT scan over the patients head. The technology needs a good wifi signal which isn't always present in the OR. There is currently only 1 headset that can be used in the OR which needs a computer of some sort to operate. The battery only lasts around 2 hours, and there is no current chemistry that could be used to extend the battery life. To be used in surgery it needs FDA approval and the patients consent, since it's still considered experimental.

The technology has its pros and cons, but will likely be very prominent in the STA bypasses relatively soon as well as other procedures.

Spatial Analysis of CD200 in High Grade Serous Ovarian Cancer

Anabella Phelps, Caroline Sweeney, Rufiaat Rashid, Tullia C. Bruno
Mt. Lebanon High School, PA; University of Pittsburgh Hillman Cancer Center Academy, Pittsburgh, PA

Abstract *The CD200/CD200R axis can be linked to the under development of tertiary lymphoid structures (TLS) in ovarian tumor tissue because of the interaction between cancer-associated mesenchymal stromal cells (CA-MSCs) and B cells that express CD200 and CD200R, respectively. immunohistochemistry was performed on multiple tissue samples to examine differences in CD200 expression and distribution.*

Introduction Being one of the most aggressive yet common epithelial ovarian cancer subtypes, high grade serous ovarian cancer (HGSOC) can rapidly metastasize, leaving its 5-year survival rate at 48% [2]. A key component to immune cell infiltration and activation lies in the organization of immune cells within tumors, and specifically, within sophisticated cellular neighborhoods known as tertiary lymphoid structures (TLS). Acting as a hub for B cell and T cell activation and proliferation, the presence of TLS with germinal centers (GC) has shown prognostic benefit in ovarian cancer patients [3]. Our spatial analyses across HGSOC anatomical sites have shown that tertiary lymphoid structures in ovarian tumors are less developed and active than in omental and fallopian tissue. Precursor stromal cells known as mesenchymal stem cells (MSCs), are paramount for optimal TLS function. However, through epigenomic reprogramming within the tumor microenvironment, normal MSCs can become cancer educated, resulting in the cancer-associated MSCs (CA-MSCs), resulting in poor prognosis and immunosuppression [2]. While the transition from MSC to CA-MSC is not fully understood, bulk RNA sequencing data from our lab has shown that it could be coordinated by the molecule CD200. The CD200 and cognate receptor CD200R checkpoint molecule pathway show similar structure to immunoglobulin family members (PD1-PDL1, CTLA4-B7) that play important roles in regulating tumor-specific immune responses [1]. CD200 is mor highly expressed by CA-MSCs and we have recently demonstrated that its gene expression is much higher in CA-MSCs from HGSOC patients with ovarian tumors. Thus, we have hypothesized that the CD200-CD200R axis expressed by CA-MSCs and B cells may play a role in the lack of TLS formation and antitumor activity within HGSOC solid tumors. Modulating this axis may promote a hospitable stromal compartment, allowing for its potential as a therapeutic to be further ratified.

Methods In order to test the potential of CD200 as a therapeutic, it was important to know where CD200 is both spatially in ovarian tumors and in what cell types. To analyze CD200 spatially in ovarian tumors, we performed immunohistochemistry on ovarian (14 slides), omentum (15 slides) and fallopian tube (8 slides) tissue slides; tonsil tissue slides were used as a positive control. Slides were first deparaffinized and then antigen retrieval was performed in EDTA buffer. Primary and secondary antibody was then applied. The slides were subsequently imaged at a 10X magnification on the Keyence and analyzed using Qupath.

Results Analyzing the trend of all 37 tissue sample slides, CD200 expression on ovarian tumor tissue samples displayed the highest cell count of positive cells with a mean value of 2251.96 positive cells per mm^2. Comparatively, omental tumor tissue samples displayed a mean value of 1399.79 positive cells per mm^2. CD200 positive cells in fallopian tumor tissue samples showed a mean value of 1469 positive cells per mm^2. Although these results are statistically insignificant, the trend shown may eventually become statistically significant with a greater tissue sample size.

Discussion The data from this immunohistochemistry analysis can be used as preliminary information to future studies surrounding the opportunity of the manipulation of the CD200/CD200R axis as a potential therapeutic against HGSOC. Further studies through multispectral immunohistochemical staining and flow cytometry can confirm the protein levels of CD200 and its receptor on respective CA-MSCs and B cells s, allowing the modulation of the stroma into a hospitable compartment and increasing the efficacy of immunotherapies.

References

1. Liu, J. Q., Hu, A., Zhu, J., Yu, J., Talebian, F., & Bai, X. F. (2020). CD200-CD200R Pathway in the Regulation of Tumor Immune Microenvironment and Immunotherapy. *Advances in experimental medicine and biology*, *1223*, 155–165. https://doi.org/10.1007/978-3-030-35582-1_8
2. MacFawn, I. P., Magnon, G., Gorecki G., Kunning S., Rshid R., Kaiza E. M., Atiya H., Ruffin T. A., Taylor, S., Soong, R., Bao, R., Coffman, G. L., Bruno C. T., (in revision). *The activity of tertiary lymphoid structures in high grade serous ovarian cancer is governed by site, stroma, and cellular interactions*.
3. Nip, Christopher, Leyi Wang, and Chengfei Liu. 2023. "CD200/CD200R: Bidirectional Role in Cancer Progression and Immunotherapy" *Biomedicines* 11, no. 12: 3326. https://doi.org/10.3390/biomedicines11123326

Title: Dose Disparity in Early Stage Breast Cancer Chemotherapy according to Race and Area Deprivation

Scholar: Rose-Carlie Pierre

High School/College/City/State: Obama Academy, Pittsburgh, PA

PI of group/lab: Dr Margaret Rosenzweig

Mentor(s): Dr Margaret Rosenzweig

Site: CoSBBI

Background: Racial survival disparity in breast cancer is present despite improved survival overall. Racial chemotherapy dose inequity may be a contributing factor.

Aims: 1) Describe and compare ESBC (Early-Stage Breast Cancer) chemotherapy received/prescribed (i.e., dose intensity) over time and compare according to race and area deprivation index;

2) Describe and compare the symptom severity and quality of life of women receiving ESBC chemotherapy over time according to race and area deprivation index;

and 3) Describe membership in symptom and quality of life score trajectories according to race, neighborhood deprivation and dose intensity of prescribed chemotherapy.

Hypothesis: Race and neighborhood deprivation, influence symptom incidence and severity during ESBC. This impacts the patient's ability to receive essential ESBC chemotherapy dose intensity.

Design: Prospective, comparative, repeated measures design **Setting:** Eleven medical oncology sites in Western Pennsylvania and Northeast Ohio, South Central, and Southwestern PA

Methods: Frequently repeated assessments, baseline, and pre/post questionnaires for up to 8 chemotherapy cycles of White and Black women. Symptoms measured by PROMIS symptom scoring, Quality of life through the Functional Assessment of Cancer Therapy and the dose of chemotherapy by chart review and calculation.

Results: Data collection August 2017 through June 2022, n=264 patients, 100 Black and 164 White. The mean area deprivation was 62.0±26.7. There were significant differences between Black and White patients and between patients from more versus less deprived neighborhoods for dose intensity of chemotherapy for dose intensity of chemotherapy received.

69.9% of Black patients received less than the benchmark 85% relative dose intensity. Black patients had greater odds of being included in trajectories of high physical symptoms and poor quality of life.

Conclusions: Racial differences in the receipt of breast cancer chemotherapy dose intensity may be important considerations in explaining observed breast cancer racial survival disparitiesand creates actionable targets. Tailored, racially sensitive symptom assessment and management may allow improved symptom management and fewer dose modifications for Black women during ESBC chemotherapy.

IL-4 Therapy Prevents Corneal Damage in Dry Eye Disease

Caroline E. Praveen[1], Alexis Nolfi, BS[2], Clint D. Skillen[2], Mangesh Kulkarni, PhD[2], Bryan N. Brown, PhD[2]

[1]South Fayette High School, Pittsburgh, PA; [2]University of Pittsburgh, Pittsburgh, PA

Abstract

The prevalence of dry eye disease (DED) and the ineptitude of existing treatments prompts investigation into novel therapeutic approaches. Because Interleukin-4 (IL-4) is effective in promoting the expression of pro-regenerative M2 macrophages, we investigated its effect on the cornea to therefore observe its ability to treat dry eye. In a rabbit model, the reduction in dye stained corneal abrasion attests to the potential of IL-4 as a long-term solution.

Introduction

Dry eye disease (DED) affects 344 million globally, stemming from inadequate corneal lubrication due to lacrimal gland inflammation and tear film instability [1, 2] Current treatments, including artificial tears, cyclosporine, and lifitegrast fail to provide complete symptom relief; the tear drops do not address the underlying mechanisms of DED, and the prescription medications are accompanied by a host of adverse effects that ultimately encourage non-compliance. On a cellular level, reduced tear production has recently been associated with an increase in inflammatory M1-like macrophages that target the lacrimal gland [3]. However, the interleukin 4 (IL-4) is a cytokine that induces the polarization of M1 macrophages into the M2 phenotype, which possesses anti-inflammatory and pro-regenerative properties. Therefore, we hypothesized that IL-4 is a pleiotropic cytokine that can be utilized as a long-term treatment for DED. We are using a pre-clinical rabbit model to test our hypothesis.

Methods

To establish a surgical model of DED, the lacrimal gland was removed in 6 New Zealand white rabbits (3.3-3.5 kg), whose corneal dimensions and architecture resemble that of a human [4]. For this study, a baseline assessment of corneal health was performed for 2 rabbits designated for this specific experiment and abstract before the surgery. Given that DED takes 3-4 weeks on average to manifest, we began assessing the corneal damage at 3 weeks post-surgery. At the peak of symptoms, the rabbit corneas were randomly assigned to a treatment vs. control group. For the next two weeks, the treatment group received 1ng of IL-4 (30 µl drops) daily, while the control group was treated with PBS. Corneal abrasion was measured using fluorescein staining under fluorescent light as well as lissamine staining under brightfield. Two to three pictures were taken of each eye with both stains at every assessment. At the end of the experimental period, the stained area in each image was quantified with pixel classification tools in QuPath biomage analysis software. Thresholds were set to classify the intensity of the stain as either medium or high in the fluorescein and lissamine images. Ultimately, these intensities were averaged and presented as percentages of their total corneal area with GraphPad Prism.

Results

As shown in Figure 1, the derived data indicates a decrease in stained area for the IL-4 treated groups. The baseline data presented with minimal staining, consistent with that of a normal cornea. At 4.5 weeks post-surgery, the graphs showed the increased corneal damage expected in the surgical model of DED. Corneal staining intensified in the control group treated with only PBS, as revealed in the R5 Left and R6 Left data groups. In contrast, the IL-4 treated groups (R5 Right and R6 Right) revealed significant decrease in corneal damage during the two weeks of treatment.

Discussion

Analyzing the trends in stained areas between control and experimental eyes demonstrates the efficacy of the IL-4 treatment and aligns with the data from the investigations subjected to the previous four rabbits. The reduction in corneal damage with the IL-4 treatment exemplifies the therapeutic potential of the interleukin in addressing the mechanisms of DED. We are in the process of completing histological assessments to quantify M1 vs. M2 macrophages as well as goblet cells in conjunctival epithelium, and the next steps involve testing controlled release systems for longer term delivery of IL-4.

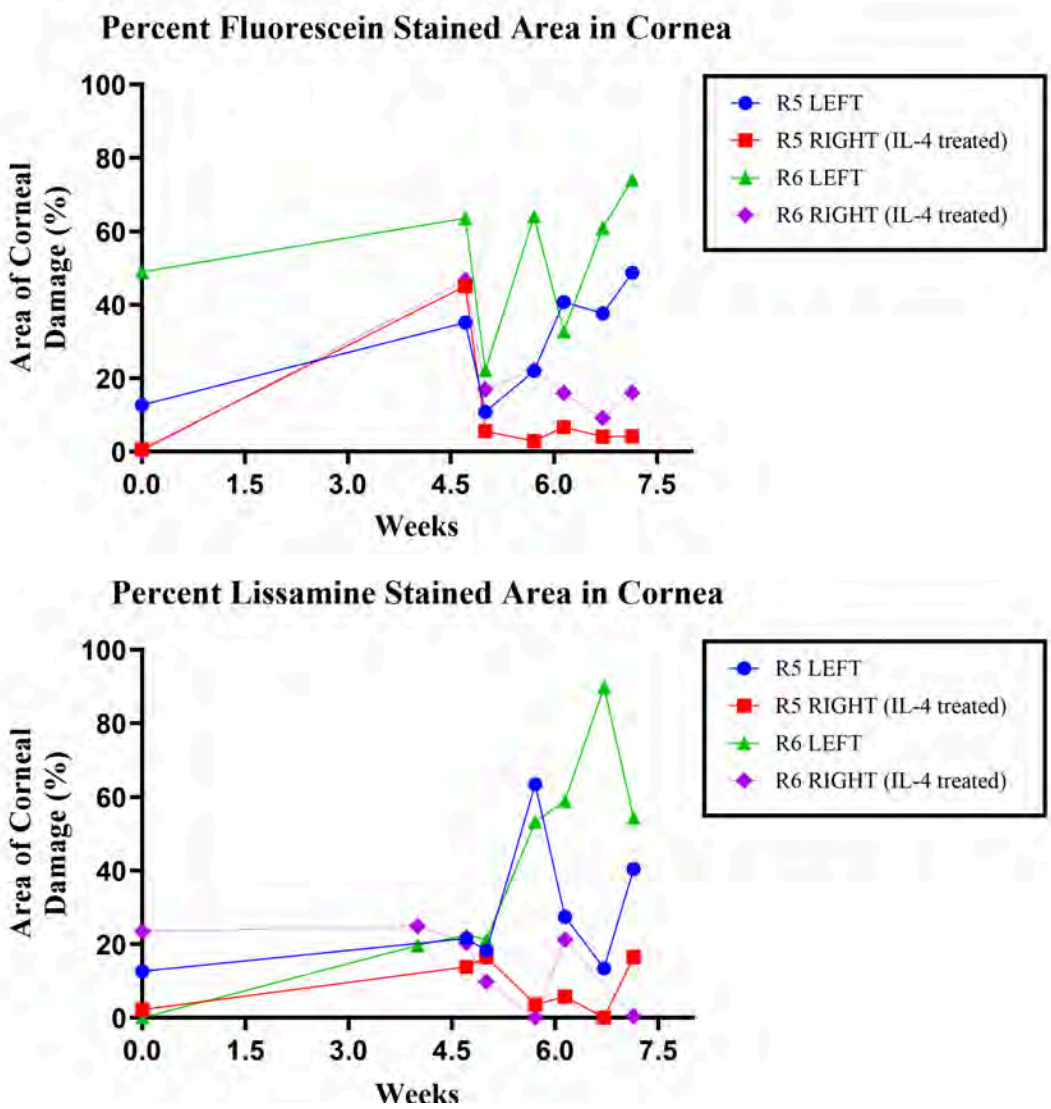

Figure 1. Graphical representations of stained corneal area in fluorescein and lissamine, presented as percentages relative to their total corneal area.

References

1. Messmer, E. M. (2015). The Pathophysiology, Diagnosis, and Treatment of Dry eye Disease. *Deutsches Ärzteblatt International*. https://doi.org/10.3238/arztebl.2015.0071
2. Stapleton, F., Velez, F. G., Lau, C., & Wolffsohn, J. S. (2024). Dry eye disease in the young: A narrative review. *˜the œOcular Surface/˜the œOcular Surface*, *31*, 11–20. https://doi.org/10.1016/j.jtos.2023.12.001
3. Ling, J., Chan, B. C., Tsang, M. S., Gao, X., Leung, P. C., Lam, C. W., Hu, J., & Wong, C. K. (2022). Current Advances in Mechanisms and Treatment of Dry Eye Disease: Toward Anti-inflammatory and Immunomodulatory Therapy and Traditional Chinese Medicine. *Frontiers in Medicine*, *8*. https://doi.org/10.3389/fmed.2021.815075
4. *Centre for Comparative Medicine Research of the University of Hong Kong*. (n.d.). https://ccmr.hku.hk/en/Animals/Animals/Animal-Strains/Rabbit/NZW

Comparing Manual, Semi-Automatic, and Automatic Segmentation for Abdominal Aortic Aneurysm CT Image Sets for Clinical Utility

Scholar: Narendra Ray
PI of group: Timothy Chung, PhD
Mentor: Katherine Kerr
Education: Canon-McMillan High School, Canonsburg, PA
Site: Tech Drive X

Introduction

Abdominal aortic aneurysm (AAA) is when the infrarenal section of the aorta expands. While individuals with AAA can lead normal lives with no complications, AAA can become life-threatening if a rupture occurs. Although surgical intervention can prevent rupture, the usual clinical metric to determine when to operate, maximum diameter, is not reliable as up to 13% rupture before this threshold is met. Morphology has been previously shown to be a strong predictor of AAA outcome. However, it requires the use of manual segmentation, which is quite slow. By employing deep learning to segment AAA computed tomography (CT) image data sets, this flaw can be circumvented. This experiment analyzed the speed and accuracy of three specific segmentation methods: manual (gold standard), semi-automated, and fully automated using a trained deep learning model.

Methods

The three types of segmentation methods was performed on CT scans of the same 15 patients diagnosed with AAA from the Mayo Clinic system (i.e., a total of 45, 15 per group). Manual segmentation used a software called 3D Slicer, where each CT scan was individually traced over using 2D axial slices. The semi-automatic segmentation was implemented using a custom MATLAB script, requiring minimal input from the user. Finally, a Stanford Machine Intelligence for Medical Imaging (MIMI) program called Comp2Comp was utilized to complete the automatic segmentation. Both the manual and automatic segmentations used a separate MATLAB script to convert the images into 3D surfaces (or .stl files), while the semi-automatic MATLAB script would output the surface after manual tracings. Then, we used a program called Autodesk Meshmixer to cut each image down to the region of interest around the aorta.

Results

The automatic segmentation, when compared with manual segmentation, was not statistically different around 70% of the time, as 16 of the 23 categories had p-values above 0.05. Semi-automatic was not statistically different about 35% of the time (8 of 23 categories). Speed-wise, the automatic segmentation finished in about 30-60 seconds, while the semi-automatic segmentation usually took about 2-3 minutes. The manual segmentation, the longest, averaged about 30 minutes per patient.

Conclusion

The automatic segmentation results were more accurate than the semi-automatic results. Part of the reason behind this difference could lie in the highly tortuous structure of each patient's aorta, or in possible human error that may have occurred when the images were being cut down. Both methods can prove to be valuable to clinicians because of their improvements in speed.

Future Directions

This method of analysis could be expanded to a wider range of patients in the future, such as the inclusion of female patients to test if a difference in sex could offer different results. Furthermore, alternative metrics, like biomechanical indices, could be analyzed to further test the similarities of segmentation methods.

Exploring the effects of proto-genes in zebrafish

Scholar: Hussain Raza

High School: Gateway High School, Monroeville, Pennsylvania

Lab: Nathan Lord

Mentor: Nathan Lord

Site: Computational Biology

Background: Proto-genes are protein coding sequences that have emerged *de novo,* and in some cases, are thought to provide a fitness advantage. Recent studies in budding yeast have suggested that many proto-genes encode transmembrane sequences and exert new functions by inserting them into cell membranes. However, it remains unclear whether this membrane insertion capacity is specific to yeast or conserved across phyla. This study's objective was to test whether transmembrane proteins encoded by yeast proto-genes can acquire this localization in the zebrafish.

Methods: We focused on three proto-genes identified in budding yeast by the Carvunis Lab: YBR196C-A, YPR126C, and YLL006W-A. Our plan is to construct N- and C-terminal GFP (Green Fluorescence Protein) fusions of each proto-gene and produce mRNA for zebrafish microinjection by *in vitro* transcription. We will visualize the proto-gene subcellular localization, in which the genes are positioned relative to cellular structures, in the early-stage embryo by microscopy. The localization may change in the earlier stages of embryonic development.

Results: We successfully cloned the proto-gene, YBR196C-A, tagged with GFP. We have subsequently produced mRNA, which is ready for microinjection into the zebrafish embryo.

Conclusion: It is important to study if the function of proto-genes are conserved across various species to better understand their evolutionary significance later. We hope to see if the membrane localization of yeast proto-genes is conserved in zebrafish.

Characterization of Adhesion Properties in SSM3 CDH1 Knockout Cells Representing ILC-like Breast Cancer

Scholar: Ny'Azia Roberts

College: Robert Morris University

PI of group/lab: Lee/Oesterreich Lab

Mentor(s): Insa Thale, PhD, Linda Klei

Site: Women's Cancer Research Center

Background: Invasive lobular carcinoma (ILC) is responsible for 10%-15% of invasive breast cancers and is the second most common type of breast cancer. To enhance the treatment for women with ILC it is important that we understand the differences of ILC compared to other types of breast cancer. One of the most distinctive characteristics of ILC is the loss of E-cadherin, which can be caused by *Cdh1* mutations. E-cadherin is a critical molecule in epithelial cell adhesion that is essential for tissue integrity and function. Without E-cadherin, cell adhesion is disrupted and more likely to have cell invasion, which is associated with cancer progression and metastasis. In general, the ILCs show better prognostic factors than NST cancers, but have a worse long-term outcome. To improve ILC research, we will analyze some characteristics of a newly designed syngeneic mouse cell line. The SSM3 cell line is an estrogen receptor positive (ER+) breast cancer cell line, derived from *STAT1* deficient mice. To mimic ILC like tumors, *Cdh1* was knocked out using CRISPR-Cas9 technology.

Methods: We will characterize how the depletion of Cdh1 in the SSM3 cell line will affect the growth and morphology in 2D environments. ECM adhesion assays were performed using the following cell lines: SUM44, SSM3 Scr, and SSM3 Cdh1 KO. The cells were plated into 96-well plates with the following coatings: Collagen I, Collagen IV, BSA, Fibronectin, Laminin, and an uncoated plate as well. After incubation, plates were imaged before and after washing with PBS, and DNA was quantified using a FluoReporter. Flow Cytometry was used to study apoptosis and cell death.

Results: When analyzing the data we see an increase of cell adhesion in the SSM3 Cdh1 KO cell line. After performing flow cytometry, the data collected shows that there is no significant difference in cell death from the SSM3 Cdh1 KO cell line.

Conclusion: We detect differences in the phenotypes of the cells. A syngeneic mouse line that is ER+ and Cdh1- that mimics ILC will allow researchers to use a critical research tool to study new immunotherapies and endocrine therapies.

Design of a Preliminary Interface for a BRAIN AI System

Alex E. Schafer[1,2,3], Eddie Perez Claudio, MS[4], Harry Hochheiser, PhD[4]
[1] Taylor Allderdice HS, Pittsburgh, PA; [2]Case Western Reserve University, Cleveland, OH; [3]University of Pittsburgh Hillman Cancer Center, Pittsburgh, PA; [4]University of Pittsburgh, Department of Biomedical Informatics, Pittsburgh, PA

Abstract

Clinical decision support systems (CDSS) are the points of contact between a clinician and patient data. The issue with these systems is that any overlooked design can lead to inefficiencies. This project aims to design a usable and transparent BRAIN AI interface for clinicians in the PICU. As a step towards this goal we created a usage scenario and low-fidelity wireframes. Heuristic evaluation showed example-based and supplementary information wireframes to have the lowest severity scores.

Introduction

CDSS is often untested for usability [1], even though there is a direct link between the use of CDSS and patient safety [2] and the misuse of these systems is a frequent cause of medication errors during drug administration [3]. This creates the necessity to create, and sufficiently evaluate, usable and transparent systems for clinicians. Usability: the extent at which a product can be used by users to achieve goals with effectiveness, efficiency, and satisfaction [2] and transparency: the ability of a human to understand factors contributing to a model's behavior [4] could provide a pathway to CDSS that is more trusted by clinicians. These attributes are important when trying to limit automation bias and complacency. By utilizing ideas from the End-User-Centered Explainable AI Framework (EUCA) [5] and heuristic evaluation, we may be able to further understand what a usable and transparent CDSS alert consists of.

Methods

The first step of the project was to create low fidelity wireframes. We utilized each EUCA explanation form: Feature-based, example-based, rules-based, and supplementary information [5]. This helped promote a wide range of offerings for each wireframe. After creating seven wireframes, four heuristic evaluations were done. In the evaluations, the fourteen Nielson-Shneiderman Heuristics brought together by Zhang et al. were used on a 0 to 4 severity scale [6]. After the evaluation, each wireframe was graded by total severity score. Usability problems that violated multiple heuristics only counted once towards total severity score, but all violated heuristics were counted.

Results

The two wireframes with the least total severity score were the example-based and supplementary information wire-frames (Figure 2), having total severity scores of 15 and 16, respectively (Figure 1). The example-based wireframe had an average severity score of 3 over 8 violated heuristics, while the Supplementary information wireframe had an average severity score of 3.2 over 10 violated heuristics (Figure 3).

Discussion

These two wireframes bring light to the differences of how a usable CDSS could look like, it is important to understand that there is not one correct solution when creating these systems. While the example-based wireframe is more quantitative for users that can easily understand numbers at glance, the supplementary information wireframe easier to understand for visual users. The next step of this research is to continue developing both wireframes. The main point of improvement for the example-based design is providing context and a range for the 'typical' column of the data. The main point of improvement for the supplementary information design is clarifying the graph and the axes. These changes will be made alongside the guidance of clinicians in the field. This guidance will help to further develop the usability and transparency of the BRAIN AI model.

Figure 1: Total severity score for all wireframes

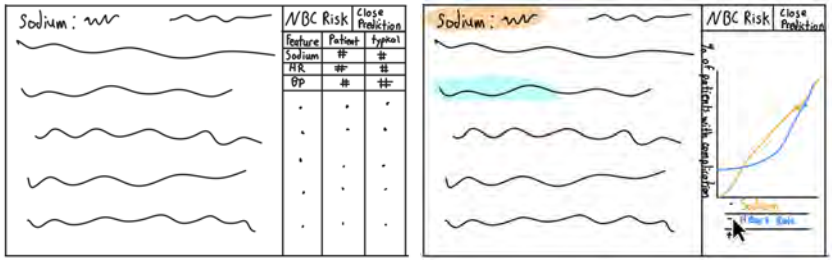

Figure 2: Example-based wireframe (left) and Supplementary information wireframe (right)

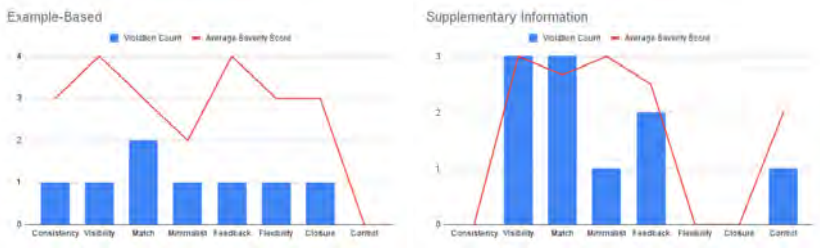

Figure 3: Violation count and average severity score for each heuristic

References

[1] Horsky J, Schiff GD, Johnston D, Mercincavage L, Bell D, Middleton B. Interface design principles for usable decision support: A targeted review of best practices for clinical prescribing interventions. Journal of Biomedical Informatics. 2012 Dec;45(6):1202-16. Available from: https://www.sciencedirect.com/science/article/pii/S1532046412001499.

[2] Guo J, Iribarren S, Kapsandoy S, Perri S, Staggers N. Usability Evaluation of An Electronic Medication Administration Record (eMAR) Application. Applied Clinical Informatics. 2011;02(02):202-24. Publisher: Schattauer GmbH. Available from: http://www.thieme-connect.de/DOI/DOI?10.4338/ACI-2011-01-RA-0004.

[3] Blandford A, Furniss D, Buchanan G, Thimbleby H, Curzon P. Who's looking? Invisible problems with interactive medical devices. Proceedings of the First International Workshop on Interactive Systems in Healthcare. 2010 Apr:4. Available from: http://www0.cs.ucl.ac.uk/staff/dfurniss/Documents/WISH2010-Ann%20Invis.pdf.

[4] Barda AJ, Horvat CM, Hochheiser H. A qualitative research framework for the design of user-centered displays of explanations for machine learning model predictions in healthcare. BMC Medical Informatics and Decision Making. 2020 Oct;20(1):257. Available from: https://doi.org/10.1186/s12911-020-01276-x.

[5] Jin W, Fan J, Gromala D, Pasquier P, Hamarneh G. EUCA: the End-User-Centered Explainable AI Framework. arXiv; 2022. ArXiv:2102.02437 [cs].

[6] Zhang J, Johnson TR, Patel VL, Paige DL, Kubose T. Using usability heuristics to evaluate patient safety of medical devices. Journal of Biomedical Informatics. 2003 Feb;36(1):23-30. Available from: https://www.sciencedirect.com/science/article/pii/S1532046403000601.

Generation of VLA-4 Engineered Fragment

Scholar: Glory Schmigel

High School: Hempfield Area High School, Greensburg, PA

Lab: Ravi Patel, MD, PhD

Mentor: Robert Edinger, PhD

Site: Cancer Biology

Very late antigen-4 (VLA-4) serves as the key molecule for the adhesion, extravasation, and homing of hematopoietic and immune cells, and shows abundant expression in metastatic melanoma and may serve as an attractive target for imaging and therapy. Previous experiments using LLP2A, a peptide that binds to VLA-4 with high affinity, have shown it to be an excellent imaging agent. However, due to high blood clearance rates of LLP2A, it is not able to be used for targeted radionuclide therapy (TRT). This study is intended to find a binding agent with a high affinity for VLA-4 that can act as an agent for TRT as well as imaging. Vascular cell adhesion protein 1 (VCAM-1) mediates the adhesion of lymphocytes, eosinophils, and basophils to vascular endothelium, and is a primary endothelial ligand for VLA-4. We hypothesized that the generation of a modified engineered fragment for VCAM-1 may act as an effective imaging and therapeutic agent for metastatic melanoma. We isolated the VCAM-1/VLA-4 interaction site, located in domain 1, and fused it to the CH3 Fc domain of IgG (VCAM-D1-CH3). Expression and isolation of VCAM-D1-CH3 was performed in bacteria, and the affinity of the protein samples was determined using a cell-based enzyme-linked immunosorbent assay (cbELISA) on the B16F10 cell line, a mouse melanoma cell line that highly expresses VLA-4.

Adaptive Noise Cancellation Algorithm to Improve Hearing Aids for Central Auditory Processing Disorder

Omisa Shah[1] and Inhee Lee[2], Ph.D.
[1] North Allegheny Senior High School, Pittsburgh, PA; [2] University of Pittsburgh, Pittsburgh, PA

Abstract

Hearing assistive technology often remains financially inaccessible for many families. This study presents an adaptive noise cancellation algorithm that adjusts its threshold based on environmental factors. Combining pure audio with generated white Gaussian noise at various ratios, we applied our algorithm and evaluated its efficacy with cross-correlation analysis. When implemented into a hearing aid, this offers a potential cost-effective alternative to existing technologies which improve real-time speech comprehension.

Introduction

CAPD is a condition affecting the perception and processing of auditory information, despite normal hearing acuity. Individuals with CAPD often experience difficulties in sound localization, processing rapid speech, isolating speech amidst auditory distractions, and retaining auditory information.[1] Current hearing assistive technology (HAT), such as frequency modulation (FM) systems and low-gain hearing aids, while effective, are often prohibitively expensive for many families, with costs reaching thousands of dollars. This study aims to develop a low-latency, energy-efficient adaptive noise cancellation algorithm suitable for implementation in hearing aids. The proposed algorithm offers a dynamic threshold tailoring itself to the user's acoustic environment, potentially providing a more affordable alternative for CAPD management.

Methods

The study utilized 10-second pure audio samples combined with additive white Gaussian noise at various signal-to-noise ratios (SNR) to simulate diverse environmental conditions. The algorithm processes this noisy audio once, mimicking real-time application. Over the first two seconds, it calculates an initial mean volume and a threshold as a percentage of this mean, and subsequently updates both values with each additional sample. Samples below the threshold are set to 0, thus silencing them. The algorithm's effectiveness was quantitatively evaluated using cross-correlation analysis, comparing the processed audio to the original. Cross-correlation analysis also determined the optimal initial threshold factor and sensitivity to mean shifts, optimizing performance across the multiple simulated acoustic environments.

Results

The cross correlation analysis returned a 99.86% similarity between the original and cleaned audio files, as opposed to a 99.75% similarity between the original file and file with white Gaussian noise. Discrepancies between the audio files are existent but faint (Figure 1). Trials reveal an optimal ideal sensitivity factor of .15 (Figure 2) and threshold factor of .15 (Figure 3) in the equation to adjust the threshold.

Discussion

The implementation of a dynamic threshold for noise cancellation demonstrates value; however, it requires further refinement prior to practical application. Benefits of the adaptive threshold over its static counterpart include superior performance with real-time and variable acoustic environments. Nonetheless, the observed improvement in audio quality is marginal. Several factors may contribute to the limited success of this approach. The similarities in volume between the target audio and background noise may impede discriminatory capability. Additionally, the trial segment may not be sufficiently representative of the entire audio file. It is also plausible the original audio file contained inherent background noise, further muddling the cleaned audio. A potential avenue for improvement involves the intersection of frequency analysis with volume assessment. In conclusion, while the current results fall short of ideal, they showcase viability. Further research and development are necessary to optimize this technique.

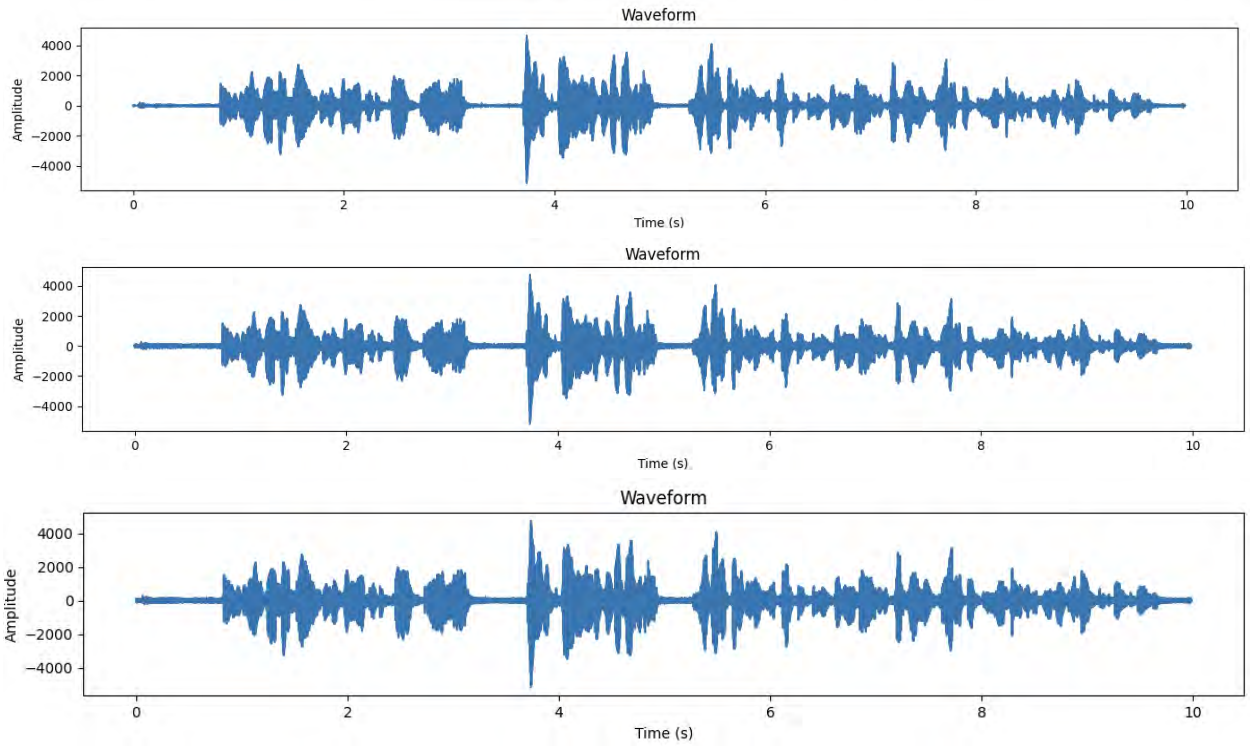

Figure 1. (top to bottom) Waveforms of the pure audio, audio combined with low-level gaussian noise, and the cleaned audio

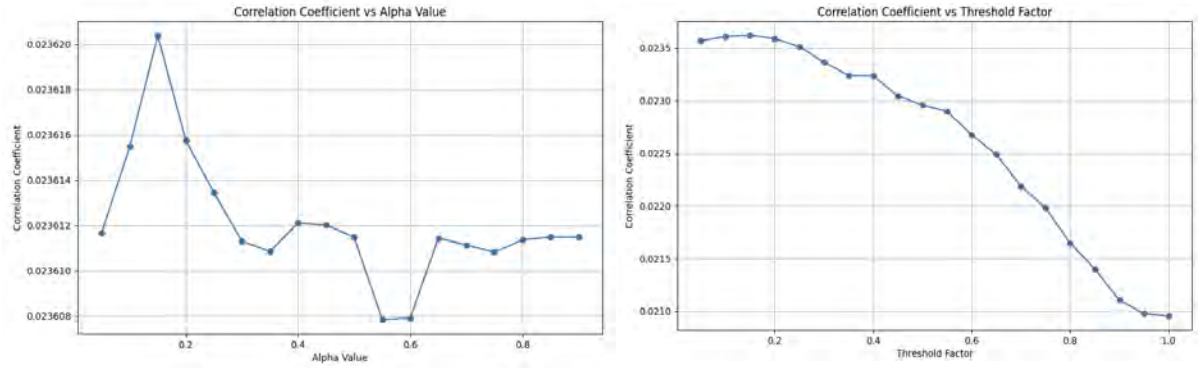

Figure 2. Graph of correlation coefficient versus alpha (smoothing factor)

Figure 3. Graph of correlation coefficient versus threshold factor

References

1. Auditory processing disorder (APD) [Internet]. Mayo Foundation for Medical Education and Research; 2023 [cited 2024 Jul 24]. Available from:https://www.mayoclinic.org/diseases-conditions/auditory-processing-disorder/diagnosis-treatment/drc-20555277

Age-Associated DNA methylation in Primary Human Invasive Lobular Breast Carcinoma

Scholar: Nathaniel Shelton
College: The Neighborhood Academy
City: Pittsburgh
State: Pennsylvania
PI of group/lab: Adrian Lee, Ph.D and Steffi Oesterreich, Ph.D
Mentor: Sanghoon Lee, Ph.D

About 42,000 women die of breast cancer in the USA every year. Aging is associated with a decline in physiological function and increased risk of mortality and incidence of breast cancer. Researching the differences in cancer biology between younger and older patients with breast cancer is necessary to develop more specific and effective cancer treatment strategies. While transcriptomic features of younger and older patients with cancer have been characterized, genome-wide epigenetic differences between the age groups remain largely unexplored. Especially, the DNA methylation patterns driving breast cancer development in older women are not well understood. DNA methylation is a key epigenetic mechanism that regulates gene expression. Therefore, we hypothesize that differences in methylation patterns between younger and older patients with breast cancer can provide insights into age-related changes in gene regulation and valuable information for patient prognosis. We characterized DNA methylation pattern differences between younger and older patients with estrogen receptor positive (ER+) invasive lobular carcinoma (ILC) (n=88) using primary tumors from the Molecular Taxonomy of Breast Cancer International Consortium (METABRIC). We divided the age groups into younger ≤ 50 and older ≥ 70 groups, excluding middle-age or perimenopausal patients aged 51 to 69. We examined the correlation between DNA methylation and chronological age, then identified distinct patterns of DNA methylation in younger and older patients with ER+ ILC. We found STOX2, CDO1, ANXA2R, and TWIST1 were hypermethylated in older patients with ER+ ILC, but their gene expressions were downregulated. On the contrary, FFAR2 and TRIM50 were hypermethylated in younger patients with ER+ ILC, but upregulated. This study reveals the distinct epigenomic features of younger and older patients with ER+ ILC. The significant genes of varying methylation patterns and gene expression with further conduct and research, may lead to more information about how DNA methylation patterns change in age related circumstances.

Identification and Characterization of GPR120 Ligands Using a Tango Assay

Ashley Shim
Mentors Cheng Zhang, Stephanie Singh

[1]North Allegheny High School, Pittsburgh, PA; [2]Hillman Academy

Abstract

GPR120, a G-protein coupled receptor identified as an omega-3 fatty acid receptor, is known for its role in mediating anti-inflammatory and insulin-sensitizing effects. A better understanding of this could aid the development of drugs to improve insulin sensitivity and mitigate inflammatory responses, potentially taking a step forward in helping the millions of individuals struggling with T2D (type 2 diabetes).

Introduction

Omega-3 fatty acids exert some of their effects through GPR120, making it a compelling target for therapeutic interventions in inflammation and metabolic disorders. Despite its significance, the full spectrum of ligands that can activate GPR120 and their therapeutic potential still need to be explored. This study aims to fill this gap by utilizing a Tango assay to identify and characterize effective ligands targeting GPR120, providing further insights that could pave the way for novel treatments.

Methods

This study incorporated GPR120 as the primary test receptor, alongside a negative control (NC) and a positive formyl peptide receptor 1 (FPR1) control to validate assay specificity and functionality. The Tango assay, a cell-based reporter gene assay, was optimized to detect receptor activation through ligand binding. HEK293 Tango cells are specifically designed to express β-arrestin-TEV fusion protein and a tTA-dependent luciferase reporter gene. They are then transfected with plasmids encoding GPR120 or FPR1. Upon ligand binding, β-arrestin recruitment to the receptor facilitated the proteolytic release of a transcription factor, driving luciferase expression as a measurable readout. We used previously studied synthetic agonist TUG-891 to benchmark receptor activation and tested a newly identified agonist compound 83 to assess its stimulation of the receptor.

Results

The positive control demonstrated robust activation of FPR1, showing high readouts and validating the assay's functionality. FPR1 was tested using fMLF/fMLP at concentrations from 10^-10 M to 10^-5 M, confirming the assay's operation. However, HEK293 Tango cells transfected with GPR120 and the negative control were not eligible for testing, likely due to issues such as low cell confluency or potential infection, highlighting the need for further optimization.

Discussion

The application of the Tango assay has the potential to provide a robust platform for identifying and characterizing ligands for GPCRs, offering further understanding of their pharmacological profiles. The overarching goal of this study is to find profound implications for the treatment of type 2 diabetes (T2D). By identifying ligands that can modulate GPR120 activity, this research has the potential to aid in the development of novel therapeutics. Further optimization of cell culture conditions is warranted to enhance assay reliability and screening efficiency.

Average Luminescence of the three replicate per Concentration of ligand

A (no ligand)	289
B (0.00001 uM)	133
C (0.0001 uM)	302
D (0.001 uM)	833
E (0.01 uM)	10311
F (0.1 uM)	14604
G (1 uM)	17903
H (10 uM)	19182

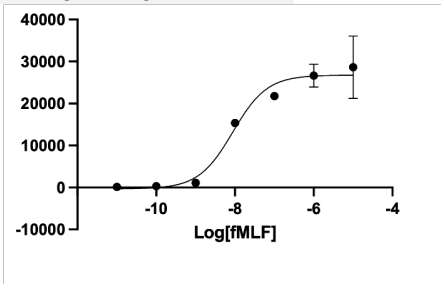

(note: Middle column was excluded from the graph)
Average luminescence (immediately after incubation + 10 minutes + 15 minutes)

A (no ligand)	219	350	297
B (0.00001 uM)	99	94	205
C (0.0001 uM)	391	255	261
D (0.001 uM)	934	309	1255
E (0.01 uM)	15378	242	15313
F (0.1 uM)	21706	267	21839
G (1 uM)	28569	418	24722
H (10 uM)	33886	291	23370

Cell culture optimizations

- Confluency
    - 50-60% confluency: resulted in 20% viability of cells after transfection
    - 90% confluency resulted in about 70-80% after transfection. After performing the luciferase assay confluency averaged 65-70%.

A	67	76	64
B	53	51	41
C	72	72	67
D	70	81	69
E	75	71	66
F	71	71	71
G	75	70	66
H	76	67	61

References

Dogra, S., Sona, C., Kumar, A., Yadav, P. N. Tango assay for ligand-induced gpcr–β-arrestin2 interaction. *Methods in Cell Biology*. 2006, 233-254. https://doi.org/10.1016/bs.mcb.2015.11.001

Oh, D. Y., Talukdar, S., Bae, E. J., Imamura, T., Morinaga, H., Fan, W., Li, P., Lu, W. J., Watkins, S. M., Olefsky, J. M. GPR120 is an omega-3 fatty acid receptor mediating potent anti-inflammatory and insulin-sensitizing effects *Cell*. 2010 *142*(5), 687-698. https://doi.org/10.1016/j.cell.2010.07.041

Tiberi, M. G *protein-coupled receptor signaling : methods and protocols*. Humana Press. 2019.

Random Forests vs Deep Learning to Classify between EASE and Control Therapies for Autistic Adolescents

Ethan L. Small, Dr. Deniz Kocanaogullari, Nathan T. Riek, and Dr. Murat Akcakaya

Central Catholic High School, Pittsburgh, Pennsylvania; University of Pittsburgh Hillman Cancer Center Academy, Pittsburgh PA

Abstract: This study explores the efficacy of machine learning models in distinguishing between adolescents with autism participating in the Early Adolescent Skills for Adults (EASE) therapy and those in a Control group, using electroencephalogram (EEG) data. We compared the performance of a Random Forest classifier and a linear neural network to classify EEG data from participants aged 12-25. Various feature selection techniques were employed to assess their impact on classification accuracy and model performance.

Introduction: An electroencephalogram (EEG) is a diagnostic tool that measures brain activity through electrodes placed at specific locations on the scalp. This study focuses on adolescents with autism, aged 12-25, who are involved in the EASE intervention and a Control group. EASE is designed to enhance the daily living and social skills of adolescents with autism, helping them transition more effectively into adulthood [1]. The Control group consists of participants not receiving the EASE intervention, serving as a baseline comparison. The primary aim of this research is to apply and compare machine learning techniques—specifically Random Forests and a linear neural network—to classify EEG data of these two groups. By analyzing the effectiveness of these classifiers, we aim to determine which model provides better differentiation between EASE and Control participants. Additionally, we test different EEG features in enhancing the classification performance of each model. This comparative analysis could offer insights into the most effective machine learning approaches for distinguishing between therapy types based on neural data, ultimately contributing to the optimization of therapeutic interventions for autistic adolescents.

Methods: The dataset for this study comprised 2,416 EEG trials from 19 channels, each lasting 1 second, and sampled at 300 Hz. The trials included 19 participants in the Control group and 17 participants in EASE . EEG data were processed to extract temporal features (mean, standard deviation , and sample entropy) and spectral features (power in frequency bands: Delta, Theta, Alpha, Beta, Gamma). We employed both a Random Forest classifier and a linear neural network to classify the data. For the Random Forest model, hyperparameters such as maximum depth, number of estimators, and loss function were optimized using grid search. The model was evaluated using three feature sets: temporal features only, spectral features only, and a combination of both. The linear neural network, structured as 57x57x1, was tested with the same feature sets. The linear neural network architecture is provided in Figure 1. Both classifiers were assessed for accuracy, precision, recall, and F1-score to determine which approach and feature set best distinguished between the EASE and Control groups.

Results: When evaluating the classifiers using only the power frequency bands as features, both the Random Forest classifier and the linear neural network yielded similar performance, achieving an Area Under the Curve (AUC) score of approximately 0.71. When temporal features were tested, the Random Forest classifier outperformed the linear neural network, achieving a slightly higher AUC score of 0.89, in comparison to an AUC score of 0.88 for the linear neural network. In contrast, when all features were combined (temporal and spectral), the linear neural network demonstrated superior performance with an AUC score of 0.90. This shows that the linear neural network was more effective in leveraging the combined feature set, while the Random Forest classifier performed better with temporal features alone. In addition to AUC scores, additional performance metrics are shown in Table 1 for the linear neural network and Table 2 for the Random Forest.

Discussion: The study reveals some exciting progress in using EEG to differentiate between EASE therapy and control groups in adolescents with autism. The Random Forest classifier stood out, performing well with temporal features and achieving an AUC of 0.89. This suggests that tracking dynamic brain activity is crucial for accurate classification. On the other hand, the linear neural network performed even better with an AUC of 0.90 by combining both temporal and spectral features. This highlights the value of using a mix of data types to boost model accuracy. Overall, these results show the benefits of blending advanced

machine learning techniques with a range of features, which could lead to more personalized and effective autism treatments. This research sets the stage for using real-time neural data to enhance and refine therapeutic approaches.

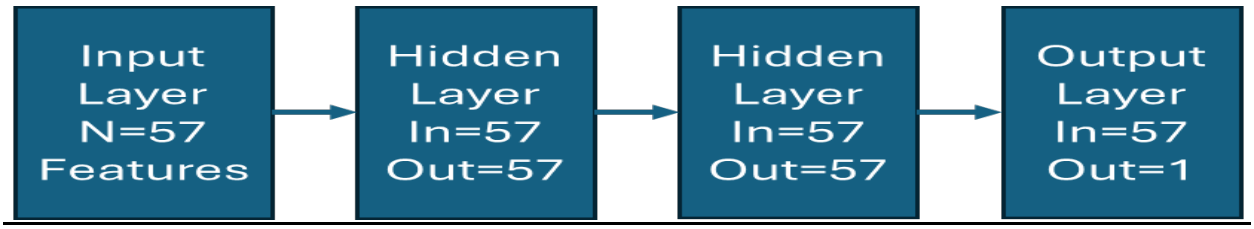

Figure 1: Linear neural network architecture

Table 1: Linear neural network performance metrics

Metrics	Temporal Features	All Features	Spectral Features
AUC	0.88	0.90	0.71
AUPRC	0.86	0.86	0.65
PPV	0.84	0.88	0.73
NPV	0.94	0.91	0.70
F1 Score	0.88	0.89	0.73
Sensitivity	0.95	0.91	0.68
Specificity	0.83	0.88	0.75

Table 2: Random Forest performance metrics

Metrics	Temporal Features	All Features	Spectral Features
AUC	0.89	0.89	0.72
AUPRC	0.86	0.86	0.65
PPV	0.92	0.91	0.71
NPV	0.88	0.88	0.74
F1 Score	0.89	0.89	0.72
Sensitivity	0.86	0.87	0.73
Specificity	0.93	0.92	0.72

References

[1] Susam, B. T., Riek, N. T., Beck, K., Eldeeb, S., Hudac, C. M., Gable, P. A., ... & Mazefsky, C. (2022). Quantitative eeg changes in youth with asd following brief mindfulness meditation exercise. IEEE transactions on neural systems and rehabilitation engineering, 30, 2395-2405.

[2] Riek, N. T., Susam, B. T., Hudac, C. M., Conner, C.M., Akcakaya, M., Yun, J., ... & Gable, P. A. (2023). Feedback Related Negativity Amplitude is Greatest Following Deceptive Feedback in Autistic Adolescents. Journal of Autism and Developmental Disorders, 1-11.

[3] Eldeeb, S., Susam, B. T., Akcakaya, M., Conner, C. M., White, S. W., & Mazefsky, C. A. (2021). Trial by trial EEG based BCI for distress versus non distress classification in individuals with ASD. Scientific reports, 11(1), 6000.

Human Corneal Limbal Epithelial Cells Immune Response to Herpes Simplex Virus type 1 Infection

Scholar: Makala Starks

High School: Obama Academy of International Studies

Lab: St. Leger

Mentor(s): Rylee N. Cisney, Anthony J. St. Leger

Site: Vision

Herpes Stromal Keratitis (HSK)is a disease of the cornea that can lead to vision loss or blindness. HSK is a leading cause of infectious blindness in developed countries, with an estimated 1.5 million cases each year. In the US, about 500,000 people are affected by HSK. The most common cause of HSK is Herpes Simplex Virus type 1 (HSV-1), which infects most of the world's adult population. Epithelial cells are a cell population located at the barrier of mucosal surfaces throughout the body, including the ocular surface. Despite human corneal limbal epithelial cells being the first to encounter HSV-1 during ocular infection, studies have largely ignored epithelial immune response(s) during the early corneal infection. We hypothesize that the production of pro-inflammatory mediators in response to HSV-1 is directly related to the pathogenicity of the virus. To test this, we infected epithelial cells *in vitro* with either a non-pathogenic strain of HSV-1 (KOS) or a highly pathogenic strain of HSV-1 (RE) at varying multiplicities of infection (MOI) for 24 & 48 hours. We then analyzed secreted pro-inflammatory mediators via Legendplex assays. We found that RE infection induced higher levels of IL-6 release from epithelial cells at 24 hours compared to KOS infection. Conversely, after 48 hours of infection, levels of IL-6 were higher in KOS infected cells compared to RE. At a 0.01 MOI, RE induced the highest levels of IL-8, another pro-inflammatory cytokine. Similar to IL-6, at 48hpi, IL-8 was similar between the KOS and RE groups. Finally, GM-CSF was downregulated during the infection compared to the media controls suggesting that HSV-1 infection interferes with the production of this factor. Overall, our data suggest that HSV-1 infection disrupts the production of pro-inflammatory mediators within epithelial cells. We have identified three factors, IL-6, IL-8, and GM-CSF, that are differentially regulated according to the pathogenicity of the virus. Therefore, we conclude that these factors can be further explored using more physiological systems and directly testing ocular pathology after epithelial cell manipulation.

Analyzing the Efficacy of Signaling and Antigen-presenting Bifunctional Receptors in Primary CD4+ Cells

Scholar: Lyra Stiglitz

School: Mount Lebanon High School, Mount Lebanon, Pennsylvania

Lab: Alok Joglekar, PhD

Mentor(s): Alok Joglekar, Sanya Arshad

Site: Immunology and Cancer Immunotherapy

Background: Signaling and Antigen-presenting Bifunctional Receptors (SABRs) allow for the determination of TCR-pMHC cognate pairs by presenting known peptides to T cell receptors (TCRs). Upon recognition of the TCR, intracellular signaling in the SABR using GFP and CD69 is induced, which can be detected using flow cytometry. Initial experiments used Jurkat cells to express SABRs; however, since immortalized cells have different properties than primary cells, future experiments must express SABRs on primary CD4+ cells, which are much less readily available than Jurkat cells. Therefore, additional research is needed to determine the minimum quantity of TCR and SABR-expressing CD4+ cells necessary to achieve detectable CD69 and GFP signaling. By co-incubating varying concentrations of TCR and SABR-expressing cells and measuring CD69 expression, SABR efficacy in primary CD4+ cells can be determined.

Methods: 293T packaging cells were transfected with DNA for BDC2.5 TCR and HIP SABR (a known cognate pair) using 8.9 and vsv-g packaging plasmids. The resulting virus was collected and transduced into CD4+ cells collected from mice by positive selection MACS sorting. The transduced cells for BDC2.5 TCR and HIP SABR were co-incubated at varying dilutions, and flow cytometry was used to measure CD69 expression.

Results: CD69 expression on SABRs varied between 100% and 6.64% as cell concentration differed. The lowest cell concentration that produced a readable CD69 signal was 1000 SABR-expressing CD4+ cells co-incubated with 1000 TCR-expressing CD4+ cells, for a CD69 expression of 51.00%.

Conclusions: These data show that SABR activation can be detected in CD4+ cells with only 1000 SABR and 1000 TCR-expressing cells. Future experiments will use this data to screen autoimmune TCRs for their cognate epitopes with SABR libraries. Identifying cognate epitopes of autoimmune TCRs may lead to the development of treatments or cures for these diseases.

Serum Arginase-1 as a Predictive Biomarker for Head and Neck Cancer

Scholar: Ella Tabish
High School: The Pingry School, Basking Ridge, New Jersey
Lab: Robert Ferris
Mentor: Lazar Vujanovic
Site: Immunology and Cancer Immunotherapy

Background: While recent advances in immuno-oncology have revolutionized how head and neck squamous cell carcinoma (HNSCC) is treated, only a subset of patients benefit from these drugs and experience deep clinical responses. Biomarker-guided identification of patients likely to respond to immunotherapy could enable superior management of HNSCC. One potential predictive biomarker is serum arginase-1 (sArg1). Unpublished data suggests that, while sArg1 is not readily found in healthy donor serum, it is detected in a cohort of HNSCC patients and may have the potential to predict HNSCC patient survival in a regimen-specific manner. This study aims to evaluate the cellular source of arginase-1 and link this biological process to the observed differences in the predictive potential of sArg1. In melanoma patients, sArg1 concentrations directly correlate with the absolute cell counts of circulating CD14lowCD3-CD19- myeloid cells. Based on this data, the hypothesis is that sArg1 may be a surrogate biomarker for a specific CD14low myeloid population that is critical for HNSCC patient response to immunotherapies.

Methods: Titrating doses of imiquimod (TLR7 agonist) were used to treat bulk peripheral blood mononuclear cells (PBMC) or MACS-isolated circulatory monocytes or dendritic cells. After treatment, cells were collected, labeled with fluorochrome-labeled antibodies, and analyzed by flow cytometry using the CytoFlex flow cytometer. Cell-conditioned media was tested using an arginase-1 ELISA.

Results: Imiquimod induced arginase-1 production in dendritic cells (DC), intermediate monocytes, and classical monocytes, but not in non-classical monocytes and monocytic myeloid-derived suppressor cells (M-MDSCs). DCs required the presence of bystander lymphocytes to produce arginase-1 in response to imiquimod.

Conclusion: This data indicates that sArg1 levels may serve as a surrogate measure of circulating DC frequencies and the fitness of tumor-specific lymphocytes. Further studies are needed to link these observations to the frequencies of DCs in HNSCC patient blood.

Effects of Exercise on Colon Cancer Liver Metastasis in a Mouse Model

Scholar: Jermaine Taylor
School: Shady Side Academy/Duquesne University, Pittsburgh, PA
Lab: Tohme Lab
Mentors: Dr. Samer Tohme
Site: Surgery

Background: Metastases is the leading cause of death in patients with cancer. Cancer exosomes, released by primary tumors, can promote liver metastasis by eliciting pre-metastatic niche formation through a multi-step process. This involves the uptake of exosomes by Kupffer cells and then hepatic stellate cell activation to generate a microenvironment that favors metastasis. Our previous work has shown that exercise can protect against liver metastases, however, the mechanisms are not fully understood. Here, we hypothesize that exercise training can decrease liver metastases by decreasing the exosome-induced pre-metastatic niche formation.

Methods: Eight-week-old mice are randomized into sedentary and exercise groups with or without cancer exosome injection to establish the hepatic pre-metastatic niche. To parallel tumor metastasis, all mice were injected with murine MC38 colon cancer cells 3 weeks after exercise. Our experimental groups were sedentary, sedentary with cancer exosomes, and exercised with cancer exosomes

Results: We confirmed that in sedentary mice, exosome injection resulted in increased premetastatic niche formation and tumor metastases compared to mice that did not receive any exosomes. However, exercised mice had a significant decrease in premetatstaic niche formation (as evident by decreased fibronectin deposition) and decreased metastatic tumors when compared to exosome-injected sedentary mice.

Conclusion: Exercise can decrease exosome induced premetastatic niches formation and metastases.

Potential mechanism regulating stability of E3 ubiquitin ligase ZBTB25, an antiviral host defense protein

Scholar: Riley Therrien

School: Highlands High School, Natrona Heights Pennsylvania

PI of group/lab: Bill Chen, PhD

Mentors: Áine Boudreau BA; Travis Lear, PhD

Site: Tech Drive X

Introduction: The ubiquitin-proteasome system (UPS) is a vital cellular pathway responsible for the focused targeting and degradation of cellular proteins. The UPS targets proteins by binding polyubiquitin chains to lysine residues, and proteins can be recognized for this pathway by phosphorylation. The human E3 ubiquitin ligase, ZBTB25, exhibits an antiviral host defense by facilitating ubiquitination and degradation of a crucial coronaviral protease. Inversely, decreased protein levels and increased ubiquitination of ZBTB25 has been shown during coronaviral infection, suggesting a viral mechanism evading host antiviral defenses. This degradation occurs post-transcriptionally; however, the precise means of ubiquitinating ZBTB25 are unknown. In this study, we aim to discover the amino acid residues responsible for ZBTB25 ubiquitination and stability. Understanding this mechanism may help improve treatments against the potential coronaviral defense mechanisms that target this antiviral protein.

Methods: Using site-directed mutagenesis (SDM), we prepared a plasmid library of HA-tagged ZBTB25 point mutants that changed predicted key lysine and serine residues to arginine and alanine, respectively. Plasmids were expressed in human bronchial epithelial cells (Beas-2B) and treated overnight with protein synthesis inhibitor cycloheximide (CHX) and proteasome inhibitor carfilzomib (CFZ). Western blotting was used to compare endogenous ZBTB25 protein levels with overexpressed ZBTB25-HA and mutant ZBTB25-HA.

Results: Endogenous ZBTB25 levels decreased with CHX and increased with CFZ, and a relatively similar pattern occurred with lysine mutations of 142, 372, and 374. Compared to ZBTB25-HA overexpressed wild type cells, ZBTB25-HA levels rose only slightly under CFZ treatment with the 375 serine to alanine mutation and the 142 lysine to arginine.

Conclusions: Serine site 375 appears to mark ZBTB25 for degradation by phosphorylation, and lysine site 148 may play a role in conjunction with other sites to facilitate ubiquitination. These data support the conclusion that ZBTB25 is degraded through the ubiquitin-proteasome system, indicating a novel pathway that coronavirus can take advantage of within a cell.

Analysis of Protein-Protein Interactions Occurring During the Initiation of DNA Replication (RNA Polymerase 3 Subunit F, Cell Division Cycle 45, and Cyclin Dependent Kinase 2) Using Split TurboID

Scholar: Isabel Vilensky

High School/City/State: Upper Saint Clair High School, Pittsburgh, PA

PI of Laboratory: Dr. Tatiana Moiseeva, PhD

Mentors: Dr. Luis Gregory Zamalloa, PhD, Dr. Tatiana Moiseeva, PhD

Site: Cancer Biology

This study focuses on using split TurboID to identify and map protein-protein interactions occurring at the initiation of DNA replication.

The initiation of DNA replication depends upon various protein-protein interactions. Prior research has found that specifically, the proteins CDC45 (cell-division cycle 45) and CDK2 (cyclin-dependent kinase 2) are proximally located to POLR3F (RNA Polymerase 3 subunit F). However, definite contact/interaction between these proteins was not confirmed in said research. For this reason, Split TurboID was essential for this study. Split TurboID is an engineered biotin ligase (catalysis agent for chemically bonding biotin to proteins). The mechanism uses two parts - Turbo C (TC) and Turbo N (TN). These parts are complementary to one another and thus attach to form a functional biotin ligase and activate Split TurboID. In order to analyze any interactions between POLR3F, CDK2, and CDC45, we cloned four constructs: POLR3F-TC, POLR3F-TN, TC-POLR3F, and TN-POLR3F. To clarify, Turbo N and Turbo C were part of the backbone sequence, and POLR3F was the insert. Then, we transfected a human line of 293T cells (transformed kidney cells) with different combinations of these proteins to create ten samples (one untransfected control, CDC45-TC matched with POLR3F-TN, TN-POLR3F, CDK2-TN, one CDC45-TC control, CDK2-TN matched with POLR3F-TC and TC-POLR3F, one CDK2-TN control, and POLR3F-TC, TC-POLR3F controls. Finally, we harvested our cells and confirmed any interaction through a streptavidin-HRP (horseradish peroxidase) analysis which illuminated any biotinylation. In conclusion, we found that the combination of TC-POLR3F and CDK2-TN produced strong biotinylation, which is evidence supporting that these proteins do come into contact with one another during DNA replication. These results are impactful because they provide further insight upon valuable protein-protein interactions occurring (as well as the positioning of the proteins) at the site of initiation of DNA replication and also demonstrate the capabilities of Split TurboID.

Assessment of a novel reporter system to detect arginine limitation in colorectal cancer

Scholar: Tiffany Wang

High School: Mt Lebanon High School, Pittsburgh, PA

PI: Dr. Dennis Hsu, MD

Mentors: Dr. Marwa Ibrahim, PhD, Alex Roberts

Site: Cancer Biology

Background: Arginine is a conditionally essential amino acid vital for various cellular functions. Although normal cells can synthesize arginine, arginine biosynthesis is impaired in cancer cells due to the downregulation of the enzyme ASS1, which leads to arginine limitation in the tumor microenvironment. During protein synthesis, arginine limitation causes ribosome stalling at arginine codons, reducing translation efficiency. To determine the pathway that drives arginine-limited translation, my lab developed a luminescence reporter sensitive to differences in arginine levels. The dual luciferase system includes the Renilla luciferase (Rluc) gene modified with two arginine codons inserted after the start codon (R^2) with the luminescence correlating with arginine concentration. A control reporter was designed with two glycine codons inserted instead of arginine (G^2). This reporter was expected to not be as sensitive to arginine levels.

Methods: To evaluate the sensitivity of the reporter to arginine limitation, the colorectal cancer cell line (RKO) was cultured under arginine fed and starved conditions. Luciferase activity and cell viability were measured using luminescence and fluorescence-based assays. RT-PCR and western blotting were performed to detect Rluc mRNA and protein abundance; respectively.

Result: Upon normalization to cell viability or firefly luciferase activity, the R^2 cells exhibited a significant decline in luciferase activity in the arginine starvation media compared to the G^2 cells, in correlation with arginine levels; confirming the reporter system's sensitivity to arginine availability. In RT-PCR analysis, mRNA abundance of Renilla was not significantly affected by arginine starvation, suggesting that the observed changes were post-transcriptional. Western blot showed that translation of the Rluc protein was impacted by arginine deprivation.

Conclusion: The decrease in bioluminescence of the arginine-modified construct is more likely due to decreased translation rather than transcription. This luminescence reporter system can potentially be used to screen for genetic factors which may affect translational efficiency under arginine limitation.

Investigating the Impact of ATR Inhibitor(ATRi) and Direct Telomerase Inhibitor 6-thio-dG in Telomerase Inhibition and DNA Damage

Scholar: Alastair Watt

High School: Deer Lakes High School, Cheswick, PA

PI of group/lab: Dr. Patricia Opresko

Mentor: Dr. Samantha Sanford

Site: Cancer Biology

Background Telomerase is a cellular enzyme that helps keep cells alive by adding DNA to telomeres, which are the ends of chromosomes. Telomerase maintains telomeres in tumor cells, preventing them from shortening and immortalizing cancer cells. ATR inhibitors, indirect telomerase inhibitors, and 6-thio-dG, a direct telomerase inhibitor and telomere uncapping agent, are used to selectively inhibit telomerase and induce DNA damage with the intention of killing cancer cells.

Methods Immunofluorescence experiments are implemented in the Opresko Lab, applying primary antibodies TRF2, a telomere marker, and γH2AX, a DNA damage marker, to U2OS and HeLa LT cancer cells treated with an 5μm ATR inhibitor (Ceralasertib by Astrazeneca) that are compared with untreated cells. The cells are then incubated with secondary antibodies Cy5, which binds to γH2AX, and Cy3, which binds to TRF2, in order to stain telomeres for cellular microscopy imaging. Metaphase analysis targeted signal free ends, chromosome ends without a telomere, as a form of telomere loss as well as fragile telomeres resulting from loss of TRF1(a telomere binding factor with a role in DNA replication), increasing stalling at the DNA replication fork. Analysis examines telomere and gamma-h2ax colocalization, the overlap between Cy3 and Cy5 stains, to detect DNA damage at telomeres and whether telomerase inhibitors ATRi and 6-thio-dG induce damage.

Results Metaphase spread analysis indicated that there were significantly more signal free ends and fragile telomeres after treatment in HeLa LT cells. The ATR inhibitor was found to cause telomere loss, indicating less DNA damage overall in LT cells due to fewer telomeres. Colocalization analysis suggested greater damage after treatment in the telomerase positive HeLa LT cells compared to the telomerase negative, U2OS cells. There were significantly more telomere positive micronuclei in both the HeLa LT and U2OS cells.

Conclusions Results indicate that when ATRi is introduced to HeLa LT and U2OS cancer cells, there is greater damage colocalization after ATRi treatment in U2OS cells and greater telomere loss in HeLa LT cells.

Title: The Impact of ATR Inhibitor and UNG Knockdown on Interferon-β Expression

Scholar: Brandon Williams

High School: Winchester Thurston Upper School, Pittsburgh, Pennsylvania

Lab PI: Christopher Bakkenist, PhD

Mentor: Reyna Jones

Site: Cancer Biology

Background: Uracil-DNA glycosylase (UNG) is an enzyme that removes deoxyuridine (dU) in DNA. dU contamination in DNA is the result of the deamination of cytosine or an imbalance in the nucleotide pool, which leads to genomic instability. Ataxia Telangiectasia and Rad3-related (ATR) kinase plays a critical role in DNA damage response ATR inhibition induces a misbalance in the nucleotide pool, dU contamination, and interferon signaling. Interferon signaling is a key regulator for innate immune responses. The goal of this study is to understand the impact of ATR inhibition-induced interferon signaling in UNG cells.

Methods: Human cell line MCF10A was transfected with siRNA specific against UNG to knockdown the UNG protein. Western blot analysis was performed to validate the knockdown efficiency. MCF10A cells were treated with 5 μM, 10 μM, or 20 μM of ATRi(AZD6738). Cells were collected at 24 hours, RNA was isolated, and purified RNA was used to make cDNA using LunaScript RT Supermix, which makes cDNA from mRNA. Gene expression analysis was performed utilizing qQuantitative PCR (qPCR).

Results: Western blot analysis showed a UNG knockdown in siRNA-targeted cells when compared to the non-targeted cells. Surprisingly, ATR inhibition did not induce interferon-β expression levels, and the UNG knockdown did not influence expression levels. Higher dosages of the ATRi did not present any significant change.

Discussion: Our study shows that there is no significant difference in interferon-β expression levels when MCF10A cells are treated with ATRi. Future studies will be done to identify the reason for the lack of a significant difference between interferon-β expression when treated with ATRi in different conditions.

Investigating Polymerase II Pausing Using a Computational Model

Sarah Winikoff[1,3], Alayna Fu [2,3], Dr. Keisuke Ishihara,[4] Dr. James R. Faeder[4], Dr. Maria Chikina[4], Dr. Tina Subic[4]
[1]Pittsburgh CAPA, Pittsburgh, PA; [2]North Allegheny Senior High School, Pittsburgh, PA; [3]UPMC Hillman Cancer Center Academy and [4] Department of Computational and Systems Biology, University of Pittsburgh School of Medicine, Pittsburgh, PA

Abstract: ChIPMOD is a computational model from 2013 that simulates simple RNAPII binding patterns on the DNA from basic transcription parameters. It outputs data such as the density profile, transcription lengths, and mRNA synthesis rates. By incorporating the findings from recent studies, we updated ChIPMOD to represent more accurate mathematical and spatial dynamics of transcription.

Introduction: Gene expression is vital to the assembly of mRNAs and the function of life. RNA polymerase II (RNAPII) is responsible for transcriptional regulation through proximal pausing. It also transcribes protein-coding mRNAs and long non-coding RNAs. When transcriptional errors occur, regulatory checkpoints signal backtracking and stalling to correct the mistake. This leads to short bursts and longer periods of inactivity in transcription. However, the physical mechanisms behind RNA Polymerase II pausing and reactivation remain unknown.

Methods: We translated the initial model from C language to Python. We implemented the RNAPII initiation as a Poisson distribution, which is the probability of an independent firing event occurring within a given timeframe. The model simulates RNA polymerase as it transcribes the body of the gene and focuses on parameters affecting initiation, pausing, elongation, and termination. As the modern technologies achieve base-pair resolution of measuring RNAPII positions on the DNA, we directly report the density of the RNAPII on the DNA rather than converting the RNAPII density into a ChIP-seq signal.We visualize simulation results with plots showing the gene length, timing of initiation, and location of active sites that change the outcome of RNA.

Results: Qualitatively, our model matches experimental data from TV-pro seq methods[3]. We successfully tracked the position, density, and state of polymerases on the gene across numerous cells. We observed periodicity in the RNAPII density with the highest peak of polymerase occupation the beginning of productive elongation. Further research is needed to confirm the validity of this finding.

Discussion: Using our model, we will expand our research to the question: *Can changes in the stability of the polymerase at the pause site explain the difference between the tracks we were observing for the body of the gene compared to the transcription from promoters and enhancers?* By understanding the concept of gene regulation expression, we will enable future research towards human development, the onset of disease, Alzheimer's, cancer, and cellular stress response. This may unlock a largely unexplored genomic landscape for therapeutics.

References

1. Andreas H. Ehrensberger, Gavin P. Kelly, Jesper Q. Svejstrup, Mechanistic Interpretation of Promoter-Proximal Peaks and RNAPII Density Maps, Cell, Volume 154, Issue 4, 2013, Pages 713-715, ISSN 0092-8674
2. Wissink, E.M., Vihervaara, A., Tippens, N.D. *et al.* Nascent RNA analyses: tracking transcription and its regulation. *Nat Rev Genet* 20, 705–723 (2019).

3. Zhang J, Cavallaro M, Hebenstreit D. Timing RNA polymerase pausing with TV-PRO-seq. Cell Rep Methods. 2021 Oct 25;1(6):None. doi: 10.1016/j.crmeth.2021.100083. PMID: 34723238; PMCID: PMC8547241.

Title: Evaluate scRANseq in PBMCs of patients treated with neoadjuvant
Scholar: Camilla Zarour
High School/City/State: Taylor Allderdice Pittsburgh, PA
PI of Lab: Dr. Diwakar
Mentors: Dr. Rodrigo Das Neves
Site: ICI (Immunotherapy)

Project Title: Evaluate scRNA-seq in PBMCs of patients treated with anti-PD1

Background: According to estimates from the American Cancer Society in 2020, there were approximately 106,110 new cases of melanoma diagnosed in the United States, representing approximately 5% of all new cancer cases. Melanoma ranks among the top five cancers with the highest incidence in the USA. Neoadjuvant therapy has been proven to enhance the chances of survival for specific types of cancer by decreasing the risk of disease recurrence and increasing the possibility of performing a complete tumor removal. T cells play a crucial role in the immune response against tumors. They recognize and eliminate cancer cells by directly secreting pro-inflammatory cytokines. However, tumors can evade the immune system by upregulating immune checkpoint molecules. A combination of immune checkpoint blockade (ICB) has emerged as an effective method for treating melanoma patients. Single-cell RNA sequencing (scRNA-seq) is a powerful technology that allows for the examination of gene expression at the individual cell level. Unlike traditional bulk RNA sequencing, which provides an average expression profile across a large population of cells, scRNA-seq captures the heterogeneity and unique transcriptomic signatures of individual cells. This capability is crucial for understanding the complexity of tissues, identifying rare cell types, and uncovering cellular responses to various conditions. In this contest, scRNA-seq has revolutionized our ability to study biological systems at an unprecedented resolution, providing deep insights into the cellular composition and functional states within tissues that would help to better understand at the cellular level why melanoma patients respond to ICB and others not.

Primary Objective: Verify the frequency of CD8 T cells at the scRNA-seq level in melanoma patients who responded and did not to ICB treatment (aPD1).

Hypothesis: The patients who responded to antiPD1 have a higher count of CD8 T Cells.

Methods: For this project, R, R studio, and The Seurat Object were all part of the process. They allowed me to perform a scRNA-sequence on two different PBMC samples, one which responded to anti-PD1 (GEX.676), and the other not (GEX.630). This allowed us to compare the CD8 T-cells frequency and see the highest frequency of genes in certain clusters.

Results: Prior to combining the two PBMC samples we knew that sample GEX.630 was the non-respondent and sample GEX.676 responded to anti-PD1. We saw that CD8A and CD8B cells were all mainly in clusters 5, 6, and 7. After seeing this, we decided to compare the two samples and see which one most of the CD8 T cells were coming from. From that we saw that sample GEX.676, the responder, had less CD8 T Cells.

Discussion: The final results do not go alongside our hypothesis as we believed that the responder would have more CD8 T cells. We came to a conclusion that the decrease in CD8 T cells in the responder sample (GEX.676) might have been because the cells might have been going to the tumor and into tumor cells (TILs) instead of the PBMC. Another reason could have been that some of the CD8 T Cells in the clusters (5,7,8) may have been exhausted.

Do T cells have a sweet tooth?: Assessing glucose utilization in therapeutic T cells for cancer treatments

Scholar: Jingyuan Zhang

High School: Bethel Park High School, Bethel Park Pennsylvania

Lab: Greg Delgoffe, PhD

Mentor: Hannah Bumgarner, Greg Delgoffe, PhD

Site: Immunology and Cancer Immunotherapy

Background: Adoptive cell therapy (ACT) is a form of immunotherapy in which T cells are isolated from a patient, genetically modified, expanded *in vitro,* and then transferred back to the patient to initiate antitumor immunity. The *in vitro* expansion step is vital for generating enough T cells to transfer back into the patient. As a result, T cells are expanded in hyperglycemic media, containing up to 10x more glucose than what is in human blood, to propagate greater proliferation. While hyperglycemic conditions might aid in the expansion step, further research has shown that it comes at the cost of T cell functionality. Given the difference in glucose concentration in the culture media, we wanted to assess glucose utilization in these cells following T cell culture

Methods: CD8+ T cells were isolated from wild-type mice, activated in 11mM and 55mM glucose medias, expanded in their respective glucose media for 7 days, and then measured for extracellular acidification rate (ECAR) via a glycolysis stress test assay on a Seahorse XF Analyzer. The CD8+ T cells cultured in 11mM and 55mM glucose were read for basal ECAR and then injected with glucose, oligomycin, and 2-deoxyglucose in order to measure glycolysis and glycolytic capacity upon blockage of mitochondrial ATP production.

Results: A comparison between the 11mM cultured CD8+ T cells and the 55mM cultured CD8+ T cells, after being injected with either 11mM glucose or 55mM glucose, revealed that CD8+ T cells activated and expanded in 55mM glucose had consistently higher ECAR values after each injection, indicating greater rates of glycolysis.

Discussion/Future directions: The data gathered from the seahorse glycolysis stress test indicates several possible reasons for the increase in glycolysis. Future directions include assessing rates of glucose uptake and exploring glucose flux through the pentose phosphate pathway and the hexosamine biosynthesis pathway.